Arterial spin labeling in space and time : new MRI sequences to probe cerebral hemodynamics

Schmid, S.

Arterial spin labeling in space and time

new MRI sequences to probe cerebral hemodynamics

Sophie Schmid

Arterial spin labeling in space and time

new MRI sequences to probe cerebral hemodynamics

Proefschrift

ter verkrijging van
de graad van Doctor aan de Universiteit Leiden,
op gezag van Rector Magnificus prof.mr. C.J.J.M. Stolker
volgens besluit van het College voor Promoties
te verdedigingen op donderdag 15 juni 2017
klokke 13.45 uur

door

Sophie Schmid

Geboren te Delfzijl
in 1987

Cover design by: Lennart Schmid and Sophie Schmid
Printed and layout by; Drukkerij Mostert & van Onderen, Leiden, The Netherlands
ISBN: 978-94-90858-49-0
PhD thesis, Leiden University, The Netherlands

The work presented in this thesis was carried out at the C.J. Gorter Center, department of Radiology at the Leiden University Medical Center, Leiden, The Netherlands.

Financial support for the publication of this thesis was kindly provided by Philips Healthcare Netherlands.

This research is supported by the Dutch Technology Foundation STW, which is part of the Netherlands Organisation for Scientific Research (NWO) and partly funded by the Ministry of Economic Affairs (project number 11047).

Promotor

Prof. dr. A.G. Webb

Co-promotor

Dr. ir. M.J.P. van Osch

Promotiecommissie

Prof. dr. M.A. van Buchem

Prof. dr. E. Achten (Ghent University, Belgium)

Dr. I. Asllani (University of Rochester, USA)

Om arteriële spin labeling technieken verder te ontwikkelen
heb je een goede verbeelding en een stapel legoblokken nodig

aangepast van Thomas Edison

Content

1

General introduction

Brain perfusion

To assure proper functioning of the brain cells, it is necessary to maintain a sufficient supply of nutrients in the form of oxygen and glucose to the tissue, and to drain waste products from the brain tissue. Despite comprising only 2% of the body's weight, the brain consumes more than 20% of daily energy intake.[1] Since there is no local storage of energy in the brain, it is dependent on continuous delivery of nutrients by the blood flow. The process of blood delivery to the brain tissue capillary bed is called the cerebral perfusion and the cerebral blood flow (CBF) is commonly expressed as the volume of blood that flows through 100 grams of tissue per minute (ml/100 gr/min). CBF is regulated by complex control mechanisms, which can quickly respond to local and global changes in energy demands. However, even short interruptions of the blood supply to parts of the brain can lead to significant tissue damage and eventually tissue death, with cognitive and/or physical impairment or even death as a consequence.[2, 3] Accurate and fast perfusion measurements are important for diagnostic and prognostic information concerning pathological conditions. Global perfusion can be assessed by measuring the total amount of blood flow to the brain in the feeding arteries. Due to the close coupling between CBF and metabolism, regional brain function can be assessed through measurements of local cerebral tissue perfusion. However, CBF is not the only parameter to provide information about the regulation of regional perfusion, since CBF simply reflects the amount of blood delivered to a certain tissue region per unit of time.

In addition to CBF, other important physiological parameters describing the cerebrovascular state are:

- cerebral blood volume (CBV), which is the relative volume of the blood vessel and is an indicator of vasodilatation,
- oxygen extraction fraction (OEF), which is related to the local oxygen use and is the difference between the oxygenation of the blood in the arterioles and venules
- cerebral metabolic rate of oxygen consumption ($CMRO_2$), which is the product of CBF and OEF and reflects the local use of oxygen.

The CBF is determined by the cerebral perfusion pressure (CPP) and the cerebrovascular resistance (CVR): [4,5]

$$CBF = CPP / CVR$$

Figure 1 shows how these parameters relate to each other and how they compensate for reductions in CPP. The blood flows from the supply side to the venous side of the vasculature due to the net pressure gradient, the CPP. The CVR is the resistance offered by the cerebral vasculature to the CPP. The CBF can be regulated by contraction and relaxation of the smooth muscle cells and pericytes in the vessel walls.

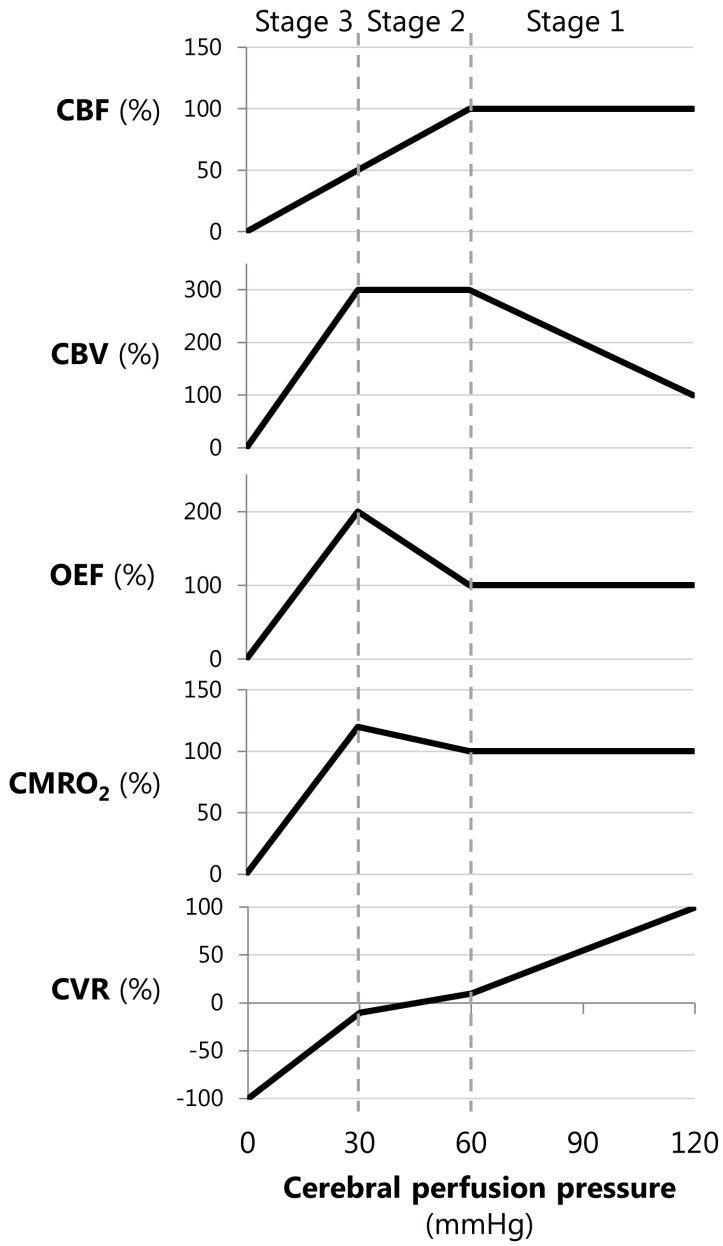

Figure 1 The change in cerebral hemodynamic variables compared to a CPP of 120 mmHg and the relation of the cerebral blood flow (CBF), cerebral blood volume (CBV) oxygen extraction fraction (OEF), cerebral metabolic rate of oxygen consumption ($CMRO_2$) and cerebrovascular resistance (CVR) as a function of the cerebral perfusion pressure (CPP). In healthy subjects the CPP is well above 60 mmHg. For a CPP below 30 mm Hg those mechanisms cannot compensate for the reduction in CBF. Figure adapted from Nemoto *et al*, Stroke, 2003. [6]

In healthy people, the CBF is regulated tightly as a function of the CPP to guarantee sufficient influx of nutrients and oxygen. This process is called the cerebral autoregulation. The autoregulation will respond to a drop in CPP by dilating the vessels, thereby increasing the CBV to stabilize the CBF at its original level (stage 1).
For a more severe reduction in CPP, and when maximum vasodilatation is reached, the OEF and $CMRO_2$ will be increased, so that a higher fraction of the oxygen is extracted from the blood, thereby enabling a continuation of aerobic energy consumption, therefore serving as compensation for the CBF reduction (stage 2).
The autoregulation and OEF can compensate for losses of CPP up to a lower limit of 30 mmHg. In the third stage, if the CPP falls below this level, the CBF will further decline and this will affect the metabolism and function of brain tissue, eventually resulting in infarction of brain tissue.

Perfusion measurement techniques

There are several modalities that can be used to measure perfusion: positron emission tomography (PET), single photon emission computed tomography (SPECT), Xenon- enhanced computed tomography (XeCT), dynamic perfusion computed tomography (pCT), dynamic susceptibility contrast MRI (DSC-MRI), dynamic contrast enhanced MRI (DCE-MRI), arterial spin labeling (ASL) MRI, and Doppler ultrasound.

Exogenous tracers

Oxygen-15 positron emission tomography (**$[^{15}O]H_2O$-PET**) is the most accurate and precise measurement method to obtain a complete quantitative evaluation of the brain hemodynamics and is considered the gold standard for perfusion measurements.[7] Nevertheless, PET has several drawbacks. The image resolution is relatively low and it requires the intravenous injection of tracers at a high dosage with a short half-life time, meaning that an onsite cyclotron is required. Due to the potential harmful radioactive and sometimes toxic characteristics of the tracers, PET is not suited for repeated measurements.

Dynamic susceptibility contrast MRI (**DSC-MRI**) is a first-passage bolus-tracking perfusion MRI-technique, which relies on the injection of a contrast agent based on the lanthanide ion gadolinium.[8] Its passage through the brain is monitored by fast dynamic MRI, usually measured for 1 minute at a 1-2 second time-resolution. The observed T_2 or T_2^*-signal changes are converted to concentration-time curves and deconvolution with the arterial input function is performed. Subsequently, perfusion parameters, such as CBF, CBV and mean transit time (MTT), are calculated from the impulse response function based upon tracer kinetic theory. The CBF equals the maximum value of the curve, the total amount of contrast present in the voxel is related to the CBV, which equals the area under the curve, and the first derivative

provides information on the amount of contrast agent that left the voxel, i.e. transit time distribution.[9]

In Dynamic contract enhanced MRI (**DCE-MRI**) T_1-weighted images are acquired at baseline and after injection of gadolinium based contrast agent. During the first passage, the contrast agent is predominantly intravascular allowing evaluation of perfusion. Including also the images acquired after the first passage of the bolus, the build-up of the contrast agent into the extravascular space can be monitored, which enables the measurement of vascular permeability and relative extravascular volume. The duration of the scans depends on the question to be answered: for perfusion measurements as for example performed for cardio applications only the first passage is important, which can be measured in a minute, while for tumours the build-up of the contrast agent needs to be captured which is typically slower (5-10 minutes), whereas the scan could take up to 25 minutes to allow detection of subtle leakage of the cerebral vasculature.[10, 11]

Endogenous tracers

Arterial spin labeling (**ASL**) is based on tracer kinetics to measure blood flow, similar to the nitrous oxide method, O^{15}-H_2O PET and to a lesser extent perfusion CT and DSC-MRI. Nevertheless, in ASL no contrast injections are used, but the blood itself is used as an endogenous contrast agent by inverting its longitudinal magnetization. A typical ASL-scan takes about 5 minutes to acquire. The water transport across the blood brain barrier is relatively unrestricted. Therefore, water protons are considered, although not completely, freely diffusible tracers.[12-16] Since ASL does not rely on the use of contrast agents or ionizing radiation, it is also suitable for pediatric patients and healthy volunteers. Furthermore, ASL can be used in patients with kidney failure and can be safely applied in groups requiring repetitive follow-ups, allowing monitoring fluctuations in CBF over time. Compared to PET, ASL has, therefore, a reduced risk of complications and is cheaper.

Arterial spin labeling

Arterial spin labeling was first proposed for perfusion imaging in the early nineties and the technique is still evolving.[12, 17] With new types of labeling schemes, readout options and models to quantify the perfusion, there are many different possibilities to acquire and process an ASL-perfusion MRI scan. This could be overwhelming and confusing, because it is not evident what would be the most robust ASL method to provide useful clinical information. In a joint effort of the ISMRM Perfusion Study Group and the European ASL in Dementia consortium a consensus paper was written with recommendations for the implementation

of ASL for clinical applications and to help the clinical community to adopt a standardized approach.[18]

General ASL concept

In arterial spin labeling the blood water is magnetically labeled by an RF-pulse that inverts or saturates the longitudinal component of the MR-signal of the blood spins. In traditional ASL-methods the labeling occurs in the feeding arteries at the distal end of the neck region. After a delay in which the labeled spins are transported further into the vasculature towards the tissue, an image of the static tissue and the tagged spins that have flown into the imaging slices is acquired. Subsequently, a control image without labeling of the static tissue and the untagged blood is acquired. The subtraction of both image types will remove the static tissue component and reflects only the inflowing tagged spins, which is a measure of the local tissue perfusion. The quality of a single subtraction image is limited, so typically 30 averages are obtained to gain sufficient SNR.

ASL can be considered as a building block system: it always consists of a labeling module, a post labeling delay (PLD) and an imaging readout sequence. Furthermore, background suppression pulses are often added during the PLD.

When available, scanning at a field strength of 3T is recommended, because of the advantages of the higher SNR and the longer T_1.[19] Other hardware considerations are the use of a multi-channel receive head coil with eight or more channels to enable the use of parallel imaging acceleration to decrease the echo time and total readout duration.[20, 21]

ASL labeling methods

The two main labeling approaches to achieve ASL for perfusion imaging are pulsed ASL (PASL)[22] and continuous ASL (CASL).[23]

In **PASL**, a large volume of blood is inverted with a short inversion pulse of about 10 – 25 ms. The many different labeling configurations that have been proposed for PASL, such as flow alternating inversion recovery (FAIR),[24-30] Signal Targeting with Alternating Radiofrequency (STAR),[31-35] Transfer insensitive labeling technique (TILT)[36, 37] and proximal inversion with a control for off resonance effects (PICORE),[38] all have in common that the labeled spins have an opposite magnetization compared with the control condition, but the positioning of the labeling plane is different for each of the methods. They have a relative high labeling efficiency, but because of imperfect slice profiles and coil geometry, blood far away from the readout center is not always perfectly inverted and therefore the edges of the bolus are not well defined, which can be a problem in quantification. Furthermore, since the labeling is

performed spatially, a dependence on the vascular layout is incorporated in the signal, resulting in an unknown temporal width of the bolus of labeled spins, thereby making quantification challenging. A better bolus definition can be achieved with Quantitative imaging of perfusion using a single subtraction, second version (QUIPSS II), that truncates the bolus length by applying saturation pulses at a certain time after labeling,[39] or with Inflow turbo-sampling EPI-FAIR (ITS-FAIR), quantitative STAR labeling of arterial regions (QUASAR) or similar multi-PLD sequences, that are capable of acquiring data at multiple time points.[35]

In **CASL**, the magnetization of water molecules in the blood flowing with a certain velocity through a thin labeling slice are continuously inverted with a flow-driven adiabatic inversion for 1–3 s. In the most common implementation of CASL there is an amplitude modulation of the RF-pulse in the control condition, which creates two inversion planes close to each other resulting in a double inversion of the spins flowing through, which also controls for magnetisation transfer effects. The labeling efficiency of CASL is lower than PASL due to loss of longitudinal magnetization in the control condition as well as the variability in the blood flow velocity over the heartbeat.[40, 41] The duration of the bolus is well-defined and CASL has a higher SNR than PASL. The main drawbacks of CASL are the high specific absorption rate (SAR) associated with the long pulse and the high demand put on the RF-amplifier, which can be overcome with a separate labeling coil.

The most popular ASL method currently for cerebral perfusion imaging is a variant of the CASL technique and is sometimes even considered as a separate, i.e. a third, labeling approach: pseudo-continuous ASL (**pCASL**).[41-43] The long continuous labeling of CASL is for pCASL replaced by a train of slice-selective, small flip-angle, RF-pulses that gradually invert spins flowing through the labeling plane. Since continuous RF is not required, the demand on the RF-amplifiers is reduced. During labeling there is no phase difference between the pulses (except to compensate for off-center localization of the labeling plane), while in the control condition a π-phase difference between the odd and even pulses is created, which effectively leaves the blood magnetization oriented in the direction of the main magnetic field, i.e. no inversion.

Currently, pCASL is advised as the labeling method for standard applications with a labeling duration of 1800 ms. This consensus recommendation was based upon the high SNR of pCASL, its easy implementation on clinical MRI scanners, and its comparable reproducibility to PET. The RF pulse spacing should be as short as possible, with slice-selective gradients ~10 mT/m with a mean gradient of ~1 mT/m, and the RF-pulses should have a mean B1 of ~1.5 mT.[41,42] Unbalanced pCASL is preferred, meaning a π-phase shift in the control condition relative to the labeling condition and a mean gradient of zero, because of decreased sensitivity to off-resonance effects. The positioning of the labeling plane can be optimized by first making a fast angiogram to find a proper location for labeling, where the arteries are relatively straight and where the labeling plane is approximately perpendicular to all brain-feeding arteries.[18]

Post labeling delay

The post labeling delay during which the labeled spins are transported further into the vasculature towards the tissue is always a compromise. On one hand, the PLD should be long enough for all spins to arrive in the brain tissue, thereby enabling accurate quantification. The time it takes for the labeled spins to go from the labeling slice to the imaging region and reach the capillary bed in healthy subjects is approximately 1.5 to 2 seconds, depending on age.[44, 45] Otherwise, the PLD is not long enough and the labeled spins will still be in the arteries or large arterioles, resulting in an angiogram instead of a perfusion image (see figure 2) and quantification of the CBF will be affected. For accurate quantification, the PLD should ideally be set slightly longer than the longest arterial arrival times (ATT) value present in the brain.[40] On the other hand, the PLD should not be chosen too long, because the labeled spins decay with the longitudinal relaxation time T_1 of the compartment in which they reside and if the PLD is too long, all signal will have decayed and no label will be detected. During the post-labeling delay period, the labeled spins will be for most of the time located in the arterial blood compartment, which has a T_1 of approximately 1650 ms at 3T. So, especially in patients

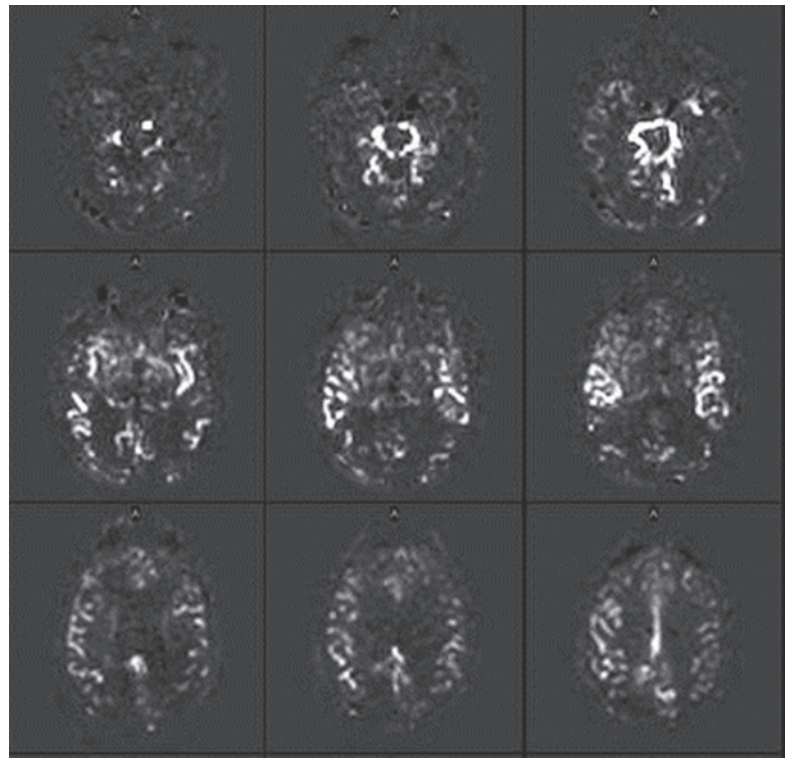

Figure 2 Example of ASL maps of a tumor patient with delayed arrival times. The presence of high signal intensity in the Circle of Willis and lateral arteries, and the lack of a clear contrast between the gray and white matter, show the delayed arrival of the label.

with cerebrovascular pathologies with collateral blood flow it can be difficult to measure the CBF with ASL due to the prolonged transport times for the label to arrive in the brain.
For pCASL, the advised PLD varies between 1500 ms for children to 1800 ms for adults and 2000 ms for elderly over 70 years old. In summary, the PLD is always a compromise between being sufficiently long for the labeled spins to arrive in the tissue and as short as possible for reduced loss of signal due to the T1-decay.[18]

Multi-PLD
When on a single-PLD acquisition an area with a low ASL signal is observed, it cannot be determined whether this is caused by a low CBF, by a much longer ATT, or by a combination of these two. It is possible to correct for the underestimation of the CBF due to long transit times by following the label dynamically with a series of images at different post labeling delays and to estimate the transit times from this dynamic data, thereby also enabling the creation of ATT-maps.[46,47, 48] However, acquiring multiple post labeling delays increases the scan time significantly and also requires more post-processing. Therefore, multi-PLD ASL methods are currently not recommended as the standard, but as a useful (research) tool to answer specific ATT-related questions as well as to obtain a potentially more precise quantification of CBF.[18]

Background suppression
Since the difference in signal intensity between the label and control condition is small, subject movement and physiological pulsations, such as from the respiratory and cardiac cycle, can lead to subtraction errors due to signal fluctuations in the static tissue. Background suppression (BGS) pulses can be employed (often during the PLD) to minimize the signal from static tissue, thereby reducing subtraction errors and significantly improving the ASL-signal stability.[49, 50]

By employing global inversion pulses the BGS affects different tissues equally. To null multiple types of tissues, more inversion pulses are needed. Although ideal inversion pulses should not attenuate the ASL signal, in reality additional pulses do lead to loss of signal due to T_2-decay during inversion and other pulse imperfections.[49] The use of 4 adiabatic inversion pulses can lead to 25% loss of ASL-signal and with 2 pulses this loss is approximately 15%. The nulling of the tissue types can only be optimized at a single time point, which is often chosen at the time of first excitation pulse of the readout module, with most tissues having a signal close to zero. The tissue signal is chosen to be slightly positive to avoid sign ambiguities and intravoxel cancellation of the signal in partial volume voxels. Because background suppression is tuned to the first excitation pulse of the readout module, lower degrees of BGS are obtained in later acquired slices for 2D imaging approaches, while more homogenous and better BGS can be achieved for 3D imaging.[49, 51, 52]

Imaging methods

2D single-shot EPI or fast low angle shot (FLASH) readouts are still the most commonly used ASL read out sequences for the brain.[53, 54] Conventionally, CASL has been frequently combined with spin echo EPI, whereas PASL is used with a gradient echo readout, but this choice mainly depends on the clinical question to be answered and is not related to the labeling approach. Spin echo sequences provide better image quality than gradient echo lower in the brain, but are also slower. For single-shot 2D readouts an ascending slice order is generally recommended with the underlying reasoning that arrival times are longer in more superior slices and that the readout should therefore 'chase the labeled spins'.

To efficiently track the transport of the created label over time, a **Look-Locker** readout can be used. Images at multiple time points are acquired employing low flip angle excitations to keep label-magnetization available for later time points. A drawback when applying Look-Locker imaging is that the low flip angle excitations affect the amount of label available for later time points and the apparent T_1 will be a function of the real T_1, the flip angle and pulse separation.[55, 56]

3D acquisitions
The above-mentioned imaging methods are all 2D, in the sense that they are acquired slice by slice. In 2005, **GRASE** (gradient and spin echo) was first used as a 3D-acquisition readout module for ASL[57, 58] The advantages of this and other 3D approaches over a 2D readout are that the background suppression is optimal over the complete imaging volume as well as higher intrinsic SNR. The drawback is that blurring in the z-direction is frequently present and can severely affect image quality.[59] To reduce too-long readout times that would lead to blurring, segmentation in the z-direction is frequently employed in 3D-GRASE readouts. Also, other 3D sequences such as stack of spirals share similar advantages as GRASE and are increasingly used for ASL. Improved image quality for 3D sequences is an active area of research and more improvements are expected in the near future. Such improvements will, hopefully, also lead to the possibility of single shot 3D-imaging, which will likely be the method of choice in the future, but currently suffers from significant blurring.

Quantification
For certain studies quantification is not essential and much information can be retrieved from scaling of ASL-images with respect to whole brain average values and considering the blood flow distribution. For example, in a clinical setting the perfusion of a tumor is frequently normalized with respect to the contralateral hemisphere or normal appearing GM. However, absolute quantification is essential for pathologies that affect the whole brain, such as large vessel occlusive disease, neurodegenerative disease and sickle cell disease, for longitudinal studies, and is especially important for clinical research in which patients are compared with

controls to improve our understanding of diseases. Factors such as transit time and labeling efficiency can differ between subjects, but also within the ASL-image of a single individual and can therefore result in quantification errors when not accounted for.

In order to quantify the CBF it is not sufficient to simply subtract the label from the control images and average these over the different dynamics. Preferably, the unsubtracted images are first corrected for motion, followed by correction for differences with global and regional scaling factors. For pCASL-data it is suggested to use the following simple quantification formula: [18]

$$CBF = \frac{6000 \cdot \lambda \cdot \left(SI_{control} - SI_{label}\right) \cdot e^{\frac{PLD}{T_{1,blood}}}}{2 \cdot \alpha_{lab} \cdot \alpha_{BGS} \cdot T_{1,blood} \cdot SI_{PD} \cdot \left(1 - e^{\frac{-\tau}{T_{1,blood}}}\right)} \left[ml/100g/\min\right]$$

where CBF is the flow in ml/100 g/min, λ is the brain/blood partition coefficient in ml/g, $SI_{control}$ and SI_{label} are the time-averaged signal intensities in the control and label images, respectively, $T_{1,blood}$ is the longitudinal relaxation time of blood, α_{lab} is the labeling efficiency, α_{BGS} is the decrease in labeling efficiency because of background suppression pulses, SI_{PD} is the signal intensity of a proton density-weighted image with similar read-out as the ASL image, and τ is the label duration. To convert the units from ml/g/s to ml/ (100 g)/min, which are used in the physiological literature, the factor of 6000 is included. Some of the multiplication factors such as α_{lab}, are chosen to have the same value for the whole image to scale to absolute perfusion. Other multiplication factors, such as SI_{PD} are applied on a voxel-by-voxel basis, to correct for differences in water content of tissue and blood, or can differ per slice, for example the post labeling delay, which should be adjusted per slice in 2D imaging to correct for the time delay between the acquisition of different slices.

New developments in ASL methods

Since the introduction of ASL, there have been many different approaches developed for new research applications, for example to measure new physiological parameters, to extend the application of ASL to outside of the brain, and to facilitate clinical implementation. Examples of these recently developed techniques used in this thesis are velocity selective ASL, Time encoded pCASL and T_2 Relaxation Under Spin Tagging.

Velocity selective ASL

For traditional ASL techniques labeling takes place proximal to the imaging region followed by a delay to allow the tagged spins to be transported towards the tissue. But in patients with slow or collateral flow prolonged transit delay time can be problematic, since the label is still in the large vessels at the moment of imaging or the PLD has to be prolonged with lower SNR as a result. In 2006 a new type of ASL labeling was introduced by Eric Wong, **velocity selective ASL** (VSASL), [60] which is a spatially non-selective labeling method based on the flow velocity of the blood spins. The main advantage of this spatially non-selective labeling method is that the labeling also occurs in the imaging region and that the label is therefore created much closer to the tissue compared to traditional ASL methods.

In the VSASL sequence, all spins with a flow velocity above a chosen cut-off velocity (often about 2 cm/s) are saturated, regardless of the spatial location, as schematically shown in figure 3. After a delay period during which the spins are transported further towards the tissue, the velocity selective labeling module is applied a second time, saturating all spins with a flow velocity above the chosen cut-off velocity again and subsequently the label image is acquired. In the control condition, the first velocity selective labeling is applied without velocity sensitivity, leaving the blood magnetization intact, and thereby creating a magnetization difference for blood spins between the label and control condition. In practice, some albeit minimal velocity sensitivity is applied in the control condition to compensate for errors related to imperfect excitation and refocusing pulses.

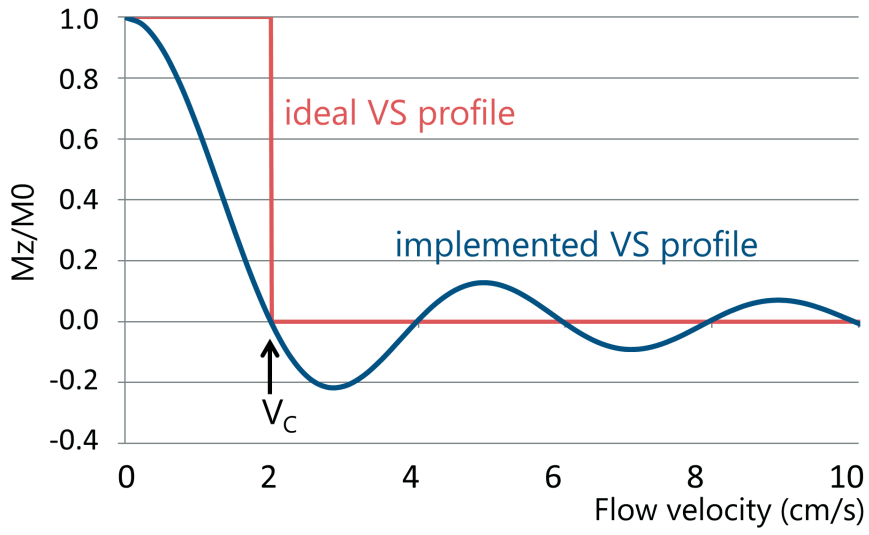

Figure 3 Longitudinal magnetization as a function of the velocity, obtained after the application VS labeling module. Ideally, the signal would be completely saturated above the chosen cut-off velocity (V_c), but the VS labeling module transforms the longitudinal signal into a sinc function. Figure adopted from Wu and Wong, JCBFM, 2007. [61]

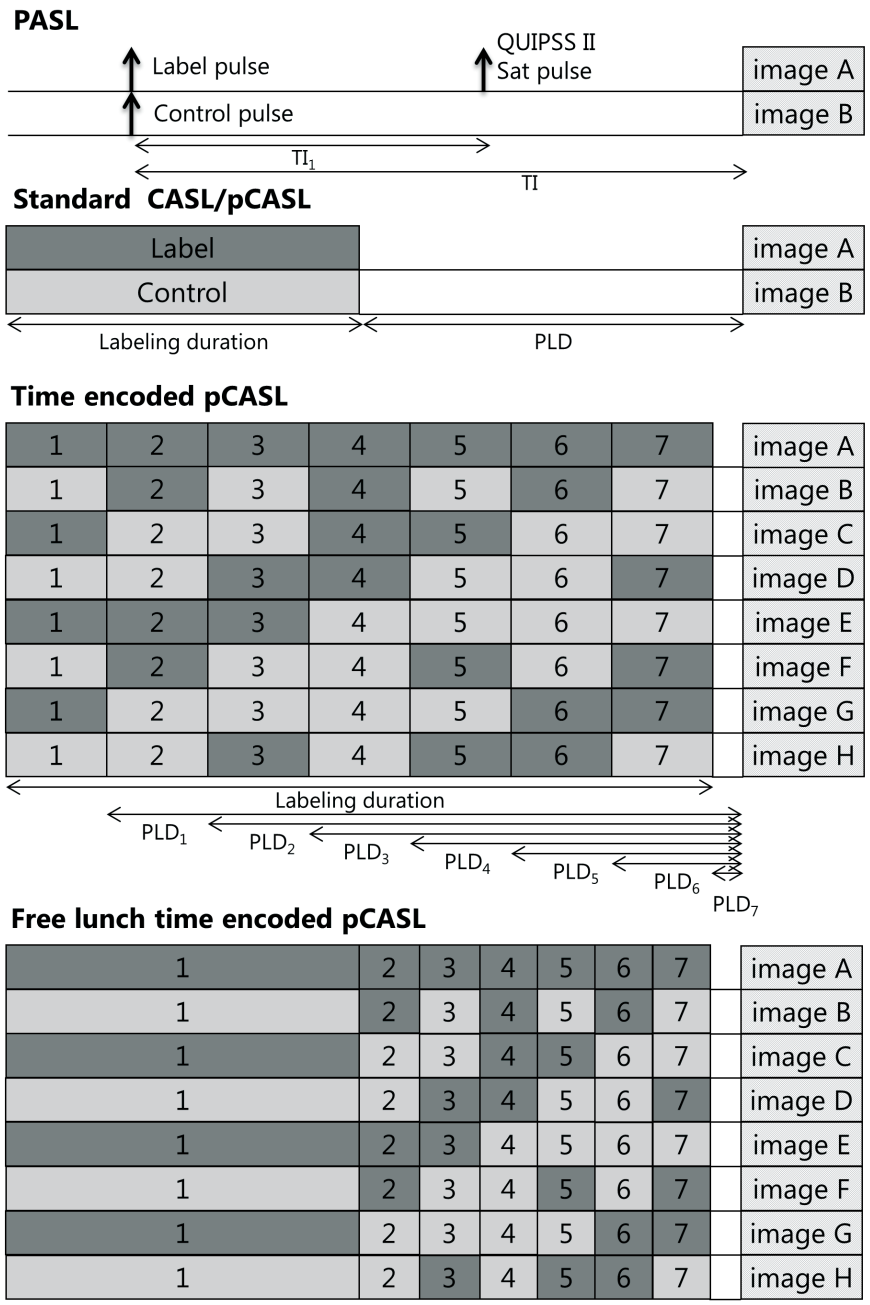

Figure 4 Schematic overview of the different ASL techniques. The darker blocks depict when labeling is performed and the lighter blocks the control condition. The time-encoded labeling module shows the 8 different encoding lines, each divided into 7 blocks. The acquisition of a single Hadamard encoding scheme encompasses 8 acquisitions, images A–H, from which 7 perfusion-weighted images can be reconstructed.

From basic physiology it is known that blood decelerates on the arterial side and accelerates on the venous side. With the labeling module placed just prior to imaging, only the spins that decelerated from above to below the cut-off velocity during the post labeling delay give signal in the image and discrimination between the arterial and venous spins is achieved in this way. Furthermore, the signal will become CBF-weighted instead of CBV-weighted and quantification of the CBF is possible, due to the well-defined bolus width. The feasibility of VSASL in functional MRI has been shown and the spatially non-selective method has been validated with xeCT in patients with Moyamoya disease, a steno-occlusive disease of the large arteries at the base of the brain, showing slight overestimations in regions with longer arrival times.[62] Results from this studie suggests that VSASL allows CBF measurements in regions that cannot be measured with traditional ASL methods using a similar PLD.

Time encoded pCASL

Temporal information is an important physiological parameter in aging, for pathologies such as stenosis or when collateral blood supply is present, and to give information about the distribution of the blood through the vasculature into the tissue. With original ASL methods information about timing was obtained by repeated acquisition with different PLDs and/or labeling durations.

In **Time encoded pCASL** (te-pCASL), also known as Hadamard encoded ASL, signal information at multiple time points is encoded in the labeling by employing a smart labeling scheme. The labeling is spatially selective as in pseudo continuous ASL with a labeling period that ends shortly before imaging, so the waiting time that is usually used for the labeled spins to be transported further into the vasculature is completely filled with labeling. This labeling period is divided into blocks that may switch between label and control according to a Hadamard matrix.[63] Whereas the standard pCASL delivers 2 types of images (label and control), with te-pCASL multiple images can be reconstructed, each characterized by the preceding labeling period. The number of different images depend on the encoding scheme applied.

In the example in figure 4 te-pCASL with a Hadamard-8 labeling scheme is applied, where 7 label and control sub-boli are captured in one image. A multiple of 8 acquisitions are measured, with signal obtained in each image from a labeling module with a different combination of label and control blocks. In post-processing, a concurrent subtraction scheme is applied that renders a perfusion map for each specific block while the signal contribution of all other blocks with different effective PLDs are cancelled out. Due to the time-encoding, the signal-time curve can be calculated at 7 different PLDs in a very time efficient way. Importantly, the perfusion image of each block will have the same SNR as a traditional pCASL scans with the same PLD, TR and labeling duration, acquired in the same scan time, i.e. one gets 7 images

with the same SNR in the time that one could traditionally only measure one of these images.[64] In te-pCASL only the labeling is adjusted compared to standard pCASL. Customization of the sequence with vascular crushing and background suppression is possible. Whereas in standard pCASL the background suppression pulses are performed during the post-labeling delay, in te-pCASL these inversion pulses (slab-selective in this case) can be applied at any time during the labeling, with a slight break in the labeling block for optimal timing of the pulses or in-between blocks with the timing adapted accordingly. To preserve the ASL signal, some modifications need to be made to the labeling scheme: the label and control condition are switched after the inversion pulse.[65]
Furthermore, any type of read-out can be added to the labeling sequence. For example to enable higher sampling rates of the signal-time curve read outs with multi slice, multi echo and even Look Locker could be used.

T2 Relaxation Under Spin Tagging pCASL

With the building block principle of ASL, not only are many variations possible for the labeling or the readout, but also adaptations are possible during the waiting time in-between those elements. **T_2 Relaxation Under Spin Tagging** (TRUST) pCASL is an example of such an approach, which enables the determination of the vascular compartment where the labeled spins reside at the moment of the readout based upon the T_2 of the label.[45] After labeling, just before imaging, a series of non-slice-selective T_2-preparation pulses are inserted into the PLD.[66] Images are acquired with several effective echo times at multi PLDs and the signal can be fitted to a monoexponential model to estimate the T_2-value. Water spins have characteristic T_2-values at 3T in the arterial, tissue and venous compartment of 160 ms (at a hematocrit of 42%) , 50 ms (at an oxygenation level of 60%)[67] and 90 ms,[68] respectively. Originally, TRUST was used to estimate the T_2 of blood signal in superior sagittal sinus,[69, 70] which was subsequently converted into venous oxygenation via a calibration plot. [71]

Regional perfusion imaging

Regional perfusion imaging (RPI) enables assessment of the perfusion territories of the major cerebral arteries, as shown in figure 5.[72] By switching gradients the labeling efficiency within the labeling plane is varied in a spatially differentiating manner over multiple acquisitions, so that using signal clustering the flow territories of left internal carotid artery (ICA), right ICA and basilar artery can be distinguished. This planning-free approach is called **vessel-encoded pCASL (VE-pCASL)** and is demonstrated to be robust.[73] VE-pCASL has the drawback that the labeling efficiency varies spatially for all arteries at the same time and voxels are designated to a single perfusion territory afterwards, although more advanced post-processing approaches do enable the detection of mixed-perfusion territories.[74]

Another approach is **superselective pCASL** which allows the imaging of a single perfusion territory by using additional time-varying gradients to enable labeling of individual arteries. The positioning of the labeling spot in super-selective pCASL may require more accurate planning.[73]
The perfusion territories of vessel encoded and super-selective pCASL-RPI agree reasonably well. Mismatches can be explained by the poorer capabilities of VE-pCASL to detect mixed perfusion or by accidental labeling of an extra vessel with a lower efficiency by super-selective pCASL.

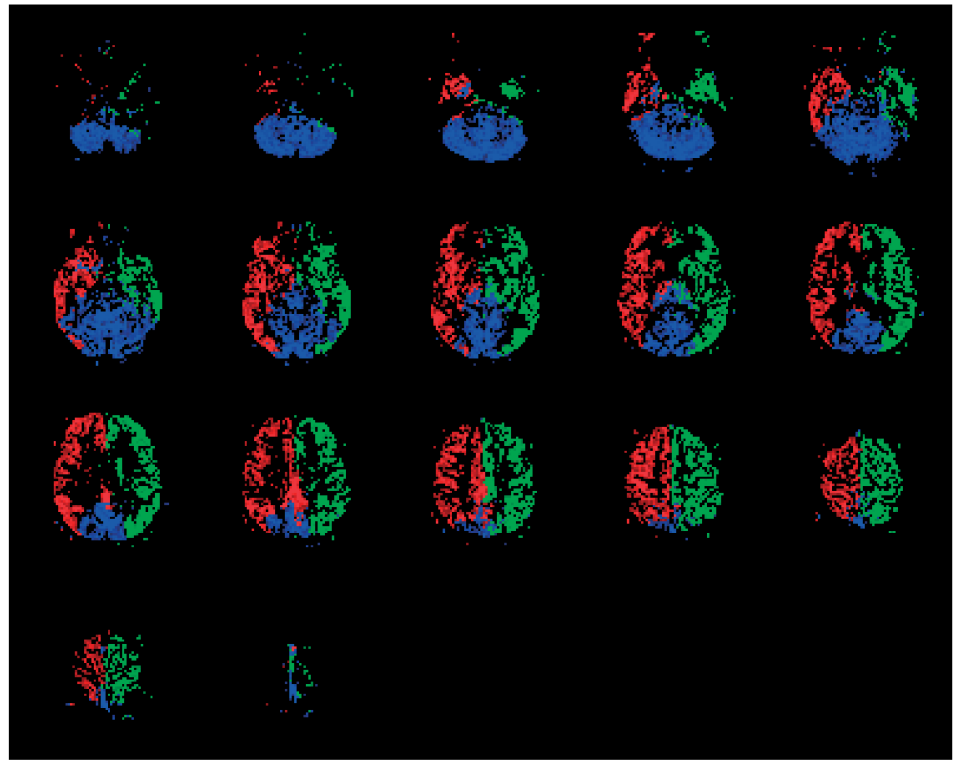

Figure 5 Example of regional perfusion maps, showing the flow territory of the right ICA in red, of the left ICA in green and of the basilar artery in blue.

References

1. Hart LA. How the Brain Works: A New Understanding of Human Learning, Emotion, and Thinking: Basic Book; 1975.
2. Mozaffarian D, Benjamin EJ, Go AS, et al. Heart Disease and Stroke Statistics—2015 Update: A Report From the American Heart Association. Circulation. 2015;131(4):e29-e322.
3. Saver JL. Time Is Brain—Quantified. Stroke. 2006;37(1):263-266.
4. Powers WJ. Cerebral hemodynamics in ischemic cerebrovascular disease. Ann Neurol. 1991;29(3):231-240.
5. van Beek AH, Claassen JA, Rikkert MGO, et al. Cerebral Autoregulation: An Overview of Current Concepts and Methodology with Special Focus on the Elderly J Cereb Blood Flow Metab. 2008;28(6):1071-1085.
6. Nemoto EM, Yonas H, Chang Y. Stages and Thresholds of Hemodynamic Failure. Stroke. 2003;34(1):2-3.
7. Mintun MA, Raichle ME, Martin WRW, et al. Brain Oxygen Utilization Measured with O-15 Radiotracers and Positron Emission Tomography. Journal of Nuclear Medicine. 1984;25(2):177-187.
8. Villringer A, Rosen BR, Belliveau JW, et al. Dynamic imaging with lanthanide chelates in normal brain: contrast due to magnetic susceptibility effects. Magn Reson Med. 1988;6(2):164-174.
9. Østergaard L. Principles of cerebral perfusion imaging by bolus tracking. J Magn Reson Imaging. 2005;22(6):710-717.
10. Paldino MJ, Barboriak DP. Fundamentals of Quantitative Dynamic Contrast-Enhanced MR Imaging. Magn Reson Imaging Clinics of North America. 2009;17(2):277-289.
11. Tofts PS, Brix G, Buckley DL, et al. Estimating kinetic parameters from dynamic contrast-enhanced t1-weighted MRI of a diffusable tracer: Standardized quantities and symbols. J Magn Reson Imaging. 1999;10(3):223-232.
12. Williams DS, Detre JA, Leigh JS, et al. Magnetic resonance imaging of perfusion using spin inversion of arterial water. Proc Natl Acad Sci USA. 1992;89:212-216.
13. Parkes LM, Tofts PS. Improved accuracy of human cerebral blood perfusion measurements using arterial spin labeling: accounting for capillary water permeability. Magn Reson Med. 2002;48(1):27-41.
14. Zhou J, Wilson DA, Ulatowski JA, et al. Two-compartment exchange model for perfusion quantification using arterial spin tagging. J Cereb Blood Flow Metab. 2001;21:440–455.
15. St Lawrence KS, Frank JA, McLaughlin AC. Effect of restricted water exchange on cerebral blood flow values calculated with arterial spin tagging a theoretical investigation Magn Reson Med. 2000 44:440-449.
16. St Lawrence KS, Owen D, Wang DJ. A two-stage approach for measuring vascular water exchange and arterial transit time by diffusion-weighted perfusion MRI. Magn Reson Med. 2012;67(5):1275-1284.
17. Detre JA, Leigh JS, Williams DS, et al. Perfusion imaging. Magn Reson Med. 1992;23:37-45.
18. Alsop DC, Detre JA, Golay X, et al. Recommended implementation of arterial spin-labeled perfusion MRI for clinical applications: A consensus of the ISMRM perfusion study group and the European consortium for ASL in dementia. Magn Reson Med. 2015;73(1):102–116.
19. Wang J, Alsop DC, Li L, et al. Comparison of quantitative perfusion imaging using arterial spin labeling at 1.5 and 4.0 Tesla. Magn Reson Med. 2002;48(2):242-254.
20. Pruessmann KP, Weiger M, Scheidegger MB, et al. SENSE: sensitivity encoding for fast MRI. Magn Reson Med. 1999;42(5):952-962.
21. Griswold MA, Jakob PM, Heidemann RM, et al. Generalized autocalibrating partially parallel acquisitions (GRAPPA). Magn Reson Med. 2002;47(6):1202-1210.
22. Edelman RR, Siewert B, Darby DG, et al. Mapping Flow and Functional Localization with Echo-planar MR Imaging and Signal Targeting Radio Frequency. Radiology. 1994;192:513-520.

23. Detre JA, Samuels OB, Alsop D, et al. Noninvasive magnetic resonance imaging evaluation of cerebral blood flow with acetazolamide challenge in patients with cerebrovascular stenosis. J Magn Reson Imaging. 1999 10:870-875.
24. Kim S-G. Quantification of relative cerebral blood flow change by flow-sensitive alternating inversion recovery (FAIR) technique: Application to functional mapping. Magn Reson Med. 1995;34(3):293-301.
25. Helpern JA, Branch CA, Yongbi MN, et al. Perfusion imaging by un-inverted flow-sensitive alternating inversion recovery (UNFAIR). J Magn Reson Imaging. 1997;15(2):135-139.
26. Zhou J, Mori S, van Zijl P. FAIR excluding radiation damping (FAIRER). Magn Reson Med. 1998;40(5):712-719.
27. Mai VM, Berr SS. MR perfusion imaging of pulmonary parenchyma using pulsed arterial spin labeling techniques: FAIRER and FAIR. J Magn Reson Imaging. 1999;9(3):483-487.
28. Tanabe JL, Yongbi M, Branch C, et al. MR perfusion imaging in human brain using the UNFAIR technique. J Magn Reson Imaging. 1999;9(6):761-767.
29. Lai S, Wang J, Jahng G-H. FAIR exempting separate T1 measurement (FAIREST): a novel technique for online quantitative perfusion imaging and multi-contrast fMRI. NMR in Biomed. 2001;14(7-8):507-516.
30. Li X, Sarkar SN, Purdy DE, et al. Improved quantification of brain perfusion using FAIR with active suppression of superior tagging (FAIR ASST). J Magn Reson Imaging. 2011;34(5):1037-1044.
31. Edelman RR, Siewert B, Adamis M, et al. Signal targeting with alternating radiofrequency (STAR) sequences: Application to MR angiography. Magn Reson Med. 1994;31(2):233-238.
32. Chen Q, Siewert B, Bly BM, et al. STAR-HASTE: Perfusion imaging without magnetic susceptibility artifact. Magn Reson Med. 1997;38(3):404-408.
33. Edelman RR, Chen Q. EPISTAR MRI: multislice mapping of cerebral blood flow. Magn Reson Med. 1998;40(6):800-805.
34. Golay X, Petersen ET, Hui F. Pulsed star labeling of arterial regions (PULSAR): a robust regional perfusion technique for high field imaging. Magn Reson Med. 2005;53(1):15-21.
35. Petersen ET, Lim T, Golay X. Model-free arterial spin labeling quantification approach for perfusion MRI. Magn Reson Med. 2006;55(2):219-232.
36. Golay X, Stuber M, Pruessmann KP, et al. Transfer insensitive labeling technique (TILT): application to multislice functional perfusion imaging. J Magn Reson Imaging. 1999;9(3):454-461.
37. Hendrikse J, Lu H, van der Grond J, et al. Measurements of cerebral perfusion and arterial hemodynamics during visual stimulation using TURBO-TILT. Magn Reson Med. 2003;50(2):429-33.
38. Jahng GH, Zhu XP, Matson GB, et al. Improved perfusion-weighted MRI by a novel double inversion with proximal labeling of both tagged and control acquisitions. Magn Reson Med. 2003;49(2):307-314.
39. Wong EC, Buxton RB, Frank JA. Quantitative imaging of perfusion using a single subtraction (QUIPSS and QUIPSS II). Magn Reson Med. 1998;39:702-708.
40. Alsop DC, Detre JA. Multisection cerebral blood flow MR imaging with continuous arterial spin labeling. Radiology. 1998;208(2):410-416.
41. Dai W, Garcia D, de Bazelaire C, et al. Continuous flow-driven inversion for arterial spin labeling using pulsed radio frequency and gradient fields. Magn Reson Med. 2008;60(6):1488-1497.
42. Wu WC, Fernandez-Seara M, Detre JA, et al. A theoretical and experimental investigation of the tagging efficiency of pseudocontinuous arterial spin labeling. Magn Reson Med. 2007;58(5):1020-1027.
43. Garcia DM, de Bazelaire C, Alsop D. Pseudo-continuous Flow Driven Adiabatic Inversion for Arterial Spin Labeling. Proc. Intl. Soc. Mag. Reson. Med. 2005.
44. Ahlgren A, Wirestam R, Petersen ET, et al. Perfusion quantification by model-free arterial spin labeling using nonlinear stochastic regularization deconvolution. Magn Reson Med. 2013;70(5):1470-1480.
45. Liu P, Uh J, Lu H. Determination of spin compartment in arterial spin labeling MRI. Magn Reson Med. 2011;65(1):120-127.

46. Golay X, Hendrikse J, Lim T. Perfusion imaging using arterial spin labeling. topics in Magnetic Resonance Imaging. 2004;15:10-27.
47. Gonzalez-At JB, Alsop D, Detre JA. Cerebral perfusion and arterial transit time changes during task activation determined with continuous arterial spin labeling. Magn Reson Med. 2000 43:739–746.
48. Dai W, Robson PM, Shankaranarayanan A, et al. Reduced resolution transit delay prescan for quantitative continuous arterial spin labeling perfusion imaging. Magn Reson Med. 2012;67(5):1252-1265.
49. Garcia DM, Duhamel G, Alsop DC. Efficiency of inversion pulses for background suppressed arterial spin labeling. Magn Reson Med. 2005;54(2):366-372.
50. Maleki N, Dai W, Alsop DC. Optimization of background suppression for arterial spin labeling perfusion imaging. MAGMA. 2012;25(2):127-33.
51. St Lawrence KS, Frank JA, Bandettini PA, et al. Noise reduction in multi-slice arterial spin tagging imaging. Magn Reson Med. 2005;53(3):735-738.
52. Ye FQ, Frank JA, Weinberger DR, et al. Noise reduction in 3D perfusion imaging by attenuating the static signal in arterial spin tagging (ASSIST). Magn Reson Med. 2000;44:92–100.
53. Barbier E, Lamalle L, Décorps M. Methodology of brain perfusion imaging. 2001.
54. Jahng GH, Weiner MW, Schuff N. Improved arterial spin labeling method Applications for measurements of cerebral blood flow in human brain at high magnetic field MRI. Medical Physics. 2007;34(11):4519–4525.
55. Günther M, Bock M, Schad LR. Arterial spin labeling in combination with a look-locker sampling strategy: Inflow turbo-sampling EPI-FAIR (ITS-FAIR). Magn Reson Med. 2001;46(5):974-984.
56. Look DC, Locker DR. Time Saving in Measurement of NMR and EPR Relaxation Times. Review of Scientific Instruments. 1970;41(2):250-251.
57. Oshio K, Feinberg DA. GRASE (Gradient-and Spin-Echo) imaging: A novel fast MRI technique. Magn Reson Med. 1991;20(2):344-349.
58. Fernandez-Seara MA, Wang Z, Wang J, et al. Continuous arterial spin labeling perfusion measurements using single shot 3D GRASE at 3 T. Magn Reson Med. 2005;54(5):1241-1247.
59. Mutsaerts HJMM, Steketee RME, Heijtel DFR, et al. Inter-Vendor Reproducibility of Pseudo-Continuous Arterial Spin Labeling at 3 Tesla. PLoS ONE. 2014;9(8):e104108.
60. Wong EC, Cronin M, Wu WC, et al. Velocity-selective arterial spin labeling. Magn Reson Med. 2006;55(6):1334-1341.
61. Qiu D, Straka M, Zun Z, et al. CBF measurements using multidelay pseudocontinuous and velocity-selective arterial spin labeling in patients with long arterial transit delays: comparison with xenon CT CBF. J Magn Reson Imaging. 2012;36(1):110-119.
62. Wu WC, Wong EC. Feasibility of velocity selective arterial spin labeling in functional MRI. J Cereb Blood Flow Metab. 2007;27(4):831-838.
63. Gunther M. Encoded Continuous Arterial Spin Labeling. Workshop on Cerebral Perfusion and Brain Function: Novel Techniques and Applications; 2007; Salvador da Bahia, Brazil
64. Dai W, Shankaranarayanan A, Alsop DC. Volumetric measurement of perfusion and arterial transit delay using hadamard encoded continuous arterial spin labeling. Magn Reson Med. 2013;69(4):1014-1022.
65. Maleki N, Dai W, Alsop DC. Optimization of background suppression for arterial spin labeling perfusion imaging. MAGMA. 2012;25(2):127-133.
66. Brittain JH, Hu BS, Wright GA, et al. Coronary Angiography with Magnetization-Prepared T2 Contrast. Magn Reson Med. 1995;33(5):689-696.
67. Chen JJ, Pike GB. Human whole blood T2 relaxometry at 3 Tesla. Magn Reson Med. 2009;61(2):249-154.
68. Lu H, Nagae-Poetscher LM, Golay X, et al. Routine clinical brain MRI sequences for use at 3.0 Tesla. J Magn Reson Imaging. 2005;22(1):13-22.
69. Liu P, Dimitrov I, Andrews T, et al. Multisite Evaluations of a T2-Relaxation-Under-Spin-Tagging (TRUST) MRI Technique to Measure Brain Oxygenation. Magn Reson Med. 2016;75(2):680-687.

70. Lu H, Ge Y. Quantitative evaluation of oxygenation in venous vessels using T2-Relaxation-Under-Spin-Tagging MRI. Magn Reson Med. 2008;60(2):357-363.
71. Lu H, Xu F, Grgac K, et al. Calibration and validation of TRUST MRI for the estimation of cerebral blood oxygenation. Magn Reson Med. 2012;67(1):42-49.
72. Hendrikse J, van der Grond J, Lu H, et al. Flow territory mapping of the cerebral arteries with regional perfusion MRI. Stroke. 2004;35(4):882-777.
73. Gevers S, Bokkers RP, Hendrikse J, et al. Robustness and Reproducibility of Flow Territories Defined by Planning-Free Vessel-Encoded Pseudocontinuous Arterial Spin-Labeling. Am J of Neurorad. 2012;33(2):E21-E25.
74. Wong EC. Vessel-encoded arterial spin-labeling using pseudocontinuous tagging. Magn Reson Med. 2007;58:1086–1091.

2

Acceleration selective arterial spin labeling

S Schmid
E Ghariq
WM Teeuwisse
A Webb
MJP van Osch

Magnetic resonance in medicine, 2014; 71(1): 191-199

Abstract

In this study a new arterial spin labeling (ASL) method with spatially non-selective labeling is introduced, based on the acceleration of flowing spins, which is able to image brain perfusion with minimal contamination from venous signal. This method is termed acceleration selective ASL (AccASL) and resembles velocity selective ASL (VSASL), with the difference that AccASL is able to discriminate between arterial and venous components in a single preparation module due to the higher acceleration on the arterial side of the microvasculature, whereas VSASL cannot make this distinction unless a second labeling module is used.

AccASL exploits the principles of acceleration encoded magnetic resonance angiography by employing motion sensitizing gradients in a T_2-preparation module. This method is demonstrated in healthy volunteers for a range of cut-off accelerations. Additionally, AccASL is compared with VSASL and pseudo-continuous ASL (pCASL), and its feasibility in functional MRI is demonstrated.

Compared with VSASL with a single labeling module, a strong and significant reduction in venous label is observed. The resulting signal-to-noise ratio is comparable to pCASL and robust activation of the visual cortex is observed.

The use of an acceleration dependent preparation module for ASL with spatially non-selective labeling was demonstrated to be able to image brain perfusion without contamination from venous signal.

Introduction

Arterial spin labeling (ASL) techniques can be used to quantify local tissue perfusion noninvasively.[1, 2] Conventional ASL methods tag arterial blood spins by saturation or inversion in a plane proximal to the imaging region. After a delay, the post labeling delay (PLD), a label image is acquired. This TI is chosen approximately equal to the T_1 of blood for cerebral perfusion imaging, representing a compromise between loss of the label due to longitudinal (T_1) relaxation and a transport time long enough for the labeled blood to reach the microvascular bed.[3] Subsequently, the sequence is repeated without labeling, thereby obtaining the so-called control image. Subtraction of the label image from the control image results in a perfusion-weighted image, which reflects solely the magnetization of the inflowing tagged spins without contamination from static tissue. Multiple interleaved averages of the label and control sequence are required to gain sufficient signal-to-noise ratio (SNR).

A major confound of conventional ASL techniques is that a significant amount of label is lost due to T_1-relaxation in the time it takes for the blood to flow from the labeling to the imaging plane, the so-called transit time. Furthermore, in several pathological brain conditions, due to slow or collateral flow the label relaxes almost completely before imaging, leading to severe underestimation of cerebral blood flow (CBF). Even in normal volunteers the variation in transit time can be up to hundreds of milliseconds across a single slice.[4]

Recently, a technique called velocity selective arterial spin labeling (VSASL) was introduced, in which spins are tagged based on flow velocity rather than spatial localization.[5-7] This enables labeling within the imaging region where perfusion is measured. By generating the label much closer to the capillaries, smaller and more uniform transit delays are obtained and therefore VSASL can provide (semi-)quantitative CBF maps even under slow and collateral flow conditions.[8]

A drawback of VSASL with a single velocity-selective labeling module (single VSASL) is its inability to discriminate between arterial and venous components of flow. All spins that flow faster than the cut-off velocity (V_C) are labeled, irrespective of whether these are located in arterial or venous blood. The use of a second velocity-selective labeling module just before imaging (dual VSASL) can exclude the venous components, since accelerating spins will be suppressed.[6] This approach suffers, however, from a reduced SNR by limiting the labeling to spins that decelerate to a velocity below V_C before the second labeling module, as well as due to increased T_2-relaxation and diffusion-weighting (DW) due to the second labeling module.

More recently, it has been shown in magnetic resonance angiography (MRA) that acceleration-encoded imaging can selectively image the arteries, without contamination from venous signal.[9] Acceleration-dependent preparation differs from a velocity-selective approach in that it does not affect the magnetization from spins flowing at a constant velocity, but dephases spins that are accelerating or decelerating.[10] In the vascular tree the average velocity of the spins decreases from the arteries towards the capillaries, after which their average velocity increases only slightly while flowing to the veins. Pulsatility is known to be higher in the

arteries than in the veins, providing a second origin for the differentiation between arterial and venous blood by employing acceleration encoding. Moreover, the tortuosity of the vessels, and especially of the capillaries, is a third origin of labeling. When the vessel orientation changes with respect to the acceleration encoding direction, there will be incomplete refocusing of the magnetization.

The aim of this study is to introduce a new ASL method, which is able to image brain perfusion without transit delay problems or contamination from venous or cerebral spinal fluid (CSF) signal, based on the principles of acceleration encoded MRA. The use of such an acceleration-dependent preparation module for ASL is demonstrated in healthy volunteers. This new method, referred to as Acceleration selective ASL (AccASL), is examined with different cut-off acceleration encodings, obtained by varying the motion-sensitizing gradients. In addition, AccASL is compared with VSASL and a conventional spatially selective ASL method, and the feasibility of AccASL in functional MRI (fMRI) is demonstrated.

Methods

Acceleration selective labeling module

The labeling module of AccASL resembles VSASL in the sense that it combines spatially non-selective hard 90° pulses with a pair of identical adiabatic 180° refocusing pulses, hereby correcting for phase shifts due to inhomogeneities of the magnetic field and chemical shifts.[11] Motion-sensitizing gradients (MSG) placed in-between these RF-pulses can be used to dephase the magnetization of flowing spins, whereas the polarity of these gradients determines whether flowing spins with constant velocity (VSASL) or accelerating (AccASL) spins are affected. A four-gradient-pulse scheme has been used to reduce eddy-current effects for VSASL.[12] The difference between the velocity sensitive and acceleration sensitive sequence is in the sign of the second and fourth gradient as shown in the schematic representation of the labeling modules in figure 1. Spins with a flow velocity or acceleration above a cut-off velocity (V_C) or cut-off acceleration (A_C), respectively, are dephased: both parameters are defined as to correspond to a phase change of π.

The effective first-gradient moment (m_1) of the velocity-sensitizing sequence can be calculated to be $m_1 = G \cdot \Delta \cdot \delta$, with G the amplitude of the gradients, δ the gradient duration and Δ the time between 90° RF-pulses (figure 1). By varying these parameters the cut-off velocity can be set, according to $V_C = \pi/(\gamma \cdot m_1)$, where γ is the gyromagnetic ratio. Penetrating arterioles exhibit a flow velocity of 1-2 cm/s in human brain [13] and have a laminar flow as their dominant flow pattern, which makes VSASL feasible.[14]

The acceleration-sensitizing sequence has an effective first-gradient moment of zero, giving no velocity sensitization, but a second-gradient moment (m_2) of $m_2 = 4 \cdot G \cdot \Delta \cdot \delta$. The relation to the cut-off acceleration is $A_C = 2 \cdot \pi/(\gamma \cdot m_2)$.[9] Deceleration could be considered as negative acceleration and is targeted with this sequence equally well.

It should be noted that the gradients not only encode motion, but also impart a diffusion sensitivity, which becomes substantial for higher moments. This diffusion sensitivity, expressed as the b-value, is dependent on the MSG parameters and scales with the square of G and δ and linearly with Δ.

MR experiments

A total of 12 healthy volunteers (4 male and 8 female, age 20-38 years) participated in this study and informed written consent was obtained from each participant. This study was part of a project for protocol development as approved by local Institutional research board (IRB). First, the influences of A_C on the signal intensity and the spatial distribution of the labeled blood were evaluated. Second, AccASL was compared with single and dual VSASL and pseudo-continuous ASL (pCASL) with respect to SNR and contamination of venous and CSF signal; the latter being introduced by diffusion weighting (DW). Finally, the feasibility of AccASL for brain activation studies was tested.

All scans were performed on a 3T scanner (Philips Healthcare, Best, The Netherlands) using a 32 channel head-coil with 17 slices acquired at a 2.75 x 2.75 x 7 mm^3 resolution (multi-slice single-shot 2D echo planar imaging). The field of view (FOV) was 220^2 mm^2 and a SENSE-factor of 2.5 was used. Spectral Presaturation Inversion Recovery (SPIR) was performed to suppress the lipid signal.

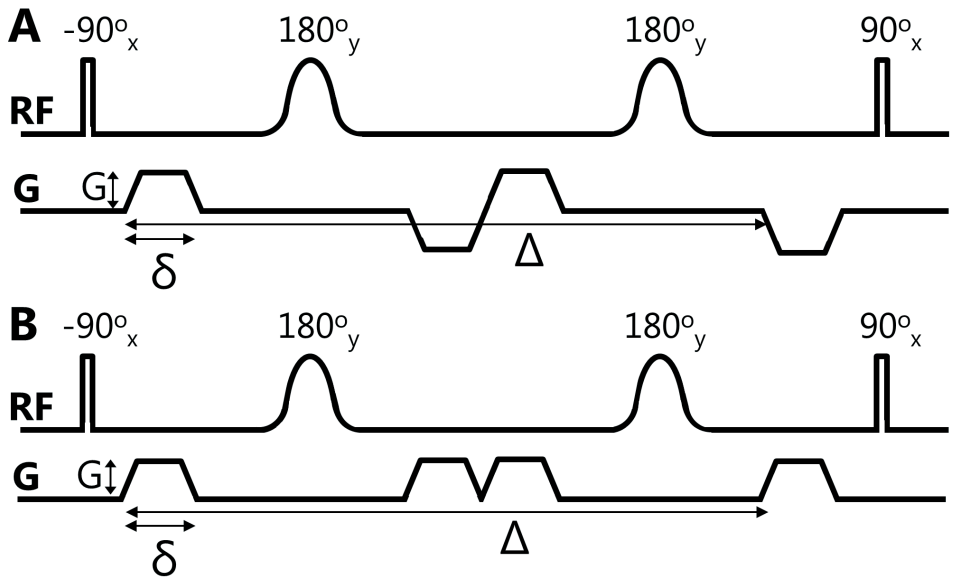

Figure 1 Schematic overview of the labeling module with velocity-sensitizing (A) and acceleration-sensitizing gradients (B), where G is the gradient amplitude, δ is the duration of the gradient, Δ is the time between the 90° RF-pulses. During the control condition, no motion sensitizing gradients are used.

Cut-off acceleration

To evaluate the influence of the value of A_C on the signal intensity and the appearance of the perfusion map, AccASL images with a range of different A_C were acquired. In 4 volunteers (2 male, 2 female, age 20-38 years) ten scans were performed in a random order with different values of G, δ and Δ, as shown in Table 1 with their corresponding acceleration-encoding parameters. In a scan time of approximately 4.5 min a total of 30 averages of both label and control images were obtained.

For analysis purposes, a high resolution 3D T_1-weighted image was obtained with a voxel size of 1.1 mm^3. A total of 200 slices with a FOV of 240 x 188 x 220 mm^3 was acquired in a scan time of circa 2.5 min with TR/TE of 7.6 / 3.5 ms.

By using the Oxford Centre for Functional MRI of the Brain (FMRIB)'s Software Library (FSL) the images were realigned over all dynamics [15, 16] and corrected for motion with Motion Correction FMRIB's Linear Image Registration Tool (MCFLIRT).[17] Subsequently, the time averages were calculated and the ASL-maps were obtained by subtracting the mean label from the mean control images. The ASL-maps were registrated to the T_1-weighted image with FMRIB's Linear Image Registration Tool (FLIRT).[17] The brain was extracted from the T_1-weighted image with the Brain Extraction Tool (BET),[18] after which the regions with grey matter (GM), white matter (WM) and cerebral spinal fluid (CSF) were segmented with FMRIB's Automated Segmentation Tool (FAST).[19] After voxelwise calculation of the SNR from the mean and standard deviation of the ASL signal over the different repeated experiments, these masks were used to calculate the mean SNR in these three specific regions of the ASL-maps.

Comparison to VSASL and pCASL

Next, the properties of the AccASL labeling module were compared with single VSASL, dual VSASL and pCASL labeling. Eight volunteers (3 male, 5 female, age 20-38 years) were scanned for this sub-study. The labeling module parameters of AccASL were G=30 mT/m, δ=1 ms and Δ=30 ms corresponding to an A_C of 2.3 m/s^2.

Single VSASL consisted of one velocity-selective labeling module, which saturated the spins above a V_C of 2 cm/s. For dual VSASL, a second velocity-selective labeling module was added 1500 ms after the first VSASL sequence, just before the imaging module. Labeling module parameters, which determine the velocity-sensitivity, were G=22 mT/m, δ=1 ms and Δ=30 ms.

For AccASL, single VSASL and dual VSASL the labeling delay was set to 1600 ms. Imaging parameters were chosen as previously stated. Background suppression was applied using two adiabatic non-selective inversion pulses at 50 and 1150 ms after labeling to increase the contrast-to-noise ratio (CNR).[20-22] For all three techniques the post acquisition delay, the time between the post-acquisition non-selective saturation and the subsequent labeling module, was set to 2000 ms. Label and control acquisitions were interleaved in time and 30 averages of both image types were obtained. TR/TE was 4272/15 ms and the total scan duration was approximately 4.5 min. Velocity and acceleration encodings were only applied along the slice encoding direction.

In a final comparison pCASL was used as the "conventional" ASL method and consisted of a labeling module of 1650 ms labeling with a 1525 ms delay before multi-slice acquisition with a TR of 3863 ms. Background suppression was applied using two inversion pulses at 1680 and 2760 ms. Total scan duration was approximately 4 min with 30 averages of both label and control images.

For the comparison of the AccASL technique to single VSASL, dual VSASL and pCASL the images were coregistrated to a standard brain with Statistical Parametric Mapping version 8 (SPM8, Matlab, The MathWorks Inc., Natick, MA).

An average CBF-weighted scan was generated from all four coregistrated images and manually thresholded to obtain a GM mask to calculate the ASL signal intensity and SNR within the GM. The SNR of the pCASL-scan was corrected for the shorter total scan time by multiplying by the square root of the relative scan times. Within the ventricles a ROI was manually selected to calculate the mean and standard deviation of the ASL signal in the CSF. In the sagittal sinus nine voxels in the central slice were selected to calculate the venous signal. Mean ROI signal intensities were compared for the four different sequences with a two-way analysis of variance (ANOVA) statistical test using Matlab.

Multiple post-labeling delay times

To get an impression of the changes in the spatial distribution of the label over time, a single slice was imaged with Look-Locker sampling scheme after labeling with an Acc or single VS labeling module in a single volunteer (female, age 22 years). The 16 post-labeling delay times varied from 300 to 3300 ms in steps of 200 ms, TR/TE was 200/14 ms and the Look-Locker flip angle 20°. The other imaging and labeling module parameters were the same as described above. A total of 30 averages was acquired in circa 10 min.

To reconstruct the multi-inflow time ASL-maps, label images were subtracted from the control images and averaged per post-labeling delay time in Matlab. The ASL-maps were corrected for the flip angle used in the Look Locker imaging strategy by multiplying each voxel by $(\cos(\alpha)^{-1})^{n-1}$, where α is the flip angle and n the number of the Look-Locker acquisition. In this way the signal loss due to the excitation pulses is corrected for and the signal intensity will be similar to that as if each scan was acquired sequentially with a 90° flip angle.

Visual stimulation

For mapping of neuronal activation, 70 dynamics of AccASL (total scan time of 10 min) were used to acquire 5 cycles of on- and off-periods with equal duration. Visual stimulation used an 8 Hz yellow and blue radial flashing checkerboard during the on-period and a black background with a white fixation point at the centre during the off-period. Two volunteers (female, age 21-24 years) viewed the projections of the stimulation via a mirror attached to the head coil. The AccASL technique was performed with A_C=2.3 m/s^2, executed with G=30 mT/m, δ=1 ms and Δ=30 ms, and 17 slices were acquired.
To aid the analysis, a Blood Oxygenation Level Dependent (BOLD) scan was acquired for each volunteer with 150 dynamics (TR/TE of 2000/30 ms, total scan time of 5 min) with the same imaging region and voxel-size as the AccASL scan, with the visual stimulation as described above, except that the duration of all blocks was only 30 s.

The fMRI data were analyzed in SPM8 and Matlab. Motion correction was performed on the label and control images from the AccASL data and images of the BOLD data separately. Then the AccASL images were registrated to the BOLD images and all images were smoothed with an 8 mm^3 full-width-half-maximum (FWHM) Gaussian kernel. A threshold on the BOLD activation map was chosen to include only the visual cortex, where the highest activation was found, and these activated voxels from the BOLD data were used to mask the ASL signal from the subtracted control and label images of the AccASL data. The signal was averaged over all voxels within the mask per time point and averaged over the stimulation and rest blocks, respectively.

Table 1 MRI acquisition parameters used for the AccASL experiment with varying motion-sensitizing gradients and their cut-off acceleration and b-values. The diffusion attenuation of the labeling module was calculated with the typical value of apparent diffusion coefficient (D): 0.8 x 10^{-3} mm^2/s for grey matter and 2.5 x 10^{-3} mm^2/s for CSF.

Cut-off acceleration (m/s^2)	Gradient strength (mT/m)	Duration labeling module (ms)	Gradient duration (ms)	b-value (m/s^2)	1-exp(-bD) (%, brain)	1-exp(-bD) (%, CSF)
0.5	30	40	3	22.7	1.80	5.51
1.3	30	60	0.5	0.97	0.077	0.24
1.3	15	60	1	0.96	0.077	0.24
2.3	30	30	1	1.92	0.15	0.48
2.3	15	30	2	1.90	0.15	0.47
3.5	20	30	1	0.85	0.068	0.21
3.5	10	30	2	0.84	0.067	0.21
4.7	15	30	1	0.48	0.038	0.12
7	10	30	1	0.21	0.017	0.053
7	5	30	2	0.21	0.017	0.053

Results

Cut-off acceleration

For all encoded cut-off accelerations (as presented in table 1) a clear WM-GM contrast typical for perfusion images was observed, as shown in figure 2, which shows a typical example of a single volunteer. In the image corresponding to A_C = 0.5 m/s^2 the signal intensity was decreased by a factor-of-four. For the signal from the CSF, the duration between the MSG plays an especially important role. With increasing Δ, and therefore decreasing A_C, the CSF contamination increases in the ventricles and in WM. In general, the mean ASL signal and SNR of the four subjects varied depending on the MSG parameters, as can be seen in figure 3. Lower A_C resulted in more inter-subject variations of the ASL signal in GM, while the standard deviation of the SNR was similar for the whole range of A_C.

Comparison of AccASL to VSASL and pCASL

The properties of AccASL were tested and compared with single VSASL, dual VSASL and pCASL. The ASL-maps in a single volunteer from the four different ASL methods are shown in figure 4. All maps have the same signal intensity scaling. AccASL and pCASL showed the highest ASL signal in GM, while the lowest signal was observed in the images acquired with dual VSASL.

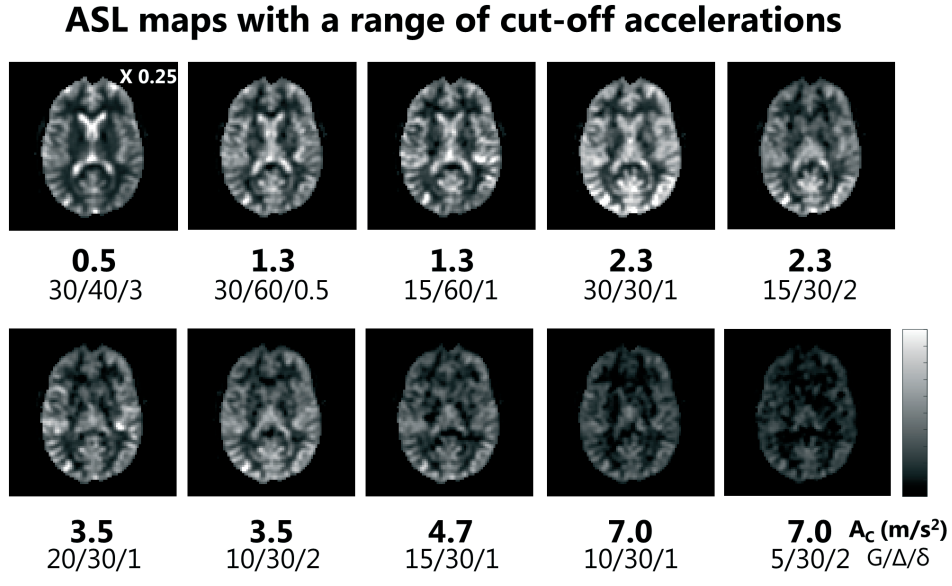

Figure 2 Representative set of single-slice ASL-maps with a range of cut-off accelerations achieved by variation of the acceleration parameters: gradient amplitude, the time between the 90° RF-pulses and the duration of the gradient, described as G/Δ/δ respectively. All images have the same scaling, except the A_C= 0.5 m/s^2, which was scaled to a range four time higher than the others.

These visual observations are confirmed by the results of statistical testing as shown in figure 5, where the mean SNR in GM and the mean ASL signal in CSF and the sagittal sinus are depicted along with a two-way ANOVA statistical comparison. This showed that the SNR for single VSASL in GM was significantly lower ($p<0.05$) compared with AccASL and the SNR for dual VSASL in GM was significantly lower ($p<0.05$) compared with all other methods. The ASL signal in the CSF and the sagittal sinus was significantly higher ($p<0.05$) for single VSASL compared with the other methods; no significant differences were observed between AccASL, pCASL and dual VSASL for either region.

Multiple post-labeling delay times

In figure 6 the ASL-maps acquired with AccASL and single VSASL are shown for the 16 post labeling delay times. In the ASL-maps at the first time points the label mainly resides in arteries

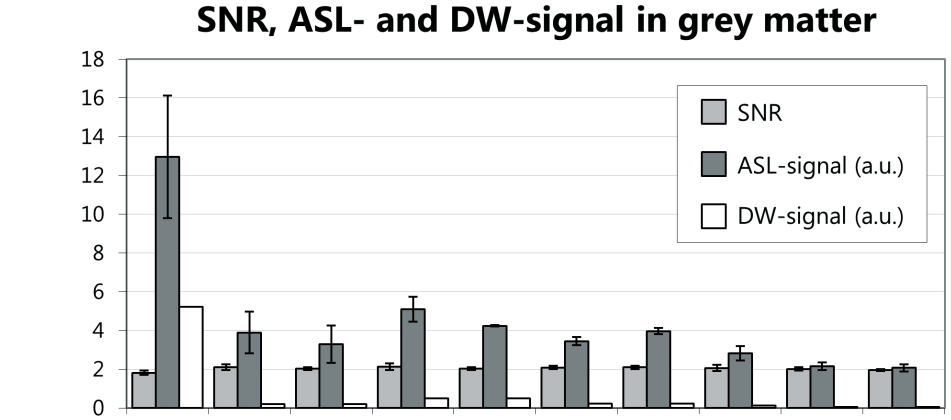

A_C (m/s²)	0.5	1.3	1.3	2.3	2.3	3.5	3.5	4.7	7.0	7.0
G (mT/m)	30	30	15	30	15	20	10	15	10	5
Δ (ms)	40	60	60	30	30	30	30	30	30	30
δ (ms)	3	0.5	1	1	2	1	2	1	1	2
DW-signal (%)	30	5	4	8	9	5	4	4	2	2

Figure 3 The mean SNR (left bar), ASL signal (middle bar) and the signal which theoretically could be attributed to diffusion weighting (DW-signal, right bar) in grey matter for a range of cut-off accelerations achieved by different contributions of acceleration encoding parameters. A grey matter mask was used to extract the voxels of interest. The error bars indicate the standard deviation of four subjects. The SNR was relatively constant for all A_Cs. The percentage of ASL signal attributable to the level of diffusion attenuation from the labeling pulses is shown underneath the acceleration encoding parameters.

and GM for AccASL, but also in large veins. During the first post-labeling delay times for the ASL-maps acquired with single VSASL the signal is especially visible in arteries and veins, and lower signal intensity can be observed in GM. The label reaches the GM at an earlier time point for AccASL and is visible with a higher intensity compared with single VSASL. While the signal intensity in the sagittal sinus in the AccASL-maps decreases over time, and vanishes around 2 s and increases again around 2.5 s, the signal in the sagittal sinus stays present at a high intensity level for single VSASL at all post labeling delay times.

Visual stimulation

The average signal time curve of the activated voxels is shown in figure 7. These curves show a block pattern with an increase of 29% in signal during the visual stimuli compared to the baseline ASL signal during rest.

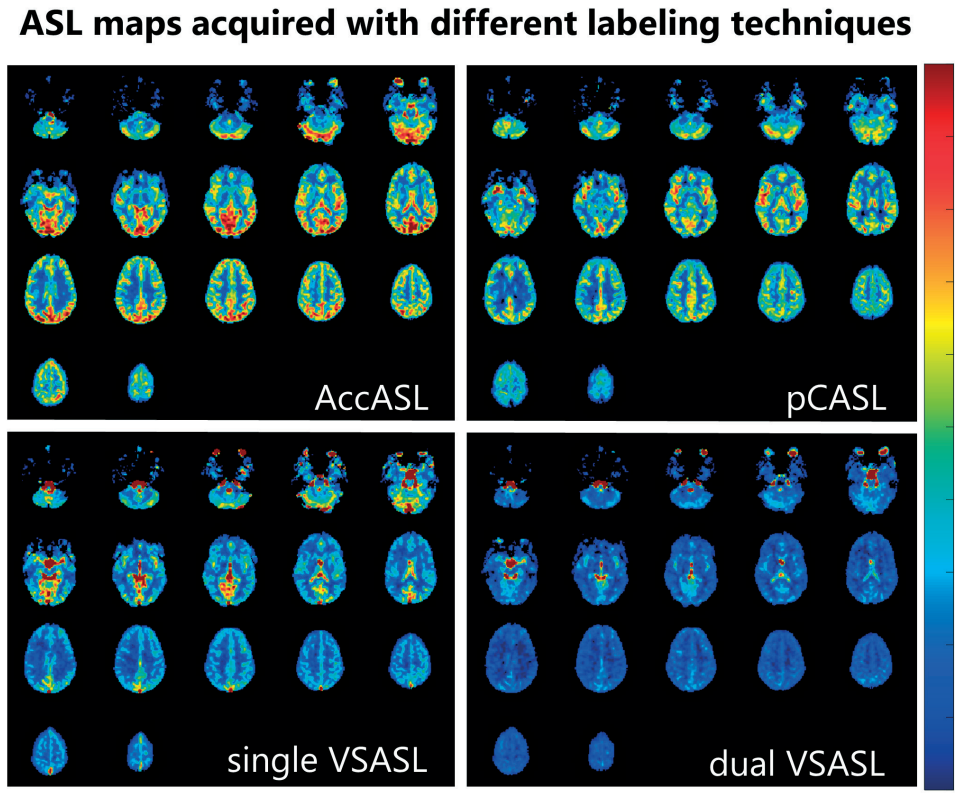

Figure 4 Representative ASL-maps averaged across 70 label/control pair images in a single volunteer. From top left clockwise: AccASL, pCASL, dual VSASL and single VSASL. Identical color scales were used for the four sets of images. The acceleration encoding was A_C= 2.3 m/s² for AccASL and the velocity encoding was V_C= 2 cm/s for both VSASL methods.

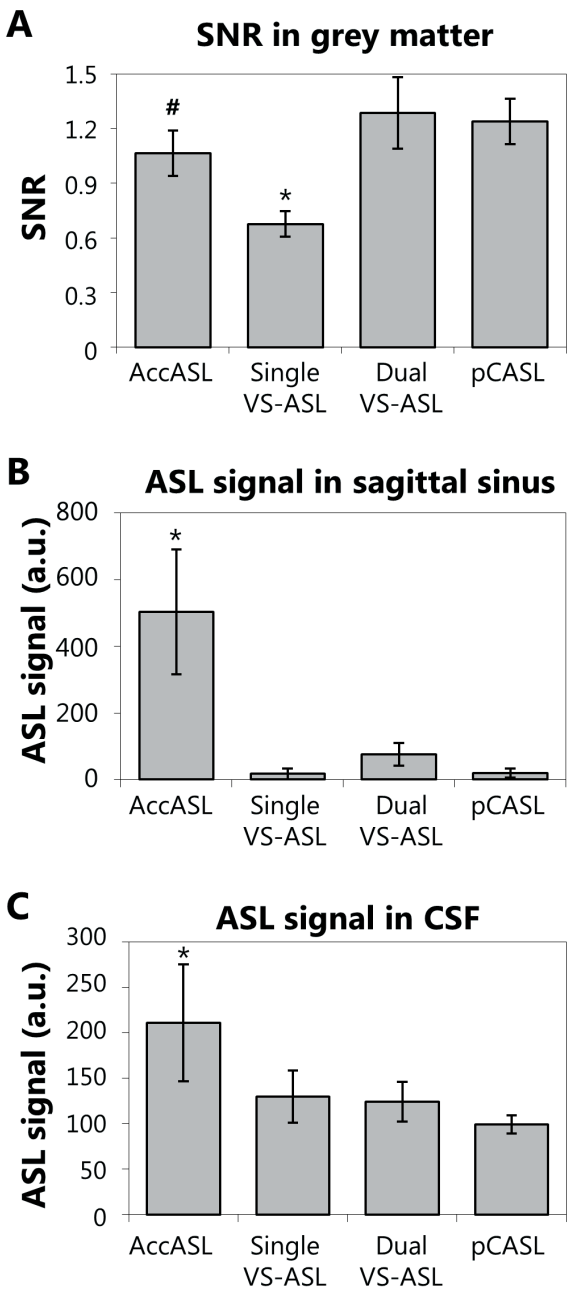

Figure 5 Mean SNR in grey matter (A), ASL signal in sagittal sinus (B) and ASL signal in CSF (C) for AccASL, single VSASL, dual VSASL and pCASL, where # represents $p<0.05$ between single VSASL and AccASL, and * represents $p<0.05$ between this method and all other methods. The acceleration encoding was A_C= 2.3 m/s^2 for AccASL and the velocity encoding was V_C= 2 cm/s for both VSASL methods. The error bars indicate the standard deviation of four subjects.

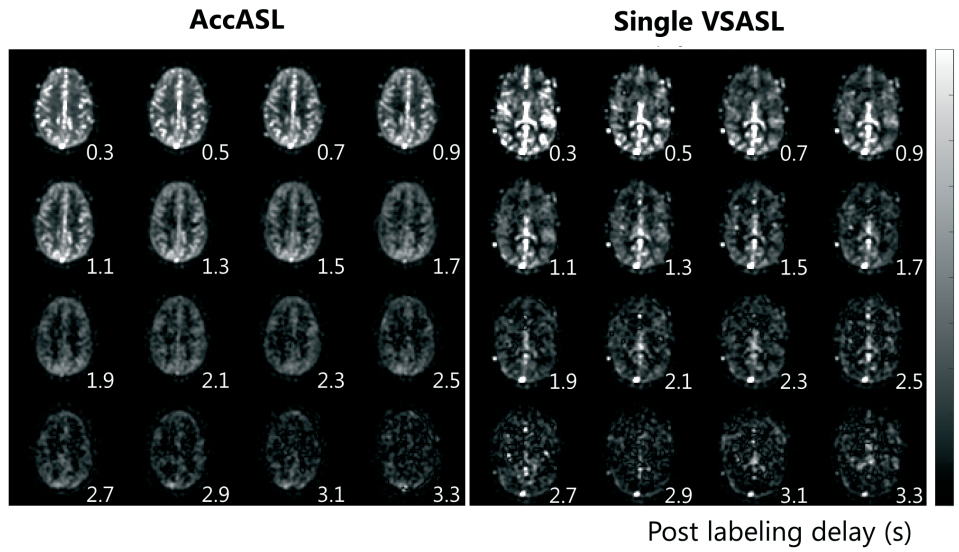

Figure 6 Single-slice AccASL (left) and single VSASL (right) ASL-maps at multiple post labeling delay times with a 200 ms interval, acquired with a Look-Locker sampling scheme. The acceleration encoding was A_C= 2.3 m/s^2 for AccASL and the velocity encoding was V_C= 2 cm/s for the VSASL methods.

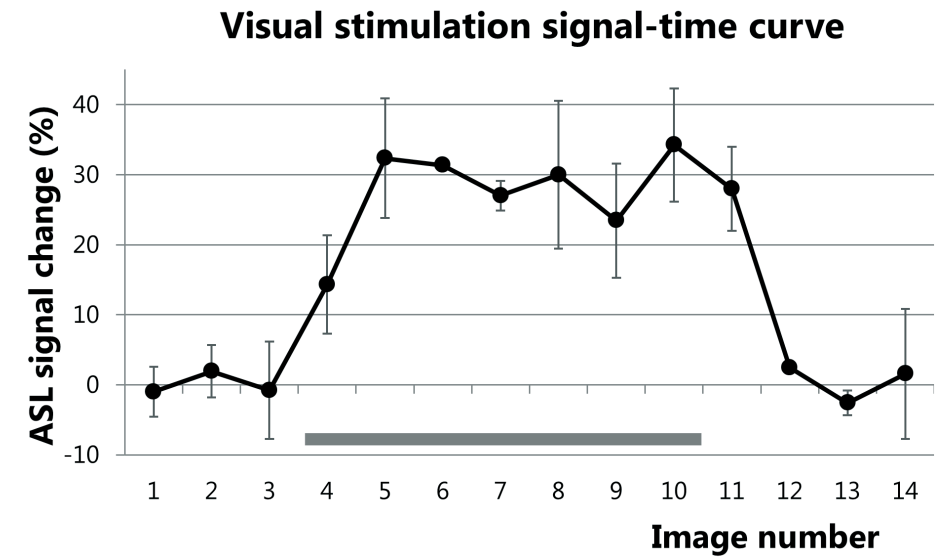

Figure 7 The signal-time curve detected by AccASL with A_C= 2.3 m/s2 for the visual stimulation fMRI experiment. Only the voxels that showed activation in the BOLD images are included. Rest and visual stimulation were altered in periods of 7 label and control pair images. The curve shows the mean signal of the included voxels averaged over the five different rest and activation periods. The error bars indicate the standard error of means of two subjects. The increase in signal in the activated region during the visual stimuli compared to the baseline signal during rest is approximately 29%. The grey line indicates the duration of the visual stimulus (1 minute).

Discussion

In this study we have proposed acceleration selection in ASL for labeling the arterial blood compartment within the imaging region without contamination from venous blood or CSF, and this sequence was successfully demonstrated in healthy volunteers to obtain resting-state perfusion maps as well as for fMRI.

By using a method with labeling not based on the spatial position of the spins, but on their acceleration, it was possible to label in the same plane as imaging, similar to VSASL. This creation of the label closer to the capillaries provides shorter and more uniform transit delays compared with traditional ASL, which makes this method theoretically suitable to use under slow or collateral flow conditions. This could also enable the use of shorter post-labeling times, resulting in a higher SNR, since there would be less loss of label through relaxation before it arrives in the microvasculature. However, compared with conventional ASL, where the label is created by inversion of the magnetization, the use of saturation leads to a lower signal difference between the label and control condition, leading to a SNR-penalty of a factor-of-2.

The origin of the label in the blood created by AccASL is the result of at least three different processes. First, the flow velocity in the vessels is not constant, but is fluctuating due to the cardiac cycle. Acceleration-dependent preparation dephases the flowing spins magnetization that are accelerating or decelerating and a pulsatile flow has both of these properties. This characteristic was used previously in MRA to achieve a good artery-vein separation, because blood flow in arteries is known to be more pulsatile than in veins.[9] Second, the general distribution of blood flow velocities over the cerebral vasculature is known to decrease for smaller vessels.[23, 24] In general, closer to the capillaries, the vasculature branches with vessels becoming smaller in diameter, but with the total surface area becoming larger, resulting in a lower blood velocity. Therefore, as the blood flows from the arterial compartment to the capillaries the blood will on average decelerate, while it will accelerate when flowing into the venous compartment. Third, the tortuosity of vessels, for example at bifurcations of vessels or due to branching, but especially at the level of the capillaries, can also be a source of labeling in AccASL. When the directionality of the vessels changes with respect to the acceleration encoding gradient direction, there will not be (complete) refocusing. This introduces some cerebral blood volume (CBV) weighting instead of the signal being only CBF-weighted. Due to the structure of the capillary bed, more label is created compared with VSASL, which can not be targeted to this region, since there is no laminar flow present.[25] In summary, several aspects can result in the creation of label in AccASL, which make it difficult to determine how much label has been created. This makes it challenging to quantify CBF by AccASL at this moment and more research is needed on this topic.

However, AccASL was shown to enable effective labeling of a large part of the arterial vasculature as proven by a similar SNR as compared to pCASL. The ASL signal intensity in GM was found to be comparable to pCASL and significantly higher compared with single and dual VSASL. Even though AccASL and VSASL both create label in the imaging plane, based on blood flow characteristics, it appears that more label is created with AccASL. Moreover, the multi-TI measurements demonstrated that at shorter post-labeling delay times more label was present in the GM of the ASL-maps acquired with AccASL compared with single VSASL. This makes it feasible to reduce the post-labeling delay and thereby improve the time resolution. Furthermore, the GM signal intensity also remained high at the later time points, proving that the label was indeed created in the arterioles and the microvasculature.

Focusing on the venous signal, the AccASL-maps showed a decreasing signal intensity in the sagittal sinus up to 2.5-3 s post-labeling, while for single VSASL a high signal in the sagittal sinus was visible at all post-labeling delay times. Therefore, it appears that only a small signal is created in the venous compartment. This showed that an efficient elimination of venous signal can be accomplished with AccASL: no significant difference in ASL signal in the sagittal sinus was measured between AccASL, dual VSASL and pCASL at a post label delay of 1600 ms, while venous contamination was clearly present in the image acquired with single VSASL. Nevertheless, elimination of the venous signal can be achieved with VSASL by the use of a second labeling module, applied just before imaging. For AccASL a waiting period is not required in order to exclude signal from the venous compartment, since labeling is based on the acceleration/deceleration during the labeling encoding module of typically 30 to 50 ms, while dual VSASL requires 1.0-1.5 s between two velocity-selective labeling modules to allow the spins to decelerate below V_C. Additionally, the use of two labeling modules enables quantification of VSASL, because the temporal width of the labeling function is fixed, i.e. the amount of label created is being controlled. However, the use of a second labeling module in dual VSASL will also diminishes the ASL signal by reduction of the labeling bolus by the second velocity-selective labeling module. Although elimination of the venous signal with AccASL was comparable to that using dual VSASL, in GM the ASL signal was significantly higher for AccASL. In future, the use of a second labeling module in AccASL should be examined to determine if this could make a valuable contribution to the quantification of the AccASL-signal.

In AccASL and both VSASL sequences the same background suppression pulses were used. Nevertheless, the CSF signal was of comparable intensity for AccASL, pCASL and dual VSASL, while it was higher for single VSASL. Therefore, the amount of CSF contamination is not only determined by the background suppression, but also by the labeling sequence. A greater amount of CSF was apparently labeled with single VSASL.

The fMRI study showed that AccASL is able to detect hemodynamic changes associated with neuronal activation. An increase of approximately 30% in signal during the visual stimuli was observed compared with the baseline ASL signal during rest. ASL methods are

in general considered more suitable than BOLD for studying slow variations in brain function over periods greater than a minute, because ASL shows stable noise characteristics over the entire frequency spectrum.[26, 27] Furthermore, ASL-based fMRI has been advocated over BOLD because of improved localization. Vascular space occupancy (VASO) techniques, which are also CBV weighted, improve localization of the activated regions during stimulation in fMRI, although at the cost of a lower SNR.[28] The great advantage compared to conventional ASL techniques, which create label proximal to the image plane, is that with AccASL the label is generated in the same region as where the neuronal activation is located, so the label is created closer to the region where the local blood flow is altered. AccASL has therefore the potential to increase the temporal resolution of CBF-weighted fMRI-techniques. Since the tagging is spatially non-selective, arterial transit time is not a limitation for anatomical coverage.

An artifactual contribution of the AccASL signal is caused by diffusion-weighting, because the motion sensitizing gradients of the labeling module also introduce diffusion sensitivity into the labeling process. The diffusion sensitivity of the sequence is characterized by the b-value and scales with the same parameters that determine the A_C, but whereas the A_C scales linearly with G and δ, the b-value scales quadratically. By varying the gradient parameters, the same A_C can be obtained with different b-values and thus different contaminations by diffusion-weighting. Table 1 indicates how much change in signal intensity due to the use of MSG could theoretically be attributed to diffusion-weighting. To calculate contribution of the diffusion-weighting to the signal, the following formula was used:

$$S/S_0 = \exp(-bD)$$

in which S is the average signal in GM during the label condition, S_0 is the average signal in GM during the control condition, b is the b-value corresponding to the gradient parameters and D=0.0008 mm^2/s for in GM.[29-32] The results from this calculation are shown in figure 3. In this study, a maximum of 9% difference of the ASL signal was observed due to diffusion-weighting, which is within acceptable limits, except for the lowest A_C with a b-value of 22.7 m/s^2, where a 34% difference in ASL signal can be attributed to diffusion-weighting. Similar diffusion-weighting was found for AccASL as compared to VSASL.[7]

Conclusion

In conclusion, the use of an acceleration-dependent preparation module for ASL with spatially non-selective labeling was demonstrated to be able to image brain perfusion without contamination from venous and CSF signal.

References

1. Williams DS, Detre JA, Leigh JS, et al. Magnetic resonance imaging of perfusion using spin inversion of arterial water. Proc Natl Acad Sci USA. 1992;89:212-216.
2. Detre JA, Leigh JS, Williams DS, et al. Perfusion imaging. Magn Reson Med. 1992;23:37-45.
3. Alsop DC, Detre JA. Reduced transit-time sensitivity in noninvasive magnetic resonance imaging of human cerebral blood flow. J Cereb Blood Flow Metab. 1996;16:1236-1249.
4. Wong EC, Buxton RB, Frank LR. Quantitative imaging of perfusion using a single subtraction (QUIPSS and QUIPSS II). Magn Reson Med. 1998;39:702-708.
5. Norris DG, Schwarzbauer C. Velocity selective radiofrequency pulse trains. J Magn Reson. 1999;137:231-236.
6. Duhamel G, de Bazelaire C, Alsop DC. Evaluation of systematic quantification errors in velocity-selective arterial spin labeling of the brain. Magn Reson Med. 2003;50:145-153.
7. Wong EC, Cronin M, Wu WC, et al. Velocity-selective arterial spin labeling. Magn Reson Med. 2006;55:1334-1341.
8. Qiu D, Moseley ME, Zaharchuk G. Comparison of Pseudocontinuous and Velocity Selective Arterial Spin Labeling with Gold Standard Xenon CT: a Study in Patients with Moyamoya Disease. Proc. Intl. Soc. Mag. Reson. Med. 2011.
9. Priest AN, Graves MJ, Lomas DJ. Acceleration Dependent Vascular Anatomy for Non-Contrast-Enhanced MRA (ADVANCE-MRA). Proc. Int. Soc. Mag. Reson. Med. 2011.
10. Nguyen TD, Rochefort LD, Spincemaille P. Effective Motion-Sensitizing Magnetization Preparation for Black Blood Magnetic Resonance Imaging of the Heart. J Magn Reson. 2009;28:1092-1100.
11. Conolly S, Glover G, Nishimura D, et al. A reduced power selective adiabatic spin-echo pulse sequence. Magn Reson Med. 1991;18:28-38.
12. Reese TG, Heid O, Weisskoff RM, et al. Reduction of eddy-current-induced distortion in diffusion MRI using a twice-refocused spin echo. Magn Reson Med. 2003;49:177-182.
13. Kobari M, Gotoh F, Fukuuchi Y, et al. Quantitative measurement of blood flow velocity in feline pial arteries during hemorrhagic hypotension and hypercapnia. Stroke. 1987;18:457-463.
14. Wu W-C, Wong EC. Intravascular effect in velocity-selective arterial spin labeling: the choice of inflow time and cutoff velocity. NeuroImage. 2006;32:122-128.
15. Smith SM, Jenkinson M, Woolrich MW, et al. Advances in functional and structural MR image analysis and implementation as FSL. NeuroImage. 2004;23:208-219.
16. Woolrich WM, Jbabdi S, Patenaude B, et al. Bayesian analysis of neuroimaging data in FSL. NeuroImage. 2009;45:173-186.
17. Jenkinson M, Bannister P, Brady M, et al. Improved optimisation for the robust and accurate linear registration and motion correction of brain images. NeuroImage 2002;17(2):825-841.
18. Smith SM. Fast Robust Automated Brain Extraction. Human Brain Mapping 2002;17(3):143-155.
19. Zhang Y, Brady M, Smith S. Segmentation of brain MR images through a hidden Markov random field model and the expectation maximization algorithm. IEEE Trans Med Imag. 2001;20(1):45-57.
20. Ye FQ, Frank JA, Weinberger DR, et al. Noise reduction in 3D perfusion imaging by attenuating the static signal in arterial spin tagging (ASSIST). Magn Reson Med. 2000;44:92-100.
21. Garcia DM, Duhamel G, Alsop DC. Efficiency of inversion pulses for background suppressed arterial spin labeling. Magn Reson Med. 2005;54(2):366-372.
22. St Lawrence KS, Frank JA, Bandettini PA, et al. Noise reduction in multi-slice arterial spin tagging imaging. Magn Reson Med. 2005;53:735-738.
23. Mulroney SE, Myers AK. Netter's essential physiology: Saunders/Elsevier; 2009.
24. Purves WK, Sadava DE. Life: The Science of Biology: W.H. Freeman & Company.
25. Wu W-C, Wong EC. Feasibility of velocity selective arterial spin labeling in functional MRI. J Cereb Blood Flow Metab. 2007;27:831-838.

26. Duong TQ, Kim DS, Uğurbil K, et al. Spatiotemporal dynamics of the BOLD fMRI signals: toward mapping submillimeter cortical columns using the early negative response. Magn Reson Med. 2000;44:231-242.
27. Aguirre GK, Detre JA, Zarahn E, et al. Experimental Design and the Relative Sensitivity of BOLD and Perfusion fMRI. NeuroImage. 2002;15(3):488-500.
28. Lu H, Golay X, Pekar JJ, et al. Functional magnetic resonance imaging based on changes in vascular space occupancy. Magn Reson Med. 2003;50:263-274.
29. Sener RN. Diffusion MRI : apparent diffusion coefficient (ADC) values in the normal brain and a classification of brain disorders based on ADC values. Comp Med Imaging and Graphics. 2001;25:299-326.
30. Newcombe VF, Williams GB, Nortje J, et al. Concordant biology underlies discordant imaging findings: diffusivity behaves differently in grey and white matter post acute neurotrauma. Acta Neurochir Suppl. 2008;102:247-251.
31. Le Bihan D. Diffusion and Perfusion Magnetic Resonance Imaging: Applications to Functional MRI. New York: Raven Press; 1995.
32. Clare S, Jezzard P. Rapid T(1) mapping using multislice echo planar imaging. Magn Reson Med. 2001;45:630-634.

3

Comparison of velocity-and acceleration-selective arterial spin labeling with [^{15}O]H_2O positron emission tomography

S Schmid*
DFR Heijtel*
HJMM Mutsaerts
R Boellaard
AA Lammertsma
AJ Nederveen
MJP van Osch

Journal of Cerebral Blood Flow & Metabolism, 2015; 35(8), 1296-1303
** both authors contributed equally to this work*

Abstract

In the last decade spatially non-selective arterial spin labeling (SNS-ASL) methods such as velocity selective ASL (VSASL) and acceleration selective ASL (AccASL), have been introduced which label spins based on their flow-velocity or acceleration rather than spatial localization. Since labeling also occurs within the imaging plane, these methods suffer less from transit delay effects than traditional ASL methods. However, there is a need for validation of these techniques.

In this study, a comparison was made between these SNS-ASL techniques with [^{15}O]H_2O positron emission tomography (PET), which is regarded as gold standard to measure quantitatively cerebral blood flow (CBF) in humans. Additionally, the question of whether these techniques suffer from sensitivity to arterial cerebral blood volume (aCBV), as opposed to producing pure CBF-contrast, was investigated.

The results show high voxelwise intracranial correlation (0.72–0.89) between the spatial distribution of the perfusion signal from the SNS-ASL methods and the PET CBF-maps. A similar GM CBF was measured by dual VSASL compared with PET (46.7±4.1 versus 47.1±6.5 ml/100g/min, respectively). Finally, only minor contribution of aCBV-patterns in GM to all SNS-ASL methods was found compared with pCASL.

In conclusion, VSASL provides a similar quantitative CBF, and all SNS-ASL methods provide qualitatively similar CBF-maps as [^{15}O]H_2O PET.

Introduction

Arterial spin labeling (ASL) is an MR technique that uses arterial blood as an endogenous tracer for non-invasive and quantitative local tissue perfusion measurements.[1] Conventional ASL methods label blood magnetically by inversion or saturation in a slab proximal to the imaging region. Subsequently, the label image is acquired after a post labeling delay (PLD), which is chosen approximately equal to the longitudinal relaxation time of blood (T_1) for cerebral perfusion imaging. The PLD represents a compromise between loss of label due to T_1 decay and transport time for labeled blood to reach the microvascular bed.[2] A so-called control image is obtained by repeating the sequence without labeling blood. By subtracting the label image from the control image, contributions from static tissue will be removed. Therefore, solely magnetization of inflowing tagged spins will be measured, resulting in a perfusion-weighted image. To gain sufficient signal-to-noise ratio (SNR) multiple interleaved repetitions of both label and control sequences are performed.

Currently, pseudo-continuous ASL (pCASL) is considered to be the most reliable and robust ASL technique.[3] However, when arrival of the labeled blood in the tissue is delayed - for example due to pathology - a longer PLD is required, leading to more relaxation of the label and thereby lower SNR. On the other hand, when the PLD is chosen too short, a severe underestimation of the cerebral blood flow (CBF) will occur. Selecting a proper PLD for accurate CBF values in clinical pathologies represents a delicate balance and would frequently lead to a need for too many signal averages to be clinically practical.

Recently, a new family of ASL techniques has been introduced. These spatially non-selective ASL (SNS-ASL) methods label spins based on their flow velocity (VSASL) or acceleration (AccASL) rather than spatial localisation.[4-7] As the label is generated globally, i.e. also within the imaging plane, it is labeled much closer to the capillaries. Therefore, the time to reach the tissue, the so-called transit delay, is smaller and more uniform and consequently these SNS-ASL techniques have the potential to be used even under slow and collateral flow conditions.[8, 9]

Although all these SNS-ASL methods are regarded to reflect perfusion information, one of them is thought to be purely CBF weighted (dual VSASL), while the others are thought to be weighted to mixed haemodynamic parameters, both CBF and CBV (single VSASL and AccASL).

Clearly, there is a need for validation of this new family of ASL techniques. Dual VSASL has already been compared with traditional ASL techniques,[6, 10] and Xenon computed tomography (CT),[8] but single VSASL and AccASL have only been compared with pCASL.[7] None of these SNS-ASL techniques have, however, been compared to the gold standard for quantifying CBF in humans: [^{15}O]H_2O positron emission tomography (PET).[11] Besides providing parametric

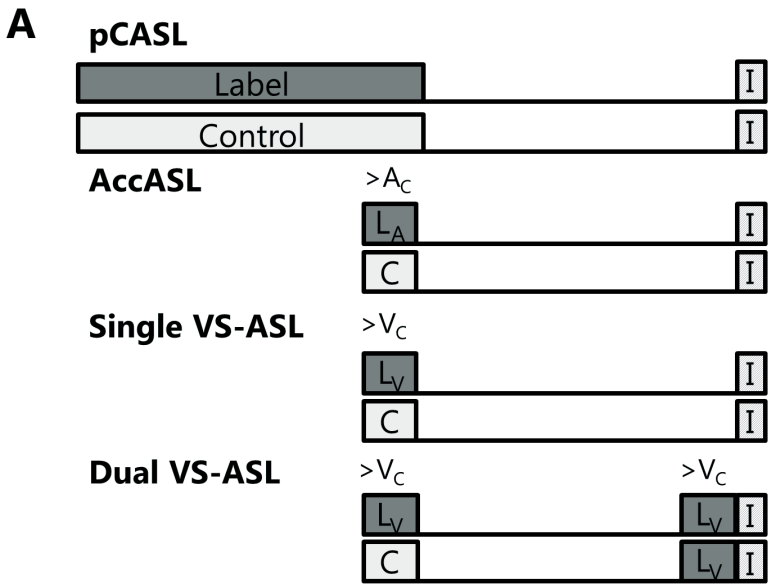

Figure 1 A) Schematic pulse sequence diagrams of the different ASL methods, where LA is the acceleration selective labeling module, LV is the velocity selective labeling module, C is the control module and I is imaging. **B)** Schematic depiction of the RF-pulses and gradients in the labeling modules of AccASL and VSASL and in the control condition.

CBF-images, [^{15}O]H_2O PET can also be used to generate arterial cerebral blood volume (aCBV) images.

Therefore, the primary aim of this study was to compare dual VSASL with [^{15}O]H_2O PET derived CBF in a quantitative way. As secondary aim, the qualitative correspondence of dual VSASL as well as of single VSASL and AccASL with PET was studied. Finally, it will be investigated whether these SNS-ASL methods have a stronger correlation to aCBV signal distribution compared with the traditional ASL method, again using [^{15}O]H_2O PET as a standard.

Materials and Methods

Subjects and study protocol

This study was performed in compliance with regulations of the Local Institutional Review Boards of the participating centres and federal authorities according to the Declaration of Helsinki 'Ethical Principles for Medical Research Involving Human Subjects' and in accordance with the guidelines for Good Clinical Practice (CPMP/ICH/135/95) and written informed consent was obtained from each participant prior to inclusion. This study was part of another study, where the accuracy and precision of pCASL measurements were compared head-to-head with [^{15}O]H_2O PET, by means of a test-retest paradigm as described by Heijtel et al. [12] In addition to the previously described results, we studied in the current study three different SNS-ASL scans, which were performed during the second visit. Only the healthy subjects who completed all required scans (three SNS-ASL scans, a pCASL scan, a pCASL scan with vascular crushing as well as the [^{15}O]H_2O PET scan) were included in the present study (n=13, 7 male and 6 female, age 20-24 years).

All MRI scans were performed on a Philips 3T Intera system (Philips Healthcare, Best, the Netherlands) using an 8 channel SENSE head-coil at the Academic Medical Center in Amsterdam. All PET examinations were performed on a Philips Gemini TF-64 PET/CT system (Philips Healthcare, Cleveland, TN, USA) at the VU University Medical Center in Amsterdam. The PET and MRI scans were performed in a random order with a maximum of 7 days between both sessions.

Three types of SNS-ASL approaches were compared with [^{15}O]H_2O PET and schematic pulse sequence diagrams of these ASL methods are shown in figure 1a.
The first type, which will be referred to as "single VSASL", uses one velocity-selective labeling module and labels all spins that flow faster than a predefined cut-off velocity (V_C). This is irrespective of whether these spins are located in arterial or venous blood and therefore this sequence is thought to have some CBV weighting.

The second type, which will be referred to as "dual VSASL", is similar to single VSASL, except that a second velocity-selective labeling module is added just before imaging in both the label and control condition. This suppresses all spins accelerating in the PLD between the labeling modules, which is assumed to be the venous component.[5] This is the only quantitative SNS-ASL method and is proposed to be predominantly CBF-weighted.[6] In literature, this technique is referred to as VSASL, but to provide more insight into the labeling process, single VSASL was also included into this study, thereby requiring a clear distinguished terminology.

The most recently introduced and third type is acceleration selective ASL (AccASL), which contains only a single labeling module and labels all spins that accelerate or decelerate during the labeling module above a certain cut-off acceleration (or deceleration) (A_c). It has been suggested that the signal is of mixed haemodynamic origin; including both CBF and CBV-weighting. The only difference between the velocity-sensitive and acceleration-sensitive labeling modules is the sign of the second and fourth gradients in the labeling module, as shown in figure 1b, inducing an effective zero first-gradient moment, giving no velocity sensitisation, but acceleration sensitisation due to a second-gradient moment.[7, 13]

pCASL, as employed in the present study for reference purposes, was previously compared with [^{15}O]H_2O PET showing good resemblance.[12, 14]

MRI acquisition

Single VSASL, dual VSASL and AccASL were acquired with interleaved label and control images. The labeling module parameters for VSASL, which determine the velocity-sensitivity, were 22 mT/m for the amplitude of the gradients (G), 1 ms for the gradient duration (δ) and 30 ms for the time between the 90° RF-pulses (Δ), corresponding to a V_c of 2 cm/s. The labeling module parameters for AccASL, which determine the acceleration-sensitivity, were G=30 mT/m, δ=1 ms and Δ=30 ms, corresponding to an A_c of 2.3 m/s^2. A schematic depiction of these labeling modules is shown in figure 1b. Velocity and acceleration encodings were only applied along the slice encoding direction (approximately feet-head direction). During the post labeling delay of 1600 ms for all three techniques background suppression was applied using two adiabatic non-selective inversion pulses at 50 and 1150 ms after labeling to increase the contrast-to-noise ratios.[15-17] The post-acquisition delay, the time between the post-acquisition non-selective saturation and subsequent labeling module, was set to 2000 ms. An overview of all imaging parameters can be found in table 1.

Balanced pCASL was used as a reference representing spatially selective or "conventional" ASL methods.[18] The labeling duration was 1650 ms with a pulse duration of 0.5 ms, a 0.5 ms pause between the pulses, and an 18° flip angle combined with a 0.6 mT/m average gradient in the direction of the blood flow. pCASL scans were acquired with and without vascular crushing (V_c=5 cm/s) to study the effect of macrovascular crushing. For positioning of the pCASL labeling plane, a time-of-flight (TOF) angiogram was acquired. The location of labeling slab was positioned such that it was perpendicular to the main brain feeding arteries and intercepts with the v3 segment of the vertebral arteries.[19]

Table 1 Scanning parameters of the various scans in the MRI protocol.

Abbreviations: Field of view (FOV), repetition time (TR), echo time (TE), time between the 90° RF-pulses of the labeling module (Δ), post labeling delay (PLD), inversion time (TI), background suppression pulses (BSup), amplitude of the gradients in the labeling module (G), gradient duration of the labeling module (δ), cut-off velocity (Vc), cut-off acceleration (Ac), sensitivity encoding (SENSE), number of signal averages (NSA), acquisition time (Tacq), inversion recovery (IR), gradient echo (GE), single shot (SSh), echo planar imaging (EPI), fast field echo (FFE), Spectral Presaturation Inversion Recovery (SPIR).
* Multi-TI IR scan was implemented as a control only pCASL scan with 'labeling duration' of 650ms

	ASL perfusion					Anatomical	$M_{0,CSF}$	Labeling efficiency	$T_{1,a}$
	Spatially non-selective ASL			Conventional ASL					
Method	**Single VS-ASL**	**Dual VS-ASL**	**AccASL**	**pCASL**	**pCASL crush**	**MPRAGE**	**Multi-TI IR***	**PC-MRI**	**Multi-TI**
FOV (mm²)	240 × 240	240 × 240	240 × 240	240 × 240	240 × 240	240 × 240	240 × 240	230 × 230	230 × 230
Resolution (mm²)	3 × 3	3 × 3	3 × 3	3 × 3	3 × 3	1 × 1	3 × 3	0.45 × 0.45	1.5 × 1.5
Slice thickness (mm)	7	7	7	7	7	1	7	4	2
Slices	17	17	17	17	17	200	17	1	1
TR/TE (ms)	4248/14	4248/14	4248/14	3850/14	3921/17	7.0/3.1	2825-4625/14	15/5.1	10000/10.9
Read-out	GE-SSh-EPI	GE-SSh-EPI	GE-SSh-EPI	GE-SSh-EPI	GE-SSh-EPI	3D-FFE	GE-SSh-EPI	2D-FFE	SSh-EPI
Labeling duration or Δ (ms)	30	30	30	1650	1650	-	-	-	-
PLD (ms)	1600	1600	1600	1525	1525	-	1100	-	190
ΔTI (ms) /nTI	-	-	-	-	-	-	200/10	-	150/60
Bsup (ms)	50/1150	50/1150	50/1150	1680/2860	1680/2860	-	-	-	-
G (mT/m)	22	22	30	-	-	-	-	-	-
δ (ms)	1	1	1	-	-	-	-	-	-
Vc or Ac	2 cm/s	2 cm/s	2.3 m/s²	-	5 cm/s	-	-	80 cm/s	-
SENSE	2.5	2.5	2.5	2.5	2.5	-	2.5	-	3
Fat suppression	SPIR	SPIR	SPIR	SPIR	SPIR	-	SPIR	-	-
NSA	35	35	35	54	38	1	2	2	6
T_{acq} (s)	297	297	297	419	301	245	78	61	130

For ASL quantification purposes, an inversion recovery sequence with equal readout properties as the ASL sequence was acquired with 10 different inversion times to estimate the longitudinal magnetization (M_0), followed by a T_1 mapping sequence of the venous blood to estimate the longitudinal relaxation of arterial blood (T_{1a}).[20]
In addition, to estimate the pCASL labeling efficiency a phase contrast scan (PC-MRI) was performed immediately after the pCASL scans, using a slice positioned at the centre of the pCASL labeling plane, in order to measure the blood flow velocity in the brain feeding arteries. For anatomical reference a whole brain T_1-weighted MPRAGE image was acquired with a 1 mm isotropic voxel size.

MRI post-processing

The Oxford Centre for Functional MRI of the Brain (FMRIB)'s Software Library (FSL) was used for realigning the unsubtracted ASL images [21, 22] and the time series were motion corrected with Motion Correction FMRIB's Linear Image Registration Tool (MCFLIRT) with a six-parameter rigid transformation [23]. ASL-maps were obtained by pairwise subtracting the label from the control images and averaging over time. To enable a valid comparison of the temporal signal-to-noise ratios (tSNR) between all different ASL methods, a fixed total ASL sequence duration of 5 min was chosen. To this end, 35 averages of the SNS-ASL scans and the first 38 averages of the pCASL scans were included in the calculation of the tSNR, using the mean and standard error of the mean (SEM).
Subsequently, CBF was calculated for dual VSASL according to the following equation. [10]

[1]

$$CBF_{VS-ASL} = \frac{\Delta M \cdot e^{PLD/T_{1a}} \cdot e^{TE/T_{2a}^*}}{\rho \cdot M_{0a} \cdot \alpha_{VS-ASL} \cdot PLD \cdot \alpha_{BSup} \cdot \left(1 - e^{(PLD-TR)/T_{1a}}\right)}$$

where CBF is the flow in ml/100g/min, ΔM the ASL signal intensity, PLD the post-labeling delay (1600 ms for the first slice and increasing with 35 ms for each following slice to correct for the ascending slice time delay), T_{1a} the longitudinal relaxation of arterial blood (as estimated by T_1 mapping of venous blood in the sagittal sinus)[20], T_{2a}* the T_2* of arterial blood (50 ms [24]), TE the echo time (14 ms), ρ the density of brain tissue (1.05 g/ml [25]), M_{0a} the equilibrium magnetization of arterial blood as determined by a multiple time-point inversion recovery scan (by fitting the M_0 of CSF and multiplying the calculated value with the blood-water partition coefficient (0.76 ml water/ml blood [25])), α_{VSASL} the labeling efficiency derived from the duration of the labeling module (30 ms) and arterial T_2 (170 ms [26]) (0.84 [6]), and α_{BSup} the decrease of labeling efficiency due to background suppression pulses (0.83 [16]).
CBF was derived from the pCASL scans according to the following equation:[12]

[2]

$$CBF_{pCASL} = \frac{\Delta M \cdot e^{t_t/T_{1a}} \cdot e^{TE/T_{2a}^*}}{\rho \cdot M_{0a} \cdot 2\alpha_{pCASL} \cdot T_{1T} \cdot \alpha_{BSup} \cdot [e^{(t_t-PLD)/T_{1T}} - e^{(\delta-\tau-PLD)/T_{1T}}]}$$

with t_t being the tissue transit time (1900 ms [27]), T_{1t} the longitudinal relaxation of brain tissue (1200 ms for GM [28], α_{pCASL} the labeling efficiency derived from the PC-MRI measurement (as simulated by Bloch equations based on the velocities in the labeled arteries [29, 30]), PLD the post-labeling delay (1525 ms for the first slice and increasing with 35 ms for each following slice), δ and τ the labeling duration (1650 ms).
For the vascular crushed pCASL scans it was assumed that only the ASL signal in relatively large arteries with a blood velocity larger than 5 cm/s was affected by crushing.[31] Therefore, quantification of these scans was performed using the same model as the non-crushed pCASL scans.
An in-plane 5 mm full width at half maximum (FWHM) Gaussian kernel was used to smooth all CBF images in order to obtain an image resolution comparable with that of $[^{15}O]H_2O$ PET images and to have a similar smoothing process.

PET acquisition

Prior to scanning, all patients received an indwelling radial artery cannula for blood sampling and a venous cannula in the opposite arm for administration of $[^{15}O]H_2O$. Each patient was positioned with the head in the centre of the field of view and immobilized with a foam mold to minimize motion. First, a 1 min low-dose CT transmission scan was acquired to enable correction of the subsequent emission scan for photon attenuation and scatter. Next, a dynamic emission scan was performed in 3D acquisition mode, starting at the time of administration of an intravenous bolus of 800 MBq $[^{15}O]H_2O$. This scan consisted of 25 frames with progressively increasing duration over a total scanning period of 10 min. The concentration in arterial blood was monitored continuously using an online blood sampler,[32] which was calibrated using three manual arterial blood samples, taken at 5.5, 8 and 10 min after injection.

PET post-processing

The $[^{15}O]H_2O$ PET data were reconstructed using the row action maximum likelihood algorithm (RAMLA) brain reconstruction protocol as provided by the vendor (128×128 matrix, 2 mm isotropic voxel size), including all common corrections (random events, dead time, photon decay, attenuation and scatter) required for quantification. Reconstructed images were smoothed with an isotropic 5 mm FWHM Gaussian kernel, resulting in an image resolution of approximately 6.5 mm isotropic FWHM. A single tissue compartment model with arterial blood volume fraction correction was used for CBF quantification:

[3]

$$C_T(t) = V_a \cdot C_a + (1 - V_a) \cdot f_{PET} \cdot e^{(-f_{pet} \cdot t \cdot V_T^{-1})} \otimes C_a(t)$$

where C_T is the tissue concentration of $[^{15}O]H_2O$, V_a the arterial blood volume (aCBV), C_a the arterial concentration of $[^{15}O]H_2O$, f_{PET} the blood flow (CBF), t the time and V_T the volume of

distribution of the water. Subsequently, parametric CBF and aCBV images were generated from the smoothed dynamic images using a basis function method implementation of the single tissue compartment model with corrections for dispersion, delay and arterial blood volume: [33, 34]

General post-processing

In FSL, the FMRIB's Automated Segmentation Tool (FAST) was used to segment the anatomical T_1-weighted scan of each subject into different tissue types (grey matter (GM), white matter (WM) and cerebrospinal fluid (CSF) probability maps). All ASL and PET CBF-maps were individually co-registered to the segmented GM probability map using FMRIB's Linear Image Registration Tool (FLIRT). A GM mask was generated using a threshold of 55% GM probability. The T_1-weighted scan of each subject was registered to the Montreal Neurological Institute (MNI) template with FMRIB's Non-Linear Image Registration Tool (FNIRT). Subsequently, all co-registered perfusion images and GM masks were warped into MNI space using the same transformation parameters.

Data analysis

For each subject, the mean GM CBF was calculated for the dual VSASL, pCASL and $[^{15}O]H_2O$ PET scans using the individual GM-masks. Next, these CBF-values were compared with each other using a paired t-test applying a two-tailed significance level of 0.05. A Bland-Altman analysis was performed to investigate the spread and measurement agreement between dual VSASL and $[^{15}O]H_2O$ PET. Bias and 95% limits of agreement were calculated as mean difference and as 1.96 × standard deviation of difference between paired measurements respectively.[35]

A one-way ANOVA was performed to compare the temporal signal-to-noise ratios (tSNR) for the different ASL techniques. To determine the tSNR in GM, both mean (μ) and SEM (σ/√n) were calculated voxel-by-voxel over the pairwise subtracted ASL-maps before averaging:

[4]

$$tSNR = \frac{\mu\sqrt{n}}{\sigma}$$

Since single VSASL and AccASL scans cannot be quantified, the comparison for these scans focussed only on the tSNR and the distribution of the signal. In Matlab (R2012b, The MathWorks Inc., Natick, MA) all scans were normalized by dividing each voxel by the average signal intensity in GM. The distribution agreement between the group-averaged normalized scans was visualized in a joint histogram: ASL versus $[^{15}O]H_2O$ derived CBF. The linear correlation coefficient (Pearson's r) was obtained to estimate the degree of correlation between ASL and $[^{15}O]H_2O$ derived CBF and between ASL and $[^{15}O]H_2O$ derived aCBV measurements.

Results

Normalized $[^{15}O]H_2O$ PET and ASL-images for both the group-average and a single subject example of these are shown in figure 2. For $[^{15}O]H_2O$ PET the lower effective resolution is noticeable. On the other hand the ASL scans had a decreased FOV in the z-direction (images not shown), whilst PET covers the entire brain. In AccASL and even more in single VSASL an increased signal intensity is visible in the sagittal sinus. Only in the $[^{15}O]H_2O$ derived aCBV maps the Circle of Willis is clearly present.

The $M0_{a,}$ measured for CBF quantifycation, was $3.8 \times 10^6 \pm 0.27 \times 10^6$ and the arterial blood T_1 was 1789 ± 42 ms for females, which was significantly higher than 1696 ± 63 ms for males ($p<0.01$, unpaired student t-test). The mean GM CBF values for dual VSASL, pCASL and $[^{15}O]H_2O$ PET are shown in table 2, together with the GM tSNR of all ASL scans. ANOVA analysis indicated a significant difference in tSNR at the $p<0.05$ level for the different ASL techniques [$F(4, 60) = 37.65$, $p = 9.82\times10^{-16}$]. Post hoc comparisons using the Tukey HSD test indicated that the mean tSNR of all ASL techniques were significantly different from each other ($p<0.05$), except for the tSNR of AccASL and non-crushed pCASL ($p=0.80$).

The Bland-Altman plot (figure 3) showed no bias between the mean GM CBF of dual VSASL and $[^{15}O]H_2O$ PET. On average the GM CBF of dual VSASL was only 0.4 ml/100g/min smaller and the paired t-test did not show a significant difference. Furthermore, regression analysis showed no significant bias ($p=0.15$). Moreover, the mean GM CBF-value of dual VSASL was significantly lower than pCASL without vascular crushing ($p<0.001$). Compared with pCASL with vascular crushing no significant differences were found with the paired t-test.

In figure 4 the intracranial and GM normalized group-average of the ASL signal versus $[^{15}O]H_2O$ derived CBF is plotted voxelwise in a joint histogram. In table 3 the correlation coefficients between ASL and $[^{15}O]H_2O$ derived CBF evaluated at subject level are shown, with an average range between 0.72 and 0.91 when only including slices above the Circle of Willis, between 0.62 and 0.85 for the all intracranial tissues and between 0.13 and 0.39 for the GM tissue only. The correlation coefficients with PET CBF for AccASL, both pCASL scans and to a lesser extent dual VSASL were comparable. Only single VSASL showed a lower correlation and larger standard deviation. In table 3 the correlation coefficients between the various ASL modalities with $[^{15}O]H_2O$ derived aCBV are presented as well. For all ASL sequences the correlation coefficients with PET aCBV were lower than PET CBF ($p<0.001$). The correlation coefficients intracranial and above the Circle of Willis with $[^{15}O]H_2O$ derived aCBV of AccASL and both pCASL scans were similar; but both VSASL methods showed a lower correlation. The correlation coefficients in GM of all SNS-ASL methods with PET aCBV were significantly lower than pCASL.

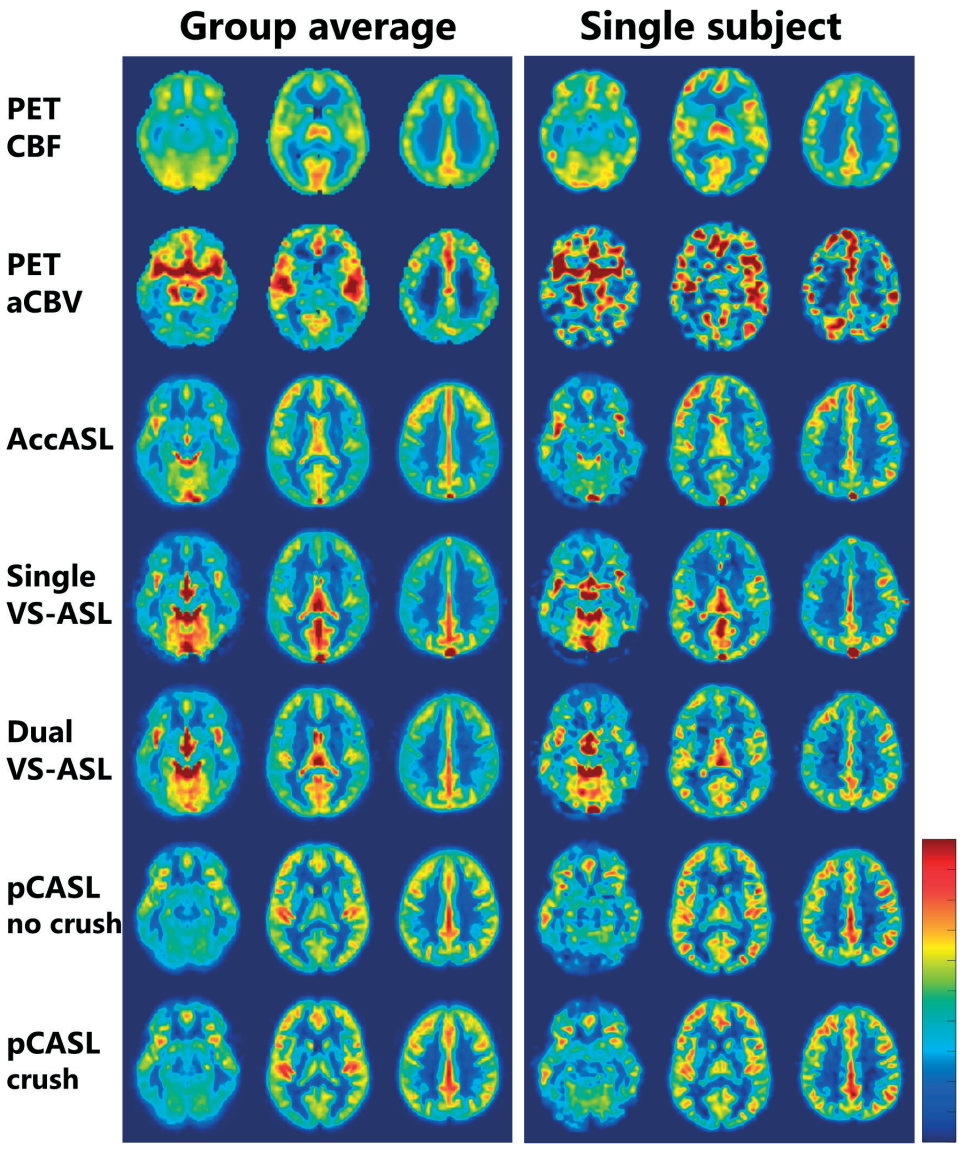

Figure 2 Example of 3 transversal slices of the $[^{15}O]H_2O$ PET and ASL maps of both the group average and a single volunteer. For comparison of the spatial distribution of the signal, all maps were normalized dividing each voxel by the average grey matter value of the corresponding map.

Table 2 The average grey matter cerebral blood flow (GM CBF, in ml/100g/min) of the quantifiable ASL and PET scans and the temporal signal-to-noise ratios (tSNR) of the 5 different ASL scans, both evaluated at subject level [mean ± SD].

	PET CBF	AccASL	Single VSASL	Dual VSASL	pCASL no crush	pCASL crush
GM CBF	47.1 ± 6.5			46.7 ± 4.1	60.7 ± 10.9	49.2 ± 9.2
tSNR		6.96 ± 1.42	5.04 ± 0.85	3.49 ± 0.50	8.40 ± 1.41	7.05 ± 1.19

Table 3 Intracranial (IC), above the Circle of Willis (CoW) and grey matter (GM) intensity normalized correlation coefficient between ASL and $[^{15}O]H_2O$ PET CBF evaluated at subject level [mean ± SD]

		AccASL	Single VSASL	Dual VSASL	pCASL no crush	pCASL crush
Correlation with PET CBF	IC	0.85 ± 0.02	0.62 ± 0.08	0.65 ± 0.03	0.84 ± 0.01	0.82 ± 0.02
	above CoW	0.89 ± 0.02	0.72 ± 0.08	0.84 ± 0.02	0.91 ± 0.01	0.91 ± 0.02
	GM	0.35 ± 0.06	0.13 ± 0.06	0.14 ± 0.06	0.38 ± 0.05	0.39 ± 0.06
Correlation with PET aCBV	IC	0.72 ± 0.06	0.54 ± 0.09	0.58 ± 0.06	0.74 ± 0.06	0.73 ± 0.06
	above CoW	0.75 ± 0.06	0.60 ± 0.10	0.70 ± 0.06	0.79 ± 0.06	0.79 ± 0.06
	GM	0.15 ± 0.06	0.03 ± 0.06	0.11 ± 0.06	0.28 ± 0.07	0.28 ± 0.07

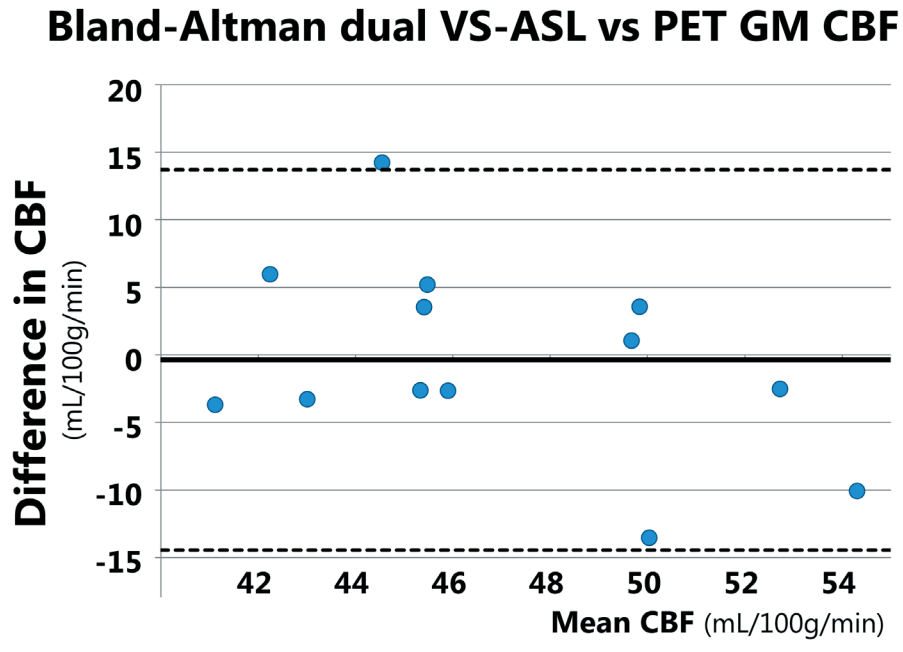

Figure 3 Bland-Altman plot of dual VSASL and $[^{15}O]H_2O$ PET CBF in grey matter. The solid line depicts the mean difference between dual VSASL and PET CBF over all volunteers, the dashed lines the corresponding 95% confidence intervals.

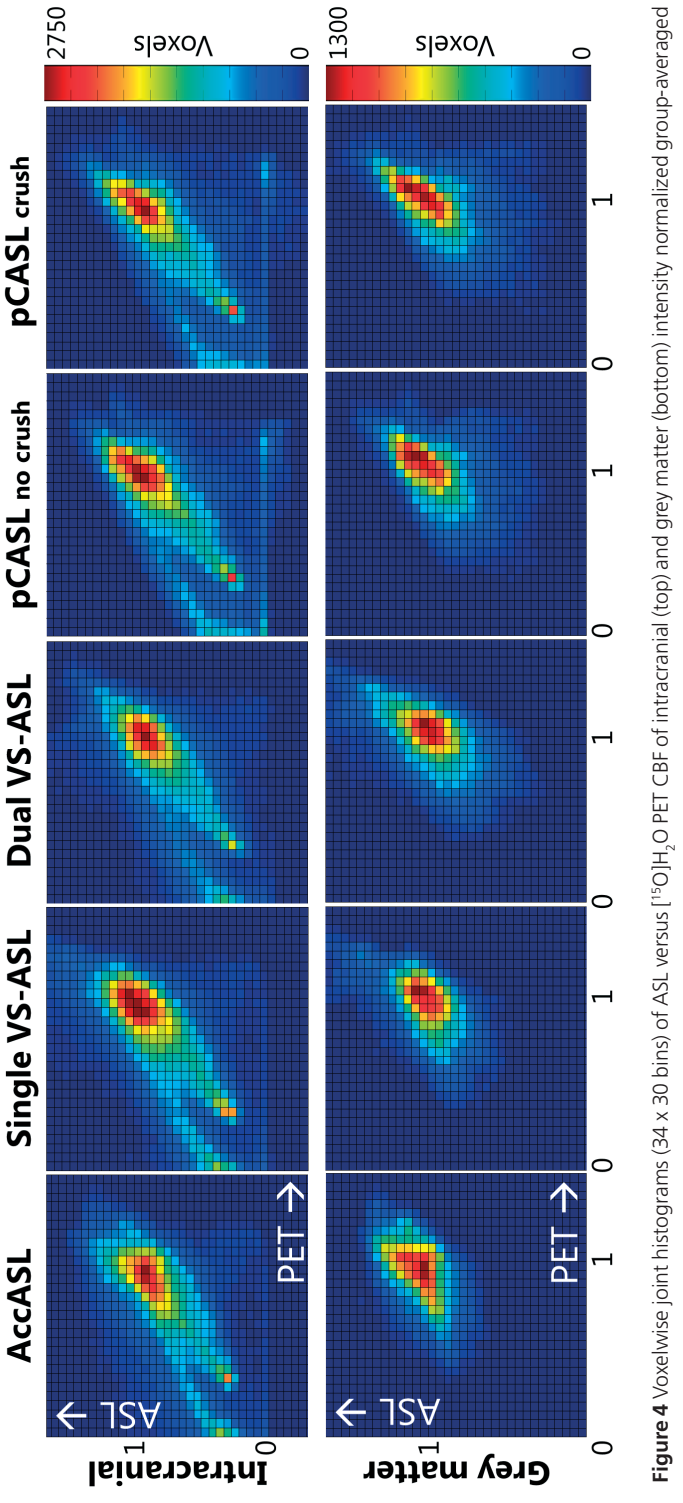

Figure 4 Voxelwise joint histograms (34 x 30 bins) of ASL versus [^{15}O]H_2O PET CBF of intracranial (top) and grey matter (bottom) intensity normalized group-averaged maps.

Discussion

In the current study we compared three spatially non-selective ASL techniques with the gold standard [^{15}O]H_2O PET and showed pCASL scans, with and without vascular crushing, as a reference for traditional, spatially selective ASL. In addition, the correlation of these ASL methods with aCBV was assessed. To the best of our knowledge this is the first study to extensively compare these SNS-ASL methods with [^{15}O]H_2O PET. The most important findings of the present study are threefold. Firstly, the GM CBF obtained with dual VSASL was similar to [^{15}O]H_2O PET. Secondly, the spatial signal distribution of the SNS-ASL methods showed good agreement with that of [^{15}O]H_2O derived CBF. Finally, for all SNS-ASL methods the aCBV signal distribution was less present compared with pCASL.

From the three SNS-ASL methods only the CBF of dual VSASL can be evaluated quantitatively. The average GM CBF was calculated using the equation proposed by Wu and Wong,[10] with an additional correction factor to account for the two background suppression pulses and a labeling efficiency term, which was estimated by the TE of the labeling module and the T_2 of arterial blood, i.e. $\exp(-TE_{lab}/T_{2a})$. No significant difference was found between the GM CBF obtained using dual VSASL and [^{15}O]H_2O PET, as shown in the Bland-Altman plot (figure 3). A limitation is that for pCASL and [^{15}O]H_2O PET a two-compartment model was used, whereas for dual VSASL a single compartment model was used to quantify the CBF. As stated in the ASL consensus paper, the single-compartment model is an oversimplification of the real situation.[3] Therefore, a more comprehensive model, expressed in equation 2, was employed to compare the traditional quantitative ASL data to the gold standard. For dual VSASL no validated two-compartment model is available yet, because it is more difficult to estimate when the transition from the arterial to the tissue compartment due to the large width of the bolus. Another limitation is that a constant, brain average blood-water partition coefficient was assumed in the ASL quantification, although it is known that this is a function of the haematocrit that may vary between subjects. Furthermore, the partition coefficient also varies throughout the brain, since the water content of the tissue is not constant for the different brain regions.[25] Since for [^{15}O]H_2O PET a region specific volume of distribution was calculated, GM-WM discrepancies might occur between both modalities. Nevertheless, the influence on the quantitative CBF comparison is hypothesized to be limited, since this was only performed in GM.

For single and dual VSASL hyper-intensities were observed in the posterior flow territory and hypo- intensities in the anterior flow territory as shown in figure 2. We think this might be caused by differences in the large vasculature in these regions, like for example the main directionally of the vessels that is more consistent in the feet-head direction for the posterior than for the anterior circulation.

With VSASL it is possible to create label closer to the tissue than with pCASL and therefore it might be considered unnecessary that the PLD for VSASL was chosen (slightly) longer than for pCASL. Since the only perfusion signal that is detected in dual VSASL is from spins whose velocity was above the cut-off velocity during labeling and below the cut-off velocity during imaging, a certain time between the labeling modules is necessary to let the labeled spins progress through the vascular tree, thereby steadily decreasing their velocity. A too short PLD would therefore lead to too little signal and the PLD in VSASL shares therefore some resemblance to the labeling duration of pCASL and the QUIPSS-time of a PASL experiment. Therefore, the PLD of VSASL was chosen similar to the labeling duration and PLD of the pCASL-experiments. For comparison reasons, the PLD of single VSASL and AccASL were kept equal to the PLD of dual VSASL.

The use of a second labeling module in dual VSASL allows quantifications of CBF, but will eliminate part of the arterial signal as well and thus decrease the amount of detected signal. This will not influence the quantitative estimation of the CBF, since it is corrected for in the quantification equation, but it will decrease the tSNR. This decrease in tSNR adds to the already lower tSNR of SNS-ASL due to the use of saturation instead of inversion for labeling.
Although the pCASL data in this study were included for reference purposes only, it was noticed that the calculated mean GM CBF values in this subgroup of subjects was 9.8 ± 4.4 ml/100g/min higher than reported by Heijtel et. al [12]. The main reason for this difference was that some volunteers who were included in the current analysis, were not included in the previously reported analysis and vice versa. When preforming the analysis with only the subjects that were included in both studies (n=10), the difference for the non-crushed pCASL CBF is then 5.1 ml/100g/min. The remaining difference can be explained by the slightly different approaches to create GM masks, such as registration to MNI instead of the use of a group-specific atlas and accompanying differences in thresholds.
The comparison of AccASL and single VSASL with $[^{15}O]H_2O$ derived CBF solely focussed on the tSNR and the spatial distribution of the signal by normalized maps, joint histograms, and the calculated correlation coefficients, as these ASL techniques cannot be quantified. When both modalities would have had the same signal distribution, the joint histograms would have shown a straight line as evidence of good agreement. As both the ASL and $[^{15}O]H_2O$ PET data were normalized to the average signal intensity of the GM, the slope of the line has no specific meaning. In figure 4 it can clearly be seen that the ASL methods showed a good intracranial correlation with PET CBF. WM is represented in the left bottom corner, because the perfusion of WM is lower than that of GM. For $[^{15}O]H_2O$ PET a region specific volume of distribution was calculated for the blood-water partition coefficient. However, the correlation coefficients were calculated using the ASL data without regional correction for the partition coefficient, which will induce GM-WM discrepancies between both modalities and might have led to lower correlation values. Some of the other discrepancies can be explained by the EPI read-out, as can be seen in figure 2: it has been shown previously that the EPI read-out

is prone to signal loss in the prefrontal brain area.[36] Furthermore, the timing of background suppression pulses was rather aggressive, which could have led to some signal loss in the lowest slices.
Focussing on the correlation coefficients as presented in table 3, it is clear that compared with all other ASL techniques single VSASL showed the lowest correlation with $[^{15}O]H_2O$ derived CBF. This weaker correlation could be explained by the presence of venous signal, of which the high signal intensity in the sagittal sinus is a good example, which is less obvious in e.g. AccASL and even absent in the other ASL sequences. Furthermore, it is known that single VSASL, and again to a lesser extent for AccASL, has higher signal in CSF regions, due to the combination of a relatively high amount of diffusion and flow in CSF. The diffusion weighting of the labeling module is strong enough to cause diffusion related attenuation in CSF and thereby contamination of the CBF-maps.[6] To incorporate this contamination into our validation analysis, it was decided to compare signal distribution over the entire brain between ASL and PET (i.e. including ventricles and sagittal sinus). In addition, the signal distribution of only the GM tissue was analysed separately. Single VSASL showed less signal than AccASL, which could be surprising since the labeling block of VSASL also exhibits a non-zero second moment, thereby also providing acceleration sensitive labeling. One could speculate that the combined velocity and acceleration sensitive signal would lead to more signal, however, this was not observed. This might be partially explained by the fact that the first and second moment of the VS-labeling module have an opposite sign and will therefore not constructively add. Furthermore, due to the difference in gradient amplitude for VSASL compared with AccASL, the acceleration cut-off is higher, which could mean that the labeling is in a different region and probably further away from the capillaries.

For both single VSASL and AccASL, it has been postulated that they would be more weighted towards CBV than CBF, since all blood above a certain velocity or acceleration is labeled.[7] To investigate this hypothesis, weighting towards aCBV was studied. by examining the intracranial and GM correlation coefficients of ASL with $[^{15}O]H_2O$ derived aCBV. The highest intracranial correlations with PET aCBV were observed for pCASL and AccASL, closely followed by dual VSASL. Only the intracranial correlation coefficient of single VSASL with PET aCBV differed from the other sequences, being approximately 20% lower than the traditional ASL methods. The GM correlations coefficients with PET aCBV of the SNS-ASL methods were lower than pCASL. The GM correlations with PET aCBV of dual VSASL showed the most resemblance to pCASL, followed by AccASL, and single VSASL again had the lowest correlation. However, all ASL methods showed lower correlation coefficients with PET aCBV than with PET CBF. aCBV-maps mainly show besides a normal GM/WM contrast, large vessels and the signal is only arterial, whereas the single VSASL and AccASL are thought to create label closer to the tissue due to the relatively long PLD and the images also include a venous component.[7, 9] In summary, the present results show that single VSASL and AccASL have much lower weighting towards aCBV compared with pCASL. Unfortunately, these findings cannot answer the

question whether those techniques are more weighted towards total CBV and this remains to be answered.

In the present study, the $[^{15}O]H_2O$ derived aCBV were used only for comparison of the relative signal distributions and not for quantitative purposes. This approach was followed because of uncertainties in quantitative accuracy of aCBV as measured by $[^{15}O]H_2O$ PET. One problem is the potential confounding effect of dispersion in the arterial line. When the dispersion is not estimated correctly due to artefacts in the image reconstruction, aCBV will become less accurate and could especially show a global bias.[9] Visual inspection of the individual aCBV-maps was performed to identify any clear errors, which were not observed. PET would be able to provide more accurate CBV-measurements by means of $[^{15}O]$-labeled carbon monoxide ($C^{15}O$).[34]

The study protocol could have been improved by acquiring the PET and ASL scans on the same day or even at the same time, thereby minimizing the effects of the physiological fluctuations in the perfusion.[38] Unfortunately, this was logistically impossible with the imaging centres at two different locations, since at the time of the study no combined PET/MRI system was available in either of the two centres. Nevertheless, it should be noted that it was verified that both pCASL and VSASL demonstrate similar variations over time, with changes on the order of 10% or less over a 6 month period.[39]

In future work, a comparison of the results from spatially non-selective ASL methods with images that are (totally) CBV-weighted should be made, to better understand in the weighting of the different ASL methods. Furthermore, the current recommended clinical application for SNS-ASL is pathology with slow or collateral flow. Therefore, a comparison between conventional and spatially non-selective ASL methods and $[^{15}O]H_2O$ or $[^{15}O]CO$ PET in patients with large vessel disease could give more insight into the preferred perfusion measurement technique for such pathologies with delayed arrival times.

Conclusion

In conclusion, dual VSASL provides a similar quantitative CBF, and qualitatively all SNS-ASL methods provide similar CBF-maps as compared to $[^{15}O]H_2O$ PET. From the SNS-ASL methods, AccASL was most similar to PET CBF, showing only a 2% lower intracranial correlation coefficient compared with pCASL. This opens up the possibility of exploring the clinical applications and validations of SNS-ASL with dual VSASL as a quantitative technique and AccASL for qualitative purposes.

References

1. Detre JA, Leigh JS, Williams DS, et al. Perfusion imaging. Magn Reson Med. 1992;23:37-45.
2. Alsop DC, Detre JA. Reduced transit-time sensitivity in noninvasive magnetic resonance imaging of human cerebral blood flow. J Cereb Blood Flow Metab. 1996;16:1236-1249.
3. Alsop DC, Detre JA, Golay X, et al. Recommended implementation of arterial spin-labeled perfusion MRI for clinical applications: A consensus of the ISMRM perfusion study group and the European consortium for ASL in dementia. Magn Reson Med. 2015;73(1):102–116.
4. Norris DG, Schwarzbauer C. Velocity selective radiofrequency pulse trains. J Magn Reson Imaging. 1999;137:231-236.
5. Duhamel G, de Bazelaire C, Alsop DC. Evaluation of systematic quantification errors in velocity-selective arterial spin labeling of the brain. Magn Reson Med. 2003;50(1):145-153.
6. Wong EC, Cronin M, Wu WC, et al. Velocity-selective arterial spin labeling. Magn Reson Med. 2006;55(6):1334-1341.
7. Schmid S, Ghariq E, Teeuwisse WM, et al. Acceleration-selective arterial spin labeling. Magn Reson Med. 2014;71(1):191-199.
8. Qiu D, Straka M, Zun Z, et al. CBF measurements using multidelay pseudocontinuous and velocity-selective arterial spin labeling in patients with long arterial transit delays: comparison with xenon CT CBF. J Magn Reson Imaging. 2012;36(1):110-119.
9. Guo J, Wong EC. Comparison of Transit Delay Sensitivity between Pseudo-Continuous ASL, Pulsed ASL and Velocity-Selective ASL. Proc. Intl. Soc. Mag. Reson. Med. 2014; Milan, Italy
10. Wu WC, Wong EC. Feasibility of velocity selective arterial spin labeling in functional MRI. J Cereb Blood Flow Metab. 2007;27(4):831-838.
11. Bokkers RPH, Bremmer JP, van Berckel BNM, et al. Arterial spin labeling perfusion MRI at multiple delay times: a correlative study with $H_2{}^{15}O$ positron emission tomography in patients with symptomatic carotid artery occlusion. J Cereb Blood Flow Metab. 2009;30(1):222-229.
12. Heijtel DFR, Mutsaerts HJMM, Bakker E, et al. Accuracy and precision of pseudo-continuous arterial spin labeling perfusion during baseline and hypercapnia: A head-to-head comparison with ^{15}O H_2O positron emission tomography. Neuroimage. 2014;92:182-192.
13. Priest AN, Graves MJ, Lomas DJ. Acceleration Dependent Vascular Anatomy for Non-Contrast-Enhanced MRA (ADVANCE-MRA) . Proc. Intl. Soc. Mag. Reson. Med. 2011; Montreal, Canada.
14. Xu G, Rowley HA, Wu G, et al. Reliability and precision of pseudo-continuous arterial spin labeling perfusion MRI on 3.0 T and comparison with ^{15}O-water PET in elderly subjects at risk for Alzheimer's disease. NMR Biomed. 2010;23(3):286-293.
15. Ye FQ, Frank JA, Weinberger DR, et al. Noise reduction in 3D perfusion imaging by attenuating the static signal in arterial spin tagging (ASSIST). Magn Reson Med. 2000;44:92-100.
16. Garcia DM, Duhamel G, Alsop DC. Efficiency of inversion pulses for background suppressed arterial spin labeling. Magn Reson Med. 2005;54(2):366-372.
17. St Lawrence KS, Frank JA, Bandettini PA, et al. Noise reduction in multi-slice arterial spin tagging imaging. Magn Reson Med. 2005;53:735-738.
18. Dai W, Garcia D, de Bazelaire C, et al. Continuous flow-driven inversion for arterial spin labeling using pulsed radio frequency and gradient fields. Magn Reson Med. 2008;60(6):1488-97.
19. Teeuwisse WM, Schmid S, Helle M, et al. 2-shim or not 2-shim, that is a question in pseudo continuous arterial spin labeling. Proc. Intl. Soc. Mag. Reson. Med. 2014; Milan, Italy.
20. Varela M, Hajnal JV, Petersen ET, et al. A method for rapid in vivo measurement of blood T1. NMR Biomed. 2011;24(1):80-88.
21. Smith SM, Jenkinson M, Woolrich MW, et al. Advances in functional and structural MR image analysis and implementation as FSL. NeuroImage. 2004;23:208-219.
22. Woolrich WM, Jbabdi S, Patenaude B, et al. Bayesian analysis of neuroimaging data in FSL. NeuroImage. 2009;45:173-186.

23. Jenkinson M, Bannister P, Brady M, et al. Improved optimisation for the robust and accurate linear registration and motion correction of brain images. NeuroImage 2002;17(2):825-841.
24. Teeuwisse WM, Nederveen AJ, Ghariq E, et al. Comparison of spin dynamics in pseudo-continuous and velocity-selective arterial spin labeling with and without vascular crushing. Proc. Intl. Soc. Mag. Reson. Med.; 2011; Montreal, Canada.
25. Herscovitch P, Raichle ME. What Is the Correct Value for the Brain-Blood Partition Coefficient for Water? J Cereb Blood Flow Metab. 1985;5(1):65-69.
26. Chen JJ, Pike GB. Human whole blood T2 relaxometry at 3 Tesla. Magn Reson Med. 2009;61(2):249-54.
27. Liu P, Uh J, Lu H. Determination of spin compartment in arterial spin labeling MRI. Magn Reson Med. 2011;65(1):120-127.
28. Lu H, Nagae-Poetscher LM, Golay X, et al. Routine clinical brain MRI sequences for use at 3.0 Tesla. J Magn Reson Imaging. 2005;22(1):13-22.
29. Wu WC, Fernandez-Seara M, Detre JA, et al. A theoretical and experimental investigation of the tagging efficiency of pseudocontinuous arterial spin labeling. Magn Reson Med. 2007;58(5):1020-1027.
30. Aslan S, Xu F, Wang PL, et al. Estimation of Labeling Efficiency in Pseudocontinuous Arterial Spin Labeling. Magn Reson Med. 2010;63:765–771.
31. Ye FQ, Mattay VS, Jezzard P, et al. Correction for vascular artifacts in cerebral blood flow values measured by using arterial spin tagging techniques. Magn Reson Med. 1997;37:226-235.
32. Boellaard R, van Lingen A, van Balen SCM, et al. Characteristics of a new fully programmable blood sampling device for monitoring blood radioactivity during PET. Europ J Nucl Med. 2001;28(1):81-89.
33. Boellaard R, Knaapen P, Rijbroek A, et al. Evaluation of Basis Function and Linear Least Squares Methods for Generating Parametric Blood Flow Images Using ^{15}O-Water and Positron Emission Tomography. Mol Imaging Biol. 2005;7(4):273-285.
34. Bremmer JP, Berckel BNM, Persoon S, et al. Day-to-Day Test–Retest Variability of CBF, CMRO2, and OEF Measurements Using Dynamic ^{15}O PET Studies. Mol Imaging Biol. 2011;13(4):759-768.
35. Bland JM, Altman DG. Statistical methods for assessing agreement between two methods of clinical measurements. the Lancet. 1986:307-310.
36. Vidorreta M, Wang Z, Rodríguez I, et al. Comparison of 2D and 3D single-shot ASL perfusion fMRI sequences. NeuroImage. 2013;66(0):662-671.
37. Lammertsma AA, Jones T. Correction for the Presence of Intravascular Oxygen-15 in the Steady-State Technique for Measuring Regional Oxygen Extraction Ratio in the Brain: 1. Description of the Method. J Cereb Blood Flow Metab. 1983;3(4):416-424.
38. Zhang K, Herzog H, Mauler J, et al. Comparison of cerebral blood flow acquired by simultaneous ^{15}O water positron emission tomography and arterial spin labeling magnetic resonance imaging. J Cereb Blood Flow Metab. 2014;10.1038/jcbfm.2014.92.
39. Zun Z, Qiu D, Rosenberg J, et al. Longitudinal Study of Cerebral Blood Flow Measurements in Normals Using Pseudocontinuous and Velocity-Selective Arterial Spin Labeling. Proc. Intl. Soc. Mag. Reson. Med. 2013; Salt Lake City, UT.

4

Insight into the labeling mechanism of Acceleration selective arterial spin labeling

S Schmid
ET Petersen
MJP van Osch

Magnetic Resonance Materials in Physics, Biology and Medicine, 2016: 30(2), 165-174

Abstract

Acceleration selective arterial spin labeling (AccASL) is a spatially non-selective labeling technique, which labels spins based on their flow acceleration rather than spatial localization, which is used in traditional ASL methods. The exact origin of the AccASL signal within the vasculature is not completely understood. To obtain more insight into this, the acceleration selective module was performed followed by a velocity selective module, which is used in velocity selective arterial spin labeling (VSASL).

Nine healthy volunteers were scanned with various combinations of the control and label conditions in both the acceleration and velocity selective module. The cut-off acceleration (0.59 m/s^2) or velocity (2 cm/s) was kept constant in one module, while it was varied over a large range in the other module. With the right subtractions this resulted in AccASL, VSASL, combined AccASL and VSASL signal, and signal from one module with crushing from the other.

The label created with AccASL has an overlap of approximately 50% in the vascular region with VSASL, but also originates from smaller vessels closer to the capillaries. In conclusion, AccASL is able to label spins both in the macro-, meso- as well as in the microvasculature.

Introduction

Arterial spin labeling (ASL) techniques can be used as a noninvasive MR technique to quantify the local tissue perfusion. In conventional ASL, the labeling is based on a spatial localized tagging of blood spins by either inversion or saturation in a plane proximal to the imaging region. The image is acquired after a post labeling delay (PLD), chosen approximately equal to the longitudinal relaxation (T_1) of blood for cerebral perfusion imaging. This choice in PLD represents a compromise between the transport time, which should be long enough for the labeled blood to reach the tissue, and the loss of label due to T_1-relaxation. However, even in healthy, young volunteers the variation in transit time within a single slice can be up to hundreds of milliseconds.[1, 2] Moreover, in elderly subjects and patients with pathological brain conditions slow and/or collateral flow is a frequently encountered confound of conventional ASL techniques leading to severe underestimation of cerebral blood flow (CBF) , because not all label will have reached the microvascular bed during readout.[2]

Recently, a new family of ASL techniques has been introduced. These spatially non-selective ASL (SNS-ASL) methods label spins by saturation based on their flow velocity (i.e. velocity-selective ASL frequently abbreviated as VSASL) or acceleration (AccASL) rather than spatial localization.[3, 4] The label is generated globally, so also within the imaging region where perfusion is measured. Since the labeling is also much closer to the capillaries, this makes the spatially non-selective techniques more robust with respect to transit time effects. Therefore VSASL can provide quantitative CBF maps even under slow and collateral flow conditions.[5, 6] Because the temporal SNR of AccASL has been found to be higher than the temporal SNR of VSASL,[4] this new technique could be an interesting alternative SNS-ASL approach, although the exact origin of the signal is not completely understood.

In VSASL the velocity-selective labeling module tags all spins that flow faster than a predefined cut-off velocity, irrespective of whether these are located in arterial or venous blood. The acceleration-dependent preparation differs from a velocity-selective approach in that it does not affect the magnetization from spins flowing at a constant velocity, but saturates spins that are accelerating or decelerating above a certain cut-off acceleration (or deceleration).[7] These different approaches to labeling result also in a difference in our understanding of the exact location in the vascular tree where the label is created. For VSASL this location can be estimated by comparing the cut-off velocity to the typical velocity within the vascular tree,[8] although these velocities are expected to vary from person to person depending on, for example, age and vessel stiffness. In the vascular tree, the average velocity of the spins decreases from the arteries toward the capillaries, after which their average velocity increases slightly while flowing into the venous system. By the use of a second velocity module approximately 1.5 - 2.0 seconds after the first, arterial label can be distinguished from venous label and quantification of CBF becomes feasible due to the fact that the temporal width

of the bolus of labeled spins is now controlled. In AccASL label is predominantly created within the arterial side of the vasculature, where the pulsatility is known to be higher than in the veins, but at what level of the vasculature the exact origin of the signal originates is poorly understood. It has been suggested that the signal is of mixed haemodynamic origin; including both CBF and CBV-weighting and that the label could originate from cardiac cycle fluctuations, general flow acceleration/deceleration in the vasculature as well as from the tortuosity of the vessels, both at macro- and microvascular level.[9]

The aim of this study was to obtain more insight into the origin of the labeling mechanism in AccASL by combining this method with a VS-module. This will show whether both approaches label at similar locations in the vascular tree or whether AccASL labels even closer to the microvasculature than VSASL.

Materials and methods

Spatially non-selective arterial spin labeling methods

The labeling module of both AccASL and VSASL combine a pair of spatially nonselective hard 90° pulses with two identical adiabatic 180° refocusing pulses to correct for phase shifts due to inhomogeneities of the magnetic field and chemical shifts.[10] Motion sensitizing gradients, placed in-between these radiofrequency pulses as shown in figure 1a, can be used to dephase the magnetization of flowing spins and the polarity of these gradients determines whether flowing spins with constant velocity (VSASL) or accelerating (AccASL) spins are affected. In the velocity-sensitive labeling module the second and fourth gradient are negative, whereas in the acceleration-sensitive labeling module all gradients are positive inducing an effective zero first-gradient moment, giving no velocity sensitisation, but acceleration sensitisation due to a second-gradient moment.[4, 11] Spins with a flow velocity or acceleration above a cut-off velocity (V_{enc}) or cut-off acceleration (A_{enc}), respectively, are dephased: both parameters are defined as to correspond to a phase change of pi.

The effective first-gradient moment (m_1) of the velocity-sensitizing sequence can be calculated to be $m_1=G\times\delta\times\Delta$, with G the amplitude of the gradients, δ the gradient duration, and Δ the time between the leading edges of the first two gradient lobes . By varying these parameters, the cut-off velocity can be set, according to $V_{enc}= \pi /(2\gamma\times m_1)$, where γ is the gyromagnetic ratio.

The acceleration-sensitizing sequence has an effective first-gradient moment of zero, giving no velocity sensitization, but a second-gradient moment (m_2) of $m_2=4\times G\times\delta\times\Delta\times\tau$, with τ the time between the leading edges of the first and the third gradient. The relation to the cut-off acceleration is $A_{enc}=2\pi/(\gamma\times m_2)$.[11] Both acceleration as well as deceleration, which could be

A

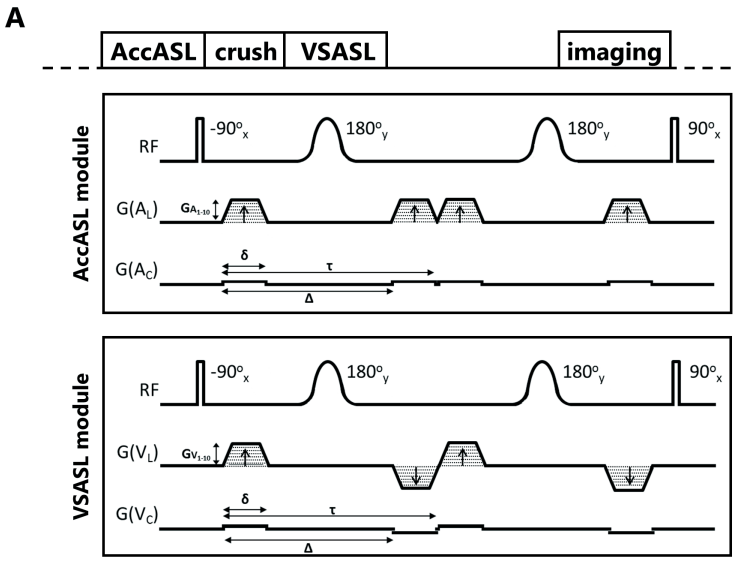

B

A_CV_C	Control	Control
A_LV_C	Label > A_{enc}	Control
A_CV_L	Control	Label > V_{enc}
A_LV_L	Label > A_{enc}	Label > V_{enc}

C

$A_CV_C - A_LV_C$ = AccASL

$A_CV_C - A_CV_L$ = VSASL

$A_CV_C - A_LV_L$ = AccASL & VSASL

$A_LV_C - A_LV_L$ = VSASL with crushing >A_{enc}

$A_CV_L - A_LV_L$ = AccASL with crushing >V_{enc}

$(A_CV_C - A_LV_C) + (A_CV_C - A_CV_L)$ = AccASL + VSASL

Figure 1 A) A schematic representation of the sequence. The gradients in the acceleration (AccASL) and velocity (VSASL) selective labeling module are described as: G the amplitude of the gradients, δ the gradient duration, and Δ the time between the leading edges of the first two gradient lobes and τ the time leading edges of the first and the third gradient **B)** Four different combinations of the control and labeling conditions are possible with the acceleration- and velocity-selective labeling modules: A_CV_C, A_LV_L, A_CV_L and A_LV_C, were A_C is the control condition of the acceleration-selective module, V_C is the control condition of the velocity-selective module, A_L is the label condition of the acceleration-selective module and V_L is the label condition of the velocity selective module. **C)** By combining and subtraction of the acquired scans different types of images can be calculated.

considered as negative acceleration, is targeted with this sequence equally well. It should be noted that the gradients not only encode motion but also impart a diffusion sensitivity, which becomes substantial for higher moments.

The sequence used in this study consisted of an acceleration-selective labeling module immediately followed by a set of crushing gradients consecutively in x-, y- and z-direction to dephase any remaining transverse magnetization, all performed with an area under the gradient of 50 mT/m×ms. Subsequently, a velocity-selective labeling module was played out. A schematic representation of the sequence is shown in figure 1a.

The control condition of VSASL and AccASL consists of the same set of RF-pulses and gradients, but with a gradient amplitude of 5% of the constant cut-off are employed . Since in our combined sequence the VS- and Acc-module can both be control or label, four different combinations are possible: A_CV_C, A_LV_L, A_CV_L and A_LV_C, were A_C is the control condition of the acceleration-selective module, V_C is the control condition of the velocity-selective module, A_L is the label condition of the acceleration-selective module and V_L is the label condition of the velocity selective module, see figure 1b. For each combination, 10 different variations in labeling velocity or acceleration were acquired.

Subtraction of ASL images

By combining and subtracting the scans acquired with different combinations of label and control condition, different types of images can be calculated, as summarised in figure 1c. The difference between A_CV_C and A_LV_C will result in signal similar to that obtained by a normal acceleration-selective scan (AccASL), since the control condition of the VS-module is assumed not to influence the longitudinal magnetization significantly and the static spins will be excluded by subtraction. Similarly, A_CV_C minus A_CV_L will yield the signal originating from the velocity-selective module (VSASL). A_CV_C minus A_LV_L results in label-signal created by joint, sequential application of the acceleration- and velocity-selective module (AccASL & VSASL). Whereas, the subtraction of A_LV_L from A_CV_L will provide the signal from the Acc-module followed immediately by crushing from the VS-module (AccASL with crushing > V_{enc}) and subtraction of A_LV_L from A_LV_C will provide the signal from the VS-module preceded by crushing from the Acc-module (VSASL with crushing > A_{enc}). When the crushing is performed with a certain cut-off, the difference with the labeling without crushing indicates the overlap in labeling, i.e. when A_LV_L - A_CV_L provides much less signal than A_LV_C - A_CV_C, then the acceleration module labeled for a large part the same spins as the velocity module for that V_{enc}.

It is important to note that the labeling modules saturate spins above the cut-off acceleration or velocity. Therefore, when some spins were already saturated by the acceleration selective labeling module, the velocity selective labeling module can never result in additional saturation of these spins, i.e. no additional label is

MR experiments

Two types of measurements were performed. First, the amplitude of the four acceleration-sensitizing gradients were varied in 10 steps (G = 0 - 30 mT/m, $A_{enc} = \infty$ - 0.59 m/s^2), while the four velocity-sensitizing gradients were kept constant (G = 15 mT/m, V_{enc} = 2 cm/s). Second, the acceleration-sensitizing gradients had constant amplitude (G = 30 mT/m, A_{enc} = 0.59 m/s^2), while the velocity-sensitizing gradients varied in 10 different values (G = 0 - 20 mT/m, $V_{enc} = \infty$ - 1.5 cm/s). When the gradient amplitude is zero, no labeling will occur (note that in the control condition gradients with an amplitude of 5% of the constant cut-off are employed)[12]. For all measurements δ = 1 ms, Δ = 17.5 ms and τ = 18.9 ms and the motion sensitizing gradients were only encoded in the z-direction. The variable gradient amplitudes are shown in table 1.

A total of 9 healthy volunteers (5 males and 4 females, mean age 29 (21–63) years) participated in this study and written informed consent was obtained from all individual participants included in the study. This study was part of a project for protocol development as approved by the local Institutional research board.

All scans were performed on a 3 T scanner (Philips Healthcare, Best, The Netherlands) using a 32-channel head coil with 17 slices acquired at a 2.75 x 2.75 x 7 mm^3 resolution (multi-slice single-shot two-dimensional echo-planar imaging). The field-of-view was 220 x 220 mm^2 and a sensitivity encoding (SENSE) factor of 2.5 was used. TR/TE = 4108/15 ms with two inversion pulses at 50 and 1150 ms for background suppression, applied during the post labeling delay of 1600 ms. Spectral presaturation inversion recovery (SPIR) was performed to suppress the lipid signal. The sequence cycled through four different labeling combinations (A_CV_C, A_LV_L, A_CV_L and A_LV_C) and 9 averages were acquired for all 10 gradient amplitudes of V_{enc} and A_{enc}. This resulted in a total scan duration of 52 min for both scans together (4 × 10 × 9 × 2 = 720 acquisitions).

Table 1. Values of the gradient amplitudes (G) and the corresponding cut-off velocities (V_c, top rows) and cut-off accelerations (A_c, bottom rows) for the measurement combined with respectively constant acceleration-sensitizing gradients (δ = 1 ms, Δ = 17.5 ms, τ = 18.9 ms, G = 30 mT/m, A_c = 0.59 m/s^2) and velocity-sensitizing gradients (δ = 1 ms, Δ = 17.5 ms, τ = 18.9 ms, G = 20 mT/m, V_c = 1.5 cm/s).

G (mT/m)	0	1.25	2.5	5	7.5	10	12.5	15	17.5	20
V_C (cm/s)	∞	24	12	6.0	4.0	3.0	2.4	2.0	1.7	1.5
G (mT/m)	0	2.5	5	10	15	20	22.5	25	27.5	30
A_C (m/s^2)	∞	7.1	3.5	1.8	1.2	0.89	0.79	0.71	0.64	0.59

Image post-processing

The unsubtracted ASL-scans were realigned and the time series were corrected for motion with Motion Correction FMRIB's Linear Image Registration Tool (MCFLIRT)[13, 14] with a six-parameter rigid transformation in Oxford Centre for Functional MRI of the Brain (FMRIB)'s Software Library (FSL).[15] The anatomic T_1-weighted scan of each subject was segmented into 3 different tissue types (grey matter (GM), white matter (WM), and cerebral spinal fluid (CSF) probability maps) using the FMRIB's automated segmentation tool (FAST, FSL, Oxford, UK). The ASL-images are subtracted according to the combinations as described in figure 1c. The T_1-weighted image was registered to the average ASL-map of AccASL, VSASL and AccASL & VSASL. A binary GM mask was generated using a threshold of 75% GM probability in Matlab. The subtractions of the different labeling combinations were normalised by the average signal intensity in the GM for the SNS-ASL contrast that was kept constant (i.e. either VSASL or AccASL): so when the V_{enc} was varied, the signal was divided by the average AccASL signal in the GM. The amount of overlap in labeling by the combined sequential labeling with the Acc- and VS-module (A_CV_C-A_LV_L) was determined by the sum of the separate labeling modules minus the sequential labeling, divided by the labeling module with the constant cut-off, expressed with the following formula when V_{enc} is constant:

$$\text{Overlap} = \Big(\big((A_CV_C - A_LV_C) + (A_CV_C - A_CV_L)\big) - (A_CV_C - A_LV_L) \Big) / (A_CV_C - A_CV_L) \quad [1]$$

Results

In figure 2 a representative set of single slice ASL maps is shown for the different V_{enc}s and A_{enc}s (as presented in table 1). The top row of figure 2a shows independent measurements of AccASL, i.e. ($A_CV_C - A_LV_C$) with constant cut-off acceleration of 0.59 m/s² and the same number of averages as the images in the other rows, to serve as reference of reproducibility and to enable easy comparison. The velocity selective module is always executed in control condition (V_C), so the varying scale of V_{enc}s of the label condition as depicted on the horizontal axis has no influence on these measurements. Similarly, figure 2b shows in the top row VSASL images with a constant cut-off velocity of 2 cm/s ($A_CV_C - A_CV_L$). For the maps with a variable cut-off velocity (second row of figure 2a) or acceleration (second row of figure 2b) the lower the cut-off velocity (acceleration), the more signal was labeled, whereas for a cut-off velocity (acceleration) of infinity only noise was measured.

Both for the variable cut-off velocity and acceleration the sum of the separate AccASL and VSASL (($A_CV_C - A_LV_C$) + ($A_CV_C - A_CV_L$), third row of figure 2a/b) has a slightly higher signal intensity than the jointly acquired AccASL and VSASL ($A_CV_C - A_LV_L$, fourth row of figure 2a/b). The ASL-maps with constant acceleration crushing (fifth row of figure 2a; similar images with constant velocity crushing in figure 2b), the signal increases for decreasing cut-off, but the signal is less than without Acc-crushing (second row). In the bottom row of figure 2a (similar

images with variable acceleration crushing in the bottom row of figure 2b), AccASL is shown with variable velocity crushing and therefore, the most right image is similar to the images of the top row.

The group-averaged signal in grey matter for variable V_{enc} and A_{enc} are shown in figure 3. The signal is normalised by dividing through the constant signal, i.e. the mean GM signal of the top row of figure 2a (or 2b). Note that this constant signal serves as a reference experiment and was depicted at all cut-off velocities/accelerations with a similar number of averages for comparison, thereby also showing the reproducibility of the measurements. For the VSASL (A_CV_C-A_CV_L) in the left graph of figure 3 at the highest V_{enc} no label is created and when the V_{enc} is decreased, more signal is created, up to 178% of the AccASL signal strength (A_{enc} = 0.59 m/s²) in GM for a V_{enc} of 1.5 cm/s. For the AccASL (A_CV_C-A_LV_C) in the right graph of figure 3 at the highest A_{enc} no label is created and the more the A_{enc} is lowered, the more signal is created, up to 94% of the VSASL signal strength (V_{enc} = 2 cm/s) in GM for an A_{enc} of 0.59 m/s².

The difference between the combined sequential labeling with the Acc- and VS-module (A_CV_C-A_LV_L) and the sum of the signal of both labeling modules acquired separately (VSASL + AccASL, i.e. (A_CV_C-A_LV_C) + (A_CV_C-A_CV_L)) is a measure for the amount of spins that are saturated by both labeling modules. In figure 4 it is shown that at the highest cut-off there is hardly any difference between the two labeling combinations, which can be explained by that there is hardly any labeling achieved by either the velocity (left) or the acceleration selective module

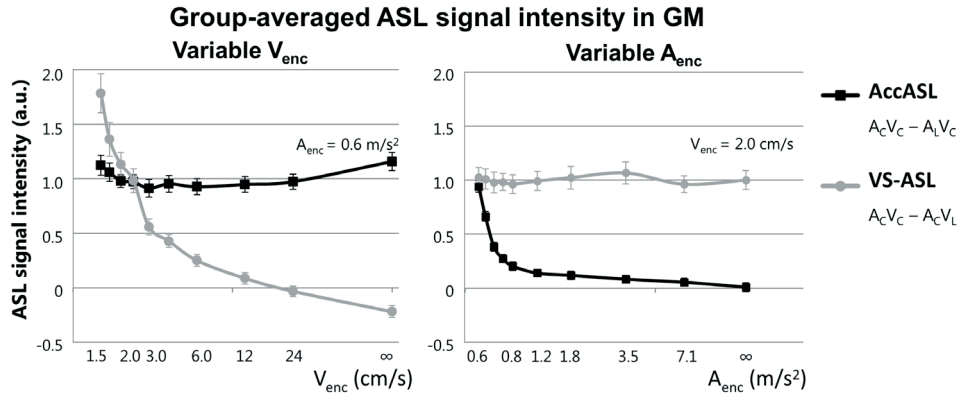

Figure 3 Group-averaged ASL signal intensities in GM of AccASL (A_CV_C-A_LV_C, dark line) and VSASL (A_CV_C-A_CV_L, light line). For the variable V_{enc} (left) the signal was normalised to the average AccASL GM signal and for the variable A_{enc} (right) normalised to the average VSASL GM signal. In VSASL with a single labeling module there is also venous label included, while for AccASL the signal is mainly arterial. Error bars indicate the standard error of the means as calculated over all subjects. Note that the constant signal was also depicted at all cut-off velocities/acceleration with a similar number of averages to illustrate the reproducibility of the measurements.

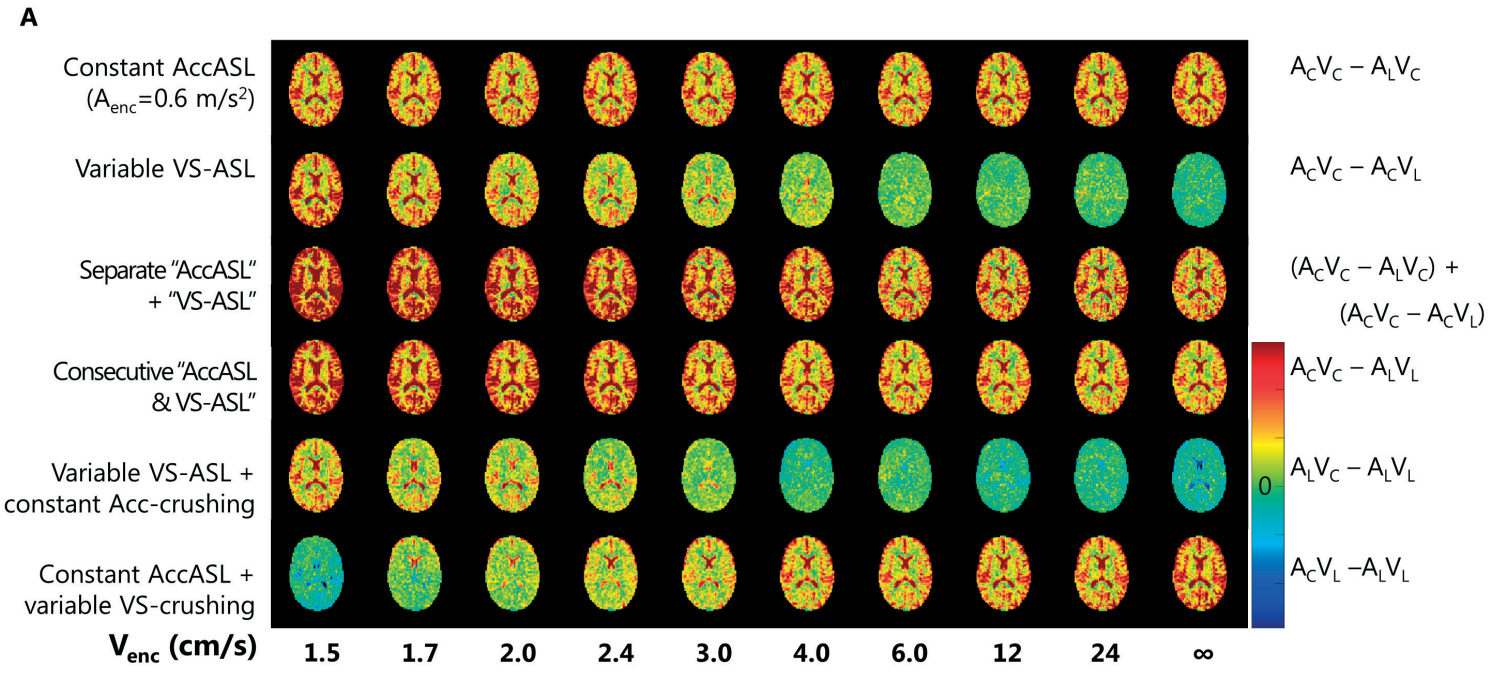

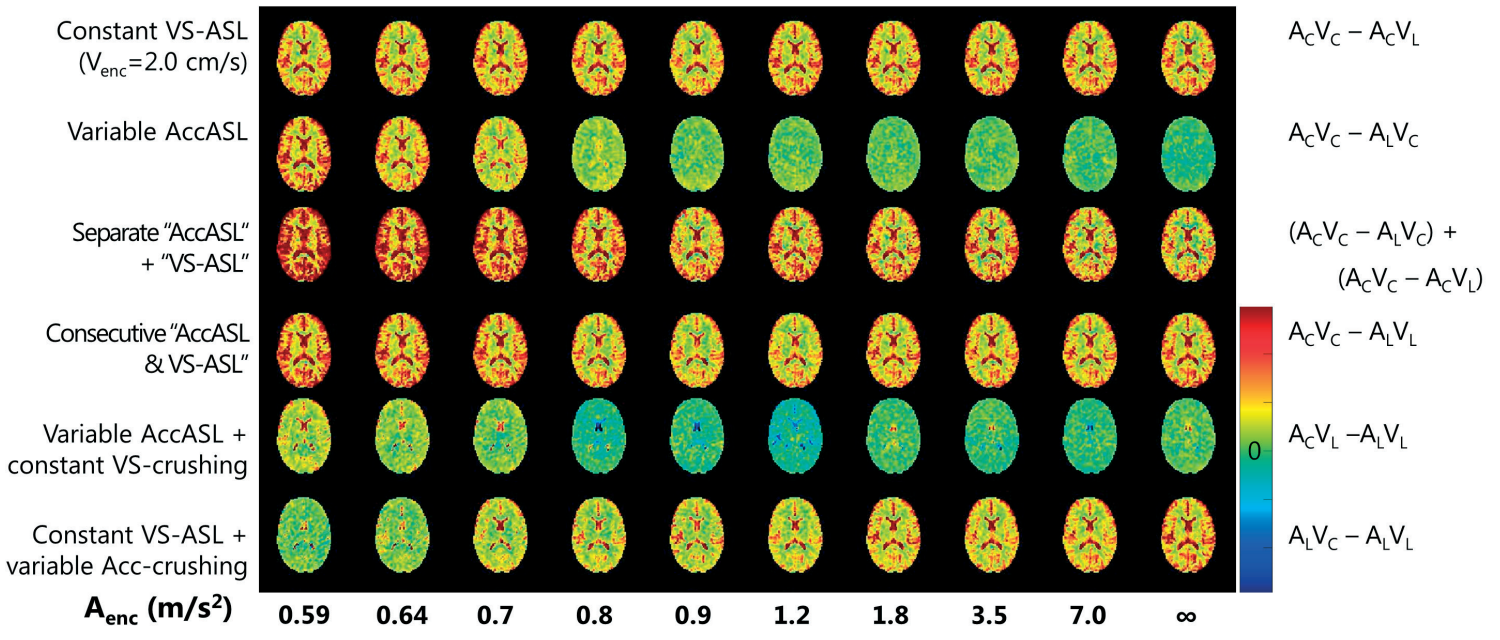

Figure 2 A representative set of single slice ASL maps acquired at different cut-off velocities **(A)** and accelerations **(B)**. The top row was acquired with a constant cut-off acceleration of 0.6 m/s² **(A)** and cut-off velocity of 2 cm/s **(B)** and was depicted with a similar number of averages to illustrate the reproducibility of the measurements.

(right). However, independent of which component of the labeling is varied, the sum of separately acquired signals are always higher than the combined labeling (up to 35% higher signal intensity at the lowest cut-off value).

To discriminate the amount of label that was uniquely labeled by one of the labeling modules from label jointly created by both labeling modules, the effect of crushing with one on the labeling by the other module was studied. In the top graphs of figure 5 the signal intensity in GM is shown when labeling had a variable cut-off and additional crushing was constant, where the difference between both labeling methods indicates the overlap in labeling. In the top left graph of figure 5 the effect of crushing with a constant A_{enc} of 0.59 m/s^2 on the variable Venc is clearly visible: a decrease up to 42% in the signal intensity at a V_{enc} of 1.5 cm/s was observed due to the crushing. A similar effect can be seen in the top right graph of figure 5, showing the effect of crushing with a constant V_{enc} of 2 cm/s on the variable A_{enc}.

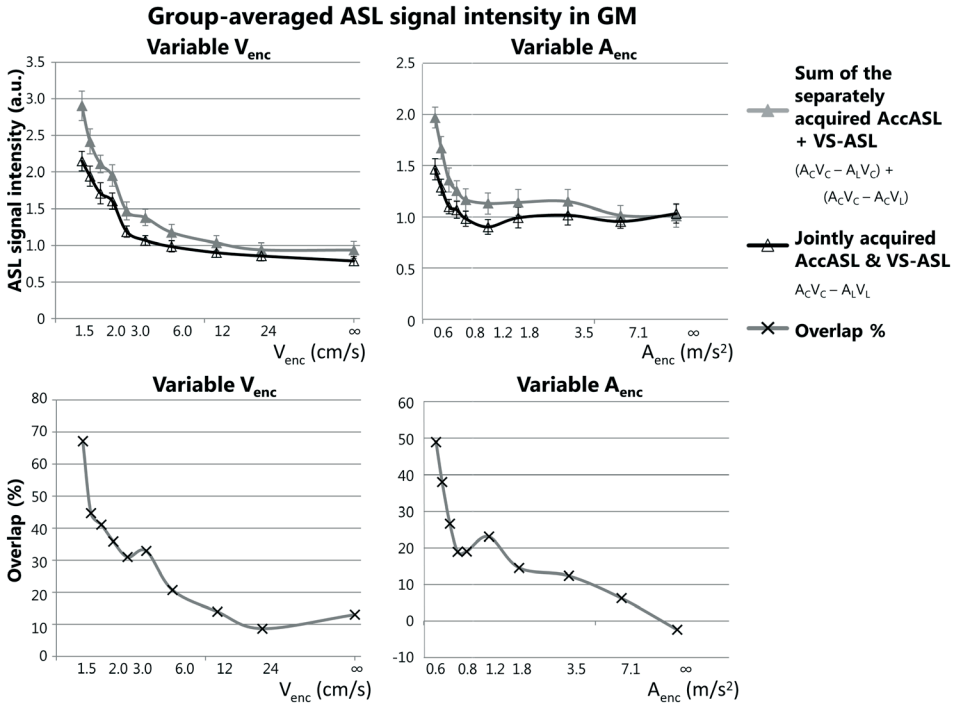

Figure 4 Group-averaged ASL signal intensities in GM (top images) of the sum of separate AccASL and VS-ASL (A_CV_C-A_LV_C + A_CV_C-A_CV_L, light line) and the joint subsequent acquisition of AccASL and VSASL (A_CV_C-A_LV_L, dark line). For the variable V_{enc} (left) the signal was normalised to the average AccASL GM signal (i.e. the mean GM signal of A_CV_C-A_LV_C, dark in left image of figure 3) and for the variable A_{enc} (right) normalised to the average VSASL (A_CV_C-A_CV_L, light in right image of figure 3) GM signal. The crossed line (bottom images) is the percentage overlap of the signal created with the variable labeling module to the signal of the constant labeling module. The error bars indicate the standard error of the mean as calculated over all subjects.

In the bottom graphs the signal intensity in GM is displayed with a constant cut-off for labeling and a variable cut-off for crushing. The difference between both curves indicates the overlap in labeling. A decrease up to 36.9% of the AccASL signal is possible with the highest V_{enc} crushing, as shown in the bottom left graph of figure 5. For the labeling with a constant cut-off velocity with crushing with a variable cut-off acceleration (bottom right graph of figure 5) a plateau with a signal intensity of 0.78 was reached between A_{enc} = 0.79 and 1.2 m/s^2, after which a steep decline in signal intensity was measured due to crushing with lower cut-off accelerations. By crushing with a variable A_{enc} the signal intensity was decreased up to 52.5%.

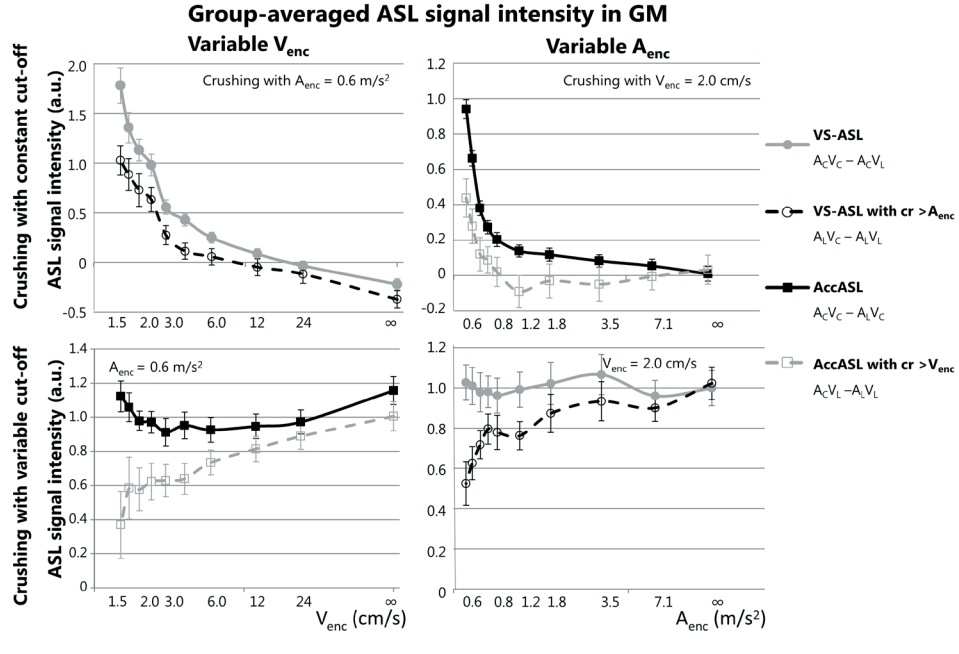

Figure 5 Group-averaged ASL signal intensities in GM of "AccASL" (A_CV_C-A_LV_C, dark, solid), "VSASL" (A_CV_C-A_CV_L, light solid), "VSASL with crushing due to AccASL" (A_LV_C-A_LV_L, dark open) and "AccASL with crushing due to VSASL" (A_CV_L-A_LV_L, light open). For the variable V_{enc} (left) the signal was normalised to the average AccASL GM signal and for the variable A_{enc} (right) normalised to the average VSASL GM signal by dividing by the constant signal. In the top row the crushing was performed with a constant cut-off and the labeling was with different gradient strengths. In the bottom row the crushing was performed with a variable cut-off, while the labeling was kept constant. The error bars indicate the standard error of the means of all subjects.

Discussion

For the recently introduced AccASL it is unknown where in the vasculature label is created. Several possible sources of the label origin have been mentioned previously, including cardiac cycle fluctuations, general flow acceleration/deceleration in the vasculature and tortuosity of the vessels leading to rapid changes in blood flow directions. Therefore, it has been suggested that the label could originate at both macro- and microvascular level and that the signal created with AccASL includes both CBF and CBV-weighting.[4] All of these effects, besides tortuosity, could explain the observation that with AccASL much more arterial than venous blood is labeled. The aim of this study was to obtain more insight into the origin of the labeling mechanism in AccASL by combining this method with a VS-module.

The most important findings of this study are that the label created with AccASL has a large overlap in vascular region with VSASL (approximately 50%), but also originates from smaller vessels closer to the capillaries. This shows that AccASL is able to label spins both in the macro-, meso- as well as in the microvasculature.

The indication that AccASL shares for a significant part the same label origin as VSASL can be seen from Figure 4 that shows that the sum of separately acquired AccASL and VSASL scans ($A_CV_C - A_LV_C + A_CV_C - A_CV_L$, in light blue) results in a higher signal intensity compared with sequentially acquired AccASL and VSASL ($A_CV_C - A_LV_L$, in dark blue). This difference reaches up to 35% for the lowest cut-off. This argument is based on the fact that spins can only be saturated once, i.e. when AccASL and VSASL would label exactly the same spins in the vascular tree, the application of the VS-module directly after the AccASL would have no effect and equal signal intensity would be measured. When assuming the signal intensity of AccASL, i.e. ($A_CV_C - A_LV_C$), to be one, the intensity of VSASL ($A_CV_C - A_CV_L$) as well as the signal of sequentially acquired AccASL and VSASL ($A_CV_C - A_LV_L$) would also be one, whereas the sum of separately acquired AccASL and VSASL scans (($A_CV_C - A_LV_C$) + ($A_CV_C - A_CV_L$)) would yield twice the amount of signal. When looking at Figure 4 at the point where AccASL and VSASL both create a similar amount of label (i.e. the point where the sum of separately acquired VSASL and AccASL equals 2.0, i.e. at a V_{enc} of 2.4 cm/s in the left graph and at an A_{enc} of 0.59 m/s^2 in the right graph), consecutive labeling ($A_CV_C - A_LV_L$) shows only 1.6 and 1.5 times the reference value, implying an overlap in signal of respectively 40 and 50%. However, the fact that the overlap was much less than 100% indicates that the two SNS-ASL modules also label spins in different parts of the vasculature. This is further confirmed by the significant higher signal (up to 120% higher signal for the lowest V_{enc}) when performing a VS-module immediately after AccASL (dark blue line from the left graph of figure 4) as compared with just AccASL (red line from the left graph of figure 3). The comparison of performing the VS-module immediately after AccASL (dark blue line from the right graph of figure 4) compared with only VSASL

(green line from the right graph of figure 3) also showed significant higher signal, up to 50% for the lowest A_{enc}. The higher signal points to the fraction of spins that could additionally be labeled by the other labeling module. When interpreting these findings, one has to keep in mind that in this study only a single velocity selective labeling module was performed, instead of using a second labeling module just before imaging as is part of the original VSASL methodology.[2] An isolated velocity selective labeling block will also generate venous signal and in previously research we showed that the amount of venous label generated by a single velocity selective module is much more than that of an acceleration module.[4] In the original VSASL sequence, this venous signal will be subsequently excluded by the second VS-module.[3,4] Some of the difference in signal intensity between the velocity and acceleration modules, will therefore be from venous spins that will be more affected by the velocity encoding than the acceleration encoding. This can explain why adding a VS-module to the AccASL scan, resulted in much more signal increase than when adding an Acc-module to the VSASL scan.

Further confirmation that a significant component of signal created by the Acc- and VS-module originates from different parts of the vasculature can be deduced from the results in which labeling was combined with crushing. When crushing with a constant V_{enc} of 2 cm/s the signal intensity in the GM decreased as shown in the top right graph from figure 5. For A_{enc}s larger than 0.79 m/s^2 the crushing is effective as shown by the fact that the orange curve is almost horizontal. This implies that for these relatively weak acceleration strengths, only spins are labeled that flow faster than 2 cm/s (the V_{enc} of the crushing). However, when the A_{enc} is decreased below 0.79 m/s^2, crushing is no longer as effective as a steep increase in signal is found, proofing that the additional label created by the stronger gradients in the acceleration module originates from spins with a velocity smaller than 2 cm/s, i.e. closer to the capillaries. For constant AccASL with variable crushing by a VS-module (lower left graph in figure 5), it can be seen that for a Venc smaller than 1.5-3 cm/s the slope of signal intensity curve gets steeper. Velocities lower than 3 cm/s are found in the arterioles, where the flow velocity rapidly decreases towards the capillaries, again pointing to significantly labeling of spins in the capillaries by AccASL. Furthermore, it should be noted that by crushing performed with the acceleration selective labeling module, like in the lower right graph of figure 5, label created by the velocity selective module that also resides in the venous compartment will not be affected, which could be an explanation for the smaller effect of the crushing. The other way around, with crushing by the velocity selective module also venous signal will be saturated twice, although this will have hardly any influence on the AccASL signal, since this label will mainly be in the arterial compartment.

For AccASL a lower Aenc could have been chosen, to label even further into the vascular tree. This was, however, not possible due to hardware restrictions of the scanner limiting the gradients amplitude (G) to these values. Smaller A_{enc}s could be achieved by increasing the time between the gradients (Δ and τ) or increasing the gradient duration (δ), however

both option would lead to an increased diffusion sensitivity. In this study, we opted for employing the same δ and Δ for all SNS-modules and only vary the gradient polarity (velocity versus acceleration) and gradient strength. Increasing the gradient strength will lead to more diffusion weighting with a maximum b-value of 2.4 s/mm^2 for AccASL with G = 30 mT/m, Δ = 17.5 ms, τ = 18.9 ms and δ = 1 ms and 1.4 s/mm^2 for VSASL with G = 20 mT/m, Δ = 17.5 ms, τ = 18.9 ms and δ = 1 ms. For typical values of brain apparent diffusion coefficient, 0.8x10^{-3} mm^2/s in GM and 2.5x10^{-3} mm^2/s in CSF, the b-values in this study could theoretically cause a systematic difference between labeled and control image of less than 1%.[1, 4] Furthermore, the influence of contamination from eddy current and/or diffusion effects was evaluated on a liquid gel phantom (shown in the supplementary material). This showed that the intensity of the artefacts was approximately only 0.1% of the M0-signal (acquired with the same imaging parameters as for the ASL scans, but no labeling performed) in the same voxels for the constant labeling module. An increase in signal was found when increasing the gradient strengths, up to 0.23% of the M0-signal for the lowest V_{enc} and A_{enc}. This indicates that contamination from eddy current/diffusion effects is very limited. Also, as expected these artefacts show as large regions of signal change, which would affect the white matter/gray matter contrast significantly in the perfusion maps of the volunteers if it would be a significant effect. No such effects were observed in the *in vivo* data in figure 2.

This study has some limitations. First of all, no cardiac triggering was applied during the measurements. The pulsatile effects from the cardiac cycle will be averaged over the dynamics and will have no specific influence on the data.

Secondly, it is important to realize that the presented results are not independent from each other, since they are all calculated by adding and subtracting four types of images. For example, the image with both labeling modules in control condition (A_CV_C), is used to calculate AccASL, VSASL, the joint AccASL & VSASL signals, whereas in the calculation of the sum of the separate AccASL and VSASL maps it is even included twice. This implies that noise and artefacts in this map will be present in the results of all these maps, which might result in erroneous conclusions. Similarly, the other three acquisitions (A_LV_L, A_CV_L, A_LV_C) are used in multiple calculations.

Thirdly, in the control condition a small gradient amplitude was used similar as proposed for VSASL with linear RF-pulses by Duhamel et al[12] to reduce the errors resulting from imperfect flip angles. In this study adiabatic RF-pulses were employed and in the labeling condition with varying gradients strengths a zero amplitude starting value was chosen. Therefore, no gradients in the control condition would have been a more optimal choice, although the amplitude (5% of the constant cut-off) of these gradients was low enough to not significantly influence the results. Finally, the gradients of the labeling modules were only applied in a single, similar direction, whereas blood flowing through the branches of the vasculature will be in all direction and will also change direction; especially in the capillaries the flow will be in random directions. So, the assumption that all spins with a flow velocity above the V_{enc} are

labeled with VSASL is not true, since only spins flowing in the z-direction with a velocity above the V_{enc} will be labeled. Nevertheless, the same directional dependency is present in the VSASL as well as in the AccASL labeling module, making the results of this study still valid.

Conclusion

In conclusion, AccASL is able to label spins in both the macro- as well as micro-vascular region and the label created with AccASL has a large overlap in vascular region with VSASL, but depending on the A_{enc} the label from AccASL could also originate from regions closer to the tissue. This might imply that AccASL could be preferable over VSASL in patients with pathologies showing prolonged arrival times, due to the label being closer to the tissue.

References

1. Wong EC, Buxton RB, Frank LR. Quantitative imaging of perfusion using a single subtraction (QUIPSS and QUIPSS II). Magn Reson Med. 1998;39:702-708.
2. Mildner T, Moller HE, Driesel W, et al. Continuous arterial spin labeling at the human common carotid artery: the influence of transit times. NMR Biomed. 2005 Feb;18(1):19-23.
3. Wong EC, Cronin M, Wu WC, et al. Velocity-selective arterial spin labeling. Magn Reson Med. 2006 Jun;55(6):1334-1341.
4. Schmid S, Ghariq E, Teeuwisse WM, et al. Acceleration-selective arterial spin labeling. Magn Reson Med. 2014;71(1):191-199.
5. Qiu D, Straka M, Zun Z, et al. CBF measurements using multidelay pseudocontinuous and velocity-selective arterial spin labeling in patients with long arterial transit delays: comparison with xenon CT CBF. J Magn Reson Imaging. 2012 Jul;36(1):110-119.
6. Guo J, Wong EC. Increased SNR efficiency in velocity selective arterial spin labeling using multiple velocity selective saturation modules (mm-VSASL). Magn Reson Med. 2015;74(3):694-705.
7. Nguyen TD, de Rochefort L, Spincemaille P, et al. Effective motion-sensitizing magnetization preparation for black blood magnetic resonance imaging of the heart. J Magn Reson Imaging. 2008 Nov;28(5):1092-100.
8. Piechnik SK, Chiarelli PA, Jezzard P. Modelling vascular reactivity to investigate the basis of the relationship between cerebral blood volume and flow under CO2 manipulation. NeuroImage. 2008 1/1/;39(1):107-118.
9. Schmid S, Heijtel DF, Mutsaerts HJ, et al. Comparison of Velocity- and Acceleration-Selective Arterial Spin Labeling with $[^{15}O]H_2O$ Positron Emission Tomography. J Cereb Blood Flow Metab. 2015 August 1, 2015;35(8):1296-1303.
10. Conolly S, Glover G, Nishimura D, et al. A reduced power selective adiabatic spin-echo pulse sequence. Magn Reson Med. 1991;18:28-38.
11. Priest AN, Taviani V, Graves MJ, et al. Improved artery–vein separation with acceleration-dependent preparation for non–contrast-enhanced magnetic resonance angiography. Magn Reson Med. 2014;72(3):699-706.
12. Duhamel G, de Bazelaire C, Alsop DC. Evaluation of systematic quantification errors in velocity-selective arterial spin labeling of the brain. Magn Reson Med. 2003 Jul;50(1):145-153.
13. Smith S, Jenkinson M, Woolrich MW, et al. Advances in functional and structural MR image analysis and implementation as FSL. NeuroImage. 2004 //;23, Supplement 1:S208-S219.
14. Woolrich MW, Jbabdi S, Patenaude B, et al. Bayesian analysis of neuroimaging data in FSL. NeuroImage. 2009 3//;45(1, Supplement 1):S173-S186.
15. Jenkinson M, Bannister P, Brady M, et al. Improved optimisation for the robust and accurate linear registration and motion correction of brain images. NeuroImage. 2002;17(2):825-841.

5

Effect of crushing with Acceleration and Velocity selective labeling modules on ASL signal at multiple post labeling delays

S Schmid
ET Petersen
MJP van Osch

Magnetic resonance materials in physics, biology and medicine, 2016;
29(Suppl 1): S55

Introduction

The recently introduced spatially non-selective acceleration selective arterial spin labeling (AccASL) [1] tags blood based on flow acceleration instead of spatial localization, like is employed in traditional ASL methods. Nevertheless, the exact origin of the AccASL signal is not completely understood. The aim of this study was to get more insight in the label origin of AccASL and especially where in the vascular tree the label is created. To this end, time-encoded pCASL (te-pCASL)[2-4] was followed by an acceleration selective module that will crush the ASL-signal whenever it is at a location in the vascular tree, where normally AccASL-signal is created. For comparison, the same procedure was repeated with a velocity selective (VS) module.[5]

Materials and methods

Six volunteers (3 male, 3 female, mean age 36 y.o. (19-63)) were scanned at 3T (Achieva MRI scanner, Philips Healthcare) using te-pCASL (see figure 1) after providing informed consent (IRB-approved protocol). The total labeling duration of 3500 ms in the Hadamard-8 labeling scheme was divided in 7 blocks of 1100, 650, 500, 350 and 3×300 ms to provide compensation for T1-decay of the label. Subsequently, a motion sensitizing gradient (MSG) labeling module with acceleration (G_A = 30 mT/m in z-direction, δ = 1 ms, Δ = 17.5 ms, τ = 18.9 ms, and A_{enc} = 0.6 m/s^2), velocity sensitive gradients (G_V = 13 mT/m in z-direction, δ = 1ms, Δ = 17.5 ms, τ = 18.9 ms, and V_{enc} = 2.4 cm/s), or without gradients (control, i.e. normal te-pCASL) was employed . A total of 408 images were acquired (single shot FFE-EPI, voxel size = 3×3×7mm, 17 slices, TR/TE/fa = 4275/14/90°, total scan time = 29 min): 8 images per Hadamard encoding scheme, repeated 17 times and 3 crushing conditions.

Results

In the early arterial phase all signal was crushed by the MSG as shown in the perfusion maps of figure 2. The amount of signal in grey matter crushed with the MSG decreased over time, see figure 3. More signal was crushed with velocity than acceleration selective gradients, with the largest difference in crushing between 1000-1500 ms.

Discussion and conclusions

Most signal was crushed at early time-points due to crushing gradients in the main flow direction and flows within the cut-off range, while less signal could be crushed at later time

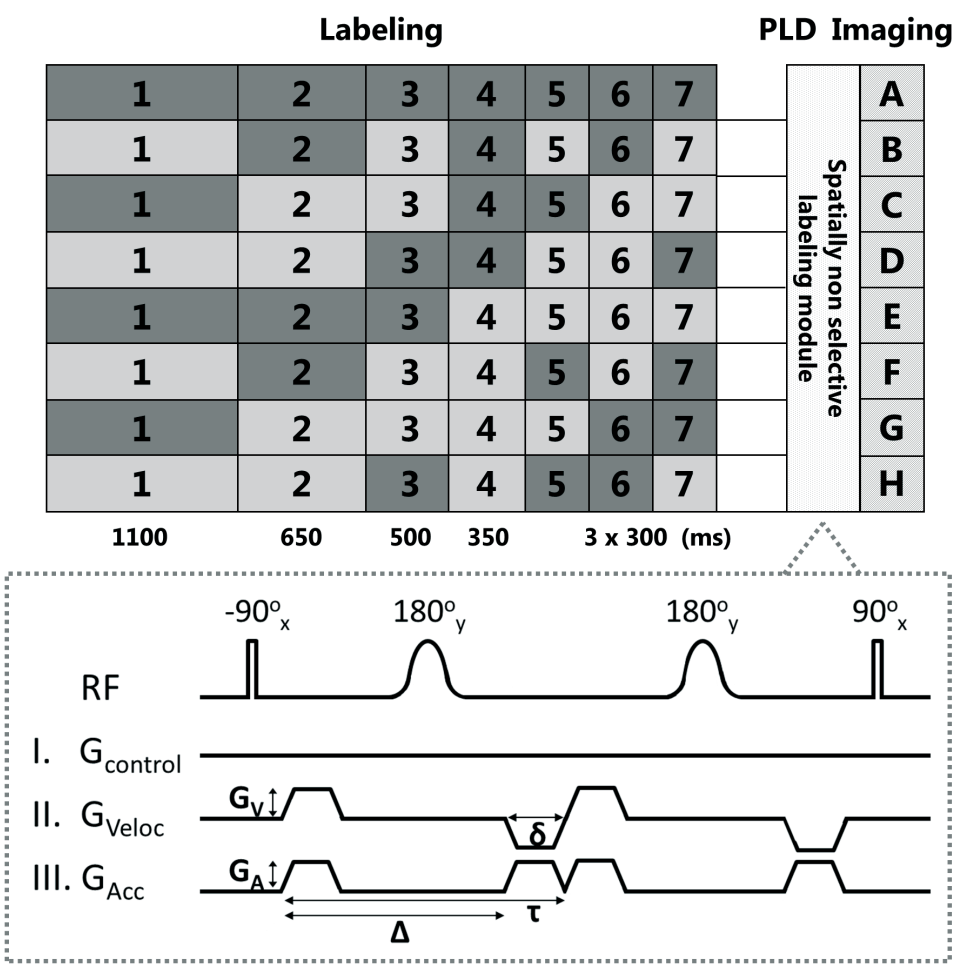

Figure 1 Schematic overview of the measurement method. Labeling scheme for time encoded pCASL with block duration below the columns. Just before imaging, at the end of the post labeling delay (PLD) 3 types of crushing (velocity or acceleration selective or no gradients) were alternatingly performed. FOCI background suppression pulses were applied at 1830 and 3150ms, after which the label and control condition were switched (not shown in this figure). Dark blocks in labeling= label, light blocks in labeling = control, G = gradient strength, δ = gradient duration, Δ = time between the first and second gradients and τ = time between the first and third gradients.

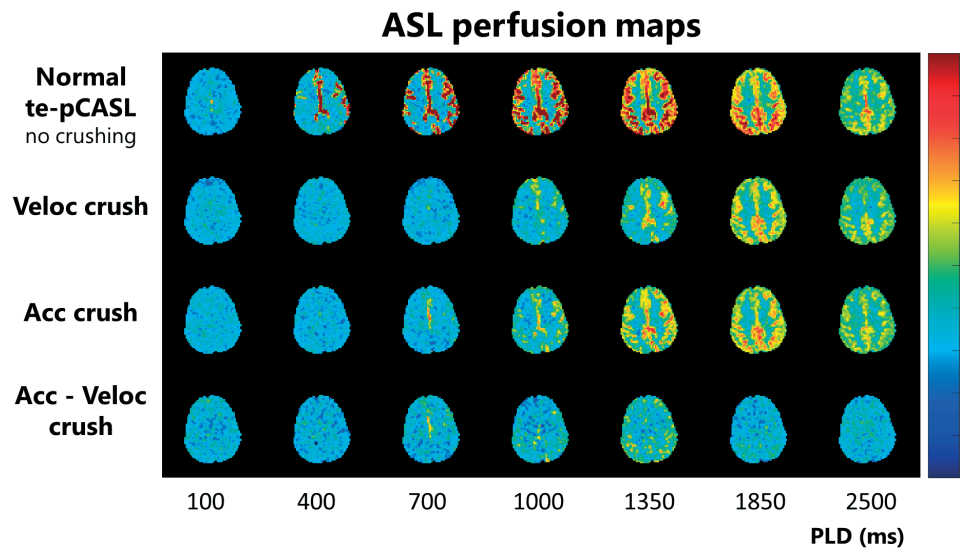

Figure 2 Perfusion maps for subsequent time points in a single volunteer. No gradients (top row), crushing with velocity (second row) and acceleration (third row) selective gradients. The maps in the bottom row show the difference between the crushing with velocity and acceleration selective gradients.

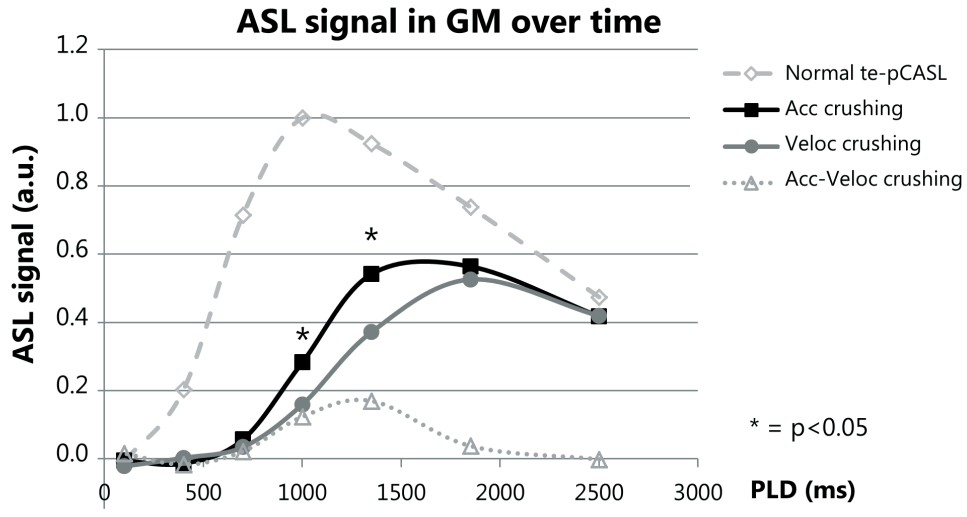

Figure 3 Group averaged ASL signal in GM over time for the 3 crushing conditions. * indicates significant difference between acceleration and velocity selective crushing (p<0.05).

points, maybe because the label did already exchange with tissue magnetization. The gradient strengths as employed in this study were chosen based on earlier studies of us that showed to generate equal amount of signal with these settings for AccASL and VSASL at a 1600ms PLD. This might indicate that AccASL does create label within the microvasculature, whereas VSASL creates more signal in the large vasculature.

References

1. Schmid S, Ghariq E, Teeuwisse WM, et al. Acceleration-selective arterial spin labeling. Magn Reson Med. 2014;71(1):191-199.
2. Gunther M. Encoded Continuous Arterial Spin Labeling. Workshop on Cerebral Perfusion and Brain Function: Novel Techniques and Applications; 2007; Salvador da Bahia, Brazil
3. Dai W, Shankaranarayanan A, Alsop DC. Volumetric measurement of perfusion and arterial transit delay using hadamard encoded continuous arterial spin labeling. Magn Reson Med. 2013;69(4):1014-22.
4. Teeuwisse WM, Schmid S, Ghariq E, et al. Time-encoded pseudocontinuous arterial spin labeling: Basic properties and timing strategies for human applications. Magn Reson Med. 2014 72:1712–1722
5. Wong EC, Cronin M, Wu WC, et al. Velocity-selective arterial spin labeling. Magn Reson Med. 2006;55(6):1334-1341.

6

Time-efficient determination of spin compartments by time-encoded pCASL T_2-relaxation-under-spin-tagging and its application in hemodynamic characterization of the cerebral border zones

S Schmid
WM Teeuwisse
H Lu
MJP van Osch

NeuroImage, 2015; 123, 72-79

Abstract

Information on the water-transport across the blood-brain-barrier can be determined from the T_2 of the arterial spin labeling (ASL) signal. However, the current approach of using separate acquisitions of multiple inversion times is too time-consuming for clinical (research) applications.

The aim of this study was to improve the time-efficiency of this method by combining it with time encoded pseudo Continuous ASL (te-pCASL). Furthermore, the hemodynamic properties of the border zone regions in the brains of healthy, young volunteers were characterized as an example-application.

The use of te-pCASL instead of multi-TI pCASL significantly reduced the total scan duration, while providing a higher temporal resolution. A significantly lower cerebral blood flow (CBF) was found in the border zone regions compared with the central regions, in both the posterior and the middle cerebral artery (MCA) flow territory. The arterial transit time (ATT) was almost two times longer in the border-zone regions than in the central regions ($p<0.05$), with an average delay in ATT of 382 ms in the posterior and 539 ms in the MCA flow territory. When corrected for the ATT, the change in T_2 over time was not significantly different for the border-zones as compared to the central regions.

In conclusion, te-pCASL-TRUST provided a time efficient method to distinguish spin compartments based on their T_2. The ATT in the border zone is significantly longer than in the central region. However, the exchange of the label from the arterial to the tissue compartment appears to be at a similar rate.

Introduction

Arterial spin labeling (ASL) can be used as a non-invasive MR technique to measure tissue perfusion by exploiting arterial blood as an endogenous tracer. Magnetic labeling is performed in a slab proximal to the imaging region, after which a delay time allows the labeled blood to travel to the cerebral microvasculature and to exchange with the spins in the tissue compartment. The transport of labeled spins from blood to the tissue can be subdivided in four stages. First, the time it takes for the labeled blood to arrive in the imaging slice, often referred to as the arterial transit time (ATT); second, the transport within the slice from the larger arteries and arterioles towards the capillary bed; thirdly, most of the water will cross the blood-brain-barrier, e.g. via aquaporins, into the tissue compartment; and fourth, the water will be eliminated via the veins either by re-uptake from the tissue compartment or via exclusive arterial-to-venous blood flow.[1]

Multi-delay ASL can be used to obtain information about the ATT, whereas the inclusion of a quantitative T_2-measurement, e.g. by Malcolm Levitt's Composite-Pulse Decoupling sequence (MLEV),[2] enables the determination of the spin compartment. The T_2-relaxation values at 3T known from literature show clear differences between the compartments: ~175 ms (at a hematocrit of 42 ± 6.4 %) in the arterial compartment,[3] ~90 ms in GM tissue,[4] and ~50 ms in the venous compartment (at an oxygenation level of 60 %).[3] Using multi-time point pseudo-Continuous Arterial Spin Labeling (pCASL) [5] acquisitions, Liu et al [6] demonstrated the feasibility of compartment determination based on T_2-measurements using T_2-Relaxation-Under-Spin-Tagging (TRUST) [7] as well as the possibility to follow changes in spin compartment localization by using four different post labeling delay (PLD) times. However, with a total scan time of more than 30 min for 4 time points, the acquisition time of this technique is too long for clinical application. Moreover, shortening the applied bolus duration can increase its sensitivity to identify compartment transitions. Another T_2-ASL method was based on a 3D-GRASE (gradient and spin echo) pulsed ASL sequence with multi-echo read-out to measure the water transfer processes between arterial blood and brain tissue and was used to voxelwise derive the mean blood to extravascular compartment transfer time.[8]

Recently a new ASL approach was proposed, named time encoded pseudo continuous ASL (te-pCASL, also known as Hadamard encoded ASL), which enables the retrieval of the ATT in a time efficient way with the same signal-to-noise ratio (SNR) compared with separate multi-time point pCASL scans.[9-12] The combination of te-pCASL with TRUST can provide a time efficient method to monitor water transport from the intra- to the extravascular compartment. Such measurements would not only be interesting to study pathology, but also to better understand normal human cerebral physiology. For example, little is known about differences in hemodynamics between the central part of flow territories and their border zone regions or watershed areas. It is well established that border zone regions are more

vulnerable to ischemia and infarction, due to acute reductions in perfusion pressure or severe systemic hypotension[13-15] and that these border zones show prolonged ATT compared to central regions. However, it is unknown whether the water transport from the larger arteries and arterioles towards the capillary bed and across the blood brain barrier into the tissue is also slower.

The aim of this study is to employ te-pCASL in combination with TRUST to enable improved and accelerated measurements of water-transport across the blood-brain barrier based on the T_2 of labeled spins, including voxelwise mapping of the T_2-evolution over time. With this method the hemodynamic properties of the border zone regions in the brains of young healthy volunteers is assessed.

Methods

Time encoded-pCASL-TRUST pulse sequence

In typical ATT measurements with multi-delay ASL, control and label images are acquired in multiple scans, each at a different post labeling delay. However, this is very time consuming due to the sequential acquisition and the idle post labeling period. For time-encoded pCASL, almost all time from the start of encoding till shortly before imaging is utilized for encoding PLD information into the ASL-signal, without having to repeat the scan for each separate

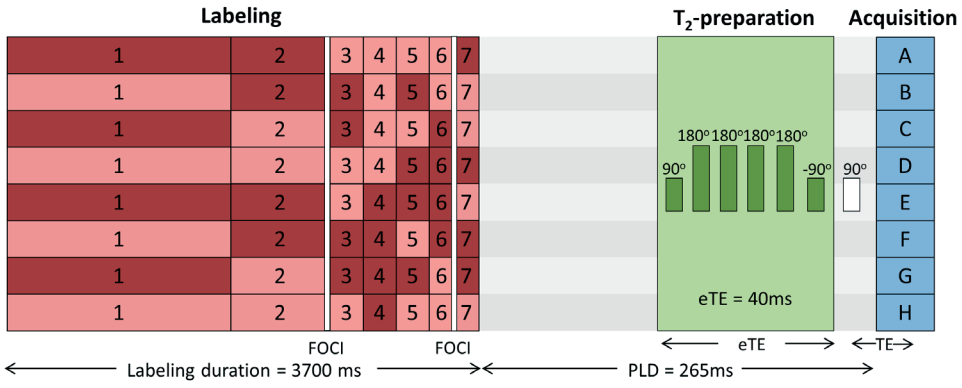

Figure 1 Schematic overview of te-pCASL-TRUST. The time encoded labeling module of 3700 ms shows the 8 different encoding lines , each divided into 7 blocks. The darker blocks depict when labeling is performed and the lighter blocks the control condition. The duration of the blocks is a balance between providing sufficient signal-to-noise ratio for blocks with longer post labeling delays and higher temporal resolution for the shorter PLDs to allow accurate ATT measurement. Just before the 90° excitation pulse for imaging, a T_2-preparation module is inserted, which consists of a series of non-slice-selective pulses that induce T_2 weighting, in this example eTE = 40 ms with four 180 ° pulses. The acquisition of a single Hadamard encoding scheme delivers 8 images, A-H.

PLD. The labeling module is divided into small blocks, which are tagged according to a Hadamard matrix to determine whether a block will contain a "label" or "control" condition, i.e. whether water spins in blood are inverted or not. A Hadamard-8 matrix was applied in this study in which the total labeling duration of 3700 ms was divided into 7 blocks of respectively 1300, 600, 3x400 and 2x300 ms, followed by a minimum PLD of 265 ms, as shown in figure 1. The durations of the time-encoded blocks were chosen to provide sufficient signal to noise ratio (SNR) in the perfusion phase, while allowing accurate ATT measurement by providing higher temporal resolution for the shorter PLDs. In post-processing, the Hadamard matrix was used to determine whether an image should be added or subtracted to calculate the signal contribution of individual labeling blocks, hence for different PLDs. Since the Hadamard scheme was repeated 9 times, effectively for each of the 7 PLDs, data are obtained from 72 acquisitions, half of which is label and the other half control, which is comparable to a single PLD ASL experiment of 36 averages. By using the time encoded method, the total scan duration will be shorter than when acquiring the same number of acquisitions with a multi-time point ASL technique, leading to a higher temporal SNR. The pCASL parameters were 0.5 ms Hanning pulses with a 1.2 ms peak-to-peak interval, 21° flip angle, a mean gradient of 0.6 mT/m and maximum gradient of 6 mT/m.

The T_2-preparation module was performed during the PLD, just before imaging with 0, 4, 8, and 16 refocusing pulses at four effective echo times (eTE): 0, 40, 80 and 160 ms. The signs of the non-selective 180°, T_2-preparation pulses were arranged in an MLEV pattern to minimize the effect of pulse imperfections due to B1 and B0 inhomogeneities.[16, 17] Background suppression was applied with frequency offset corrected inversion (FOCI) pulses (β = 810 s^{-1}, μ = 6.2, duration = 15.3 ms, BW = 1.599 kHz) [18] reaching from the labeling slab to above the highest slice of the imaging region, which requires inversion of the Hadamard scheme between these pulses. The FOCI pulses at 1900 and 3400 ms are positioned between the labeling blocks and the timing of the pulses was optimized to achieve the best possible suppression of cerebral spinal fluid (CSF), grey matter (GM) and white matter (WM) signal, with the use of only 2 pulses.

MRI experiments

Eight healthy volunteers (age 21-30 y, 5 female, 3 male) participated in this study. This study was part of a project for protocol development as approved by local Institutional Research Board and informed written consent was obtained for each participant before inclusion. All scans were performed on a 3T Achieva-TX scanner (Philips Healthcare, Best, The Netherlands) using a 32-channel head coil. 11 slices were acquired at a 3.2 × 3.2 × 6 mm^3 resolution (multi slice single-shot two-dimensional echo-planar imaging). The field-of-view was 220x220 mm^2 and a sensitivity encoding (SENSE) factor of 2.5 was used. Spectral pre-saturation inversion recovery (SPIR) was performed to suppress the lipid signal.

A total of 36 acquisitions formed one complete te-pCASL-TRUST dataset, which consisted of 9 acquisitions per eTE, multiplied by 4 eTE values. Each acquisition is defined as the complete Hadamard scheme of 8 encoding steps. Two te-pCASL-TRUST datasets were collected in each participant, one with and the other without vascular crushing gradients (crushers with V_C = 5 cm/s along three axes played out simultaneously resulting in an effective V_C of 2.9 cm/s) with a respective acquisition time of 22:34 min (TR/TE = 4423/17 ms) and 22:57 min (TR/TE = 4501/17 ms).

A Regional Perfusion Imaging (RPI) scan was performed to determine the 3 major flow territories (left ICA, right ICA and posterior) with the same geometry and orientation as the ASL scan (labeling duration 1650 ms, PLD 1525 ms, background suppression).[19] A GM mask was created by only including voxels with a signal intensity higher than the 55th percentile of a histogram of the perfusion-weighted signal of the RPI scan.

Data analysis

Using the Oxford Centre for Functional MRI of the Brain (FMRIB)'s Software Library (FSL), the unsubtracted ASL time series were motion corrected with Motion Correction FMRIB's Linear Image Registration Tool (MCFLIRT) with a six-parameter rigid transformation.[20] The ASL signal at each PLD was calculated by applying the Hadamard scheme to determine whether an image should be added or subtracted. Signal strength was normalized through dividing by the block duration. The subtraction of the crushed from the non-crushed scans was used to identify the intravascular signal. After smoothing with a 3x3 Gaussian kernel with a standard deviation of 0.5, the following mono-exponential function was used to fit the signal of the scans with vascular crushing over the different eTEs for each PLD.

$$\Delta M(eTE) = \Delta M(0) \cdot \exp\left(\frac{-eTE}{T_2}\right) \quad [1]$$

This delivered a voxelwise map of the T_2-value as well as the amplitude of the ASL signal, $\Delta M(0)$.[7] In addition, the T_2-value of the average vascular crushed GM signal of each flow region was calculated.

Border zone regions

Three major border zone regions can be distinguished: between the cortical branches of the anterior cerebral artery (ACA) and the middle cerebral artery (MCA) lies the anterior border zone region; between the cortical branches of the MCA and the posterior cerebral artery lies the posterior border zone region; and between the superficial branches of the MCA and ACA, which is along and above the lateral ventricle, lies the internal border zone region.[13-15] Since the label that is created in the internal carotid arteries (ICA) reaches both the MCA and ACA flow territory, we focussed on the posterior border zone region in this study. The distinction of the flow territories from the RPI scan data was performed with the clustering function "kmeans" from Matlab (The MathWorks, Inc, Natick, MA). Ten voxels were manually selected on the edge of the flow territories on either side of the posterior border zone. To limit contamination from the white matter, only voxels with a signal intensity within the top 15 percentile of the histogram of the perfusion-weighted signal of the RPI scan were included. These ten border zone voxels were compared with 10 voxels selected from the central region of the posterior and MCA flow territory using the same selection criteria. The signal averaged over the central or border zone voxels was then fitted to the kinetic perfusion model of Buxton to estimate the CBF and ATT.[21] These hemodynamic properties were statistically compared using paired t-tests. For each PLD the T_2 was calculated with a mono-exponential fit (equation 1) on the average signal of these voxels. The T_2-curves were shifted individually by the subject specific ATT of the flow territory to align the curve based on the transition and remove the delay caused by the arrival time. These shifted curves were interpolated at a 50 ms interval in Matlab. An ANOVA with 2 factors was applied with $\alpha<0.05$ followed by Bonferroni correction for multiple comparison to compare the moment of transition of the labeled spins from the arterial towards the tissue compartment.

Results

ASL-signal over time

In figure 2a the ASL-maps (3 slices) with and without vascular crushing from a single volunteer at different PLDs at eTE = 0 ms are shown. The signal in the large arteries was calculated from the difference between the crushed and non-crushed scans. For short PLDs the ASL signal intensity increases in the arteries, before spreading out into the tissue. The intravascular signal (with a flow velocity greater than 2.9 cm/s) is clearly visible in the posterior flow territory until 1265 ms post labeling, while at that time point the ASL signal in the left and right ICA flow territory has already left the larger vessels. The average GM signal intensity of all subjects at eTE = 0 ms for each PLD is shown in figure 2b. The maximal intravascular signal is reached around 565 ms, followed by a rapid decrease and after 2000 ms the signal reaches noise level. The signal outside the vasculature had a very low intensity during the first two PLDs. Between 1000 and 1500 ms the maximum ASL-signal is observed in the GM tissue demonstrated by the sequence with flow crushing. signal was calculated from the difference between the non-crushed and crushed signal. Error bars show the standard error of the mean (SEM).

The signal intensity decreased at the longer PLDs due to T_1-relaxation and at the longer eTEs due to the T_2-relaxation, as shown in figure 3 showing a single slice example of one of the subjects. For the longest eTE at the later PLDs there is hardly any signal left.

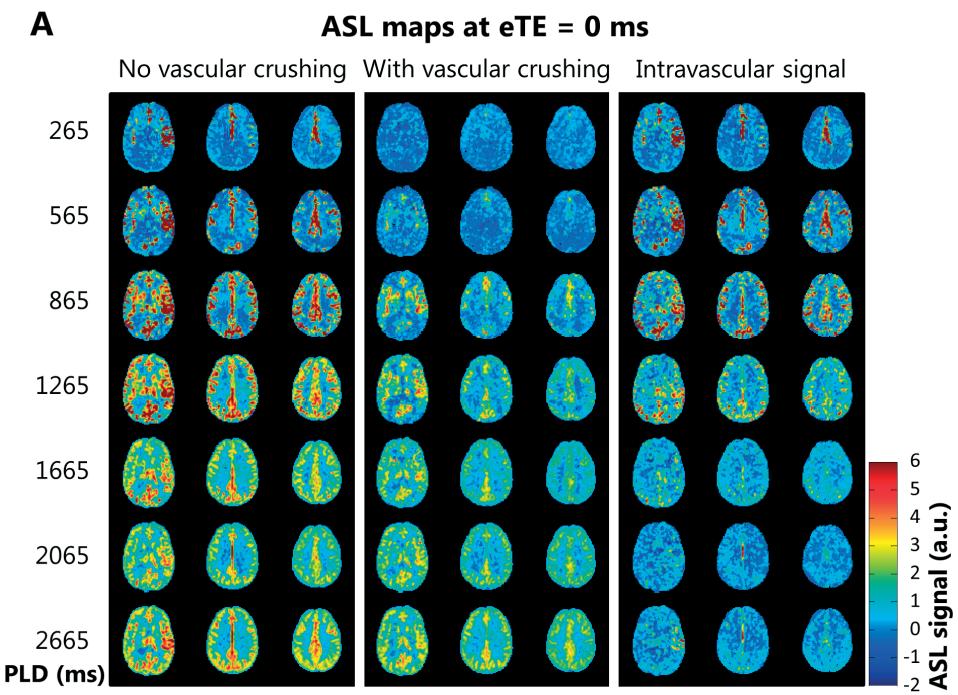

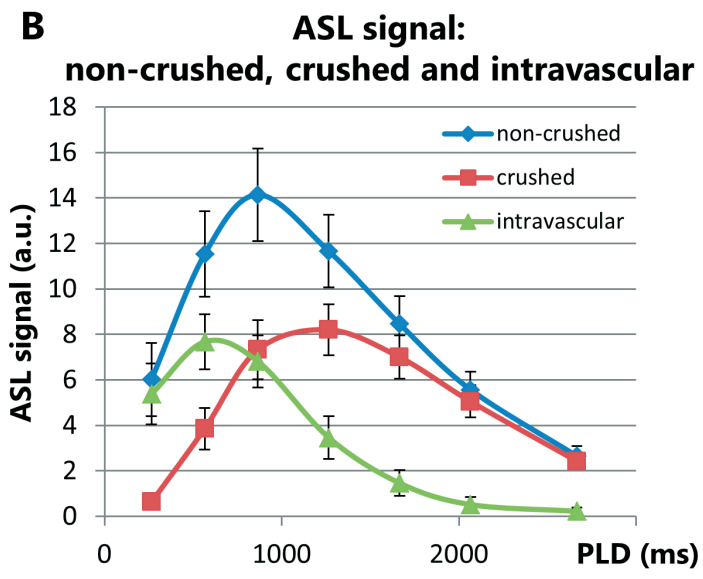

Figure 2 A) ASL-maps of a single subject at eTE = 0 ms. For each post labeling delay (PLD) 3 slices are shown for the scans without vascular crushing (left), with vascular crushing (middle) and for the arterial signal (right). **B)** The average normalized grey matter ASL-signal intensity at eTE = 0 ms at the different PLDs for non-crushed (blue), crushed (red) and arterial signal (green). The arterial

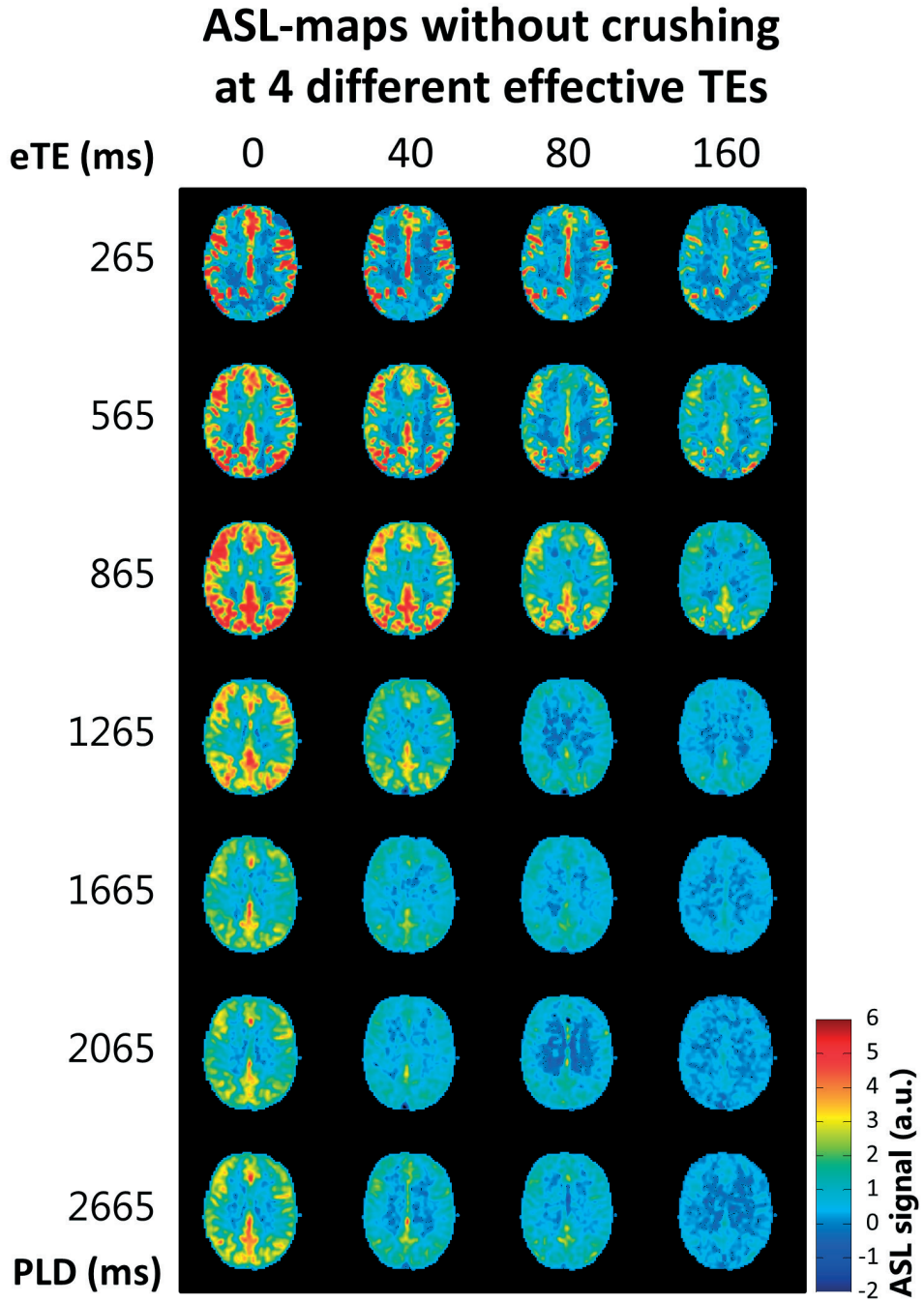

Figure 3 Single slice ASL-maps without vascular crushing of a single subject at eTE = 0, 40, 80 and 160 ms for all PLDs. The change in signal over the PLDs is due to inflow of the label and T_1-relaxation, whereas signal decay for longer eTEs is due to the T_2-relaxation of the label.

T2 at different post labeling delays

Figure 4 gives an example of the voxelwise mono-exponentially fitted T_2-maps. For the shortest PLD, it was not possible to get a proper fit in all voxels, since there was only label present in the arteries and not yet in the tissue. For later PLDs reliable fits of the T_2 could be obtained in GM tissue, whereas in the WM this was not always the case, due to low SNR or lack of signal. The fit was considered reliable when the error (root sum-of-squared differences between fit and measured signal divided by the measured signal) was smaller than 0.05. Notice the clear chi-pattern found in the first 3 slices of the T_2-maps at a PLD of 865-1665 ms showing the border zone regions. The delay in T_2-decay compared with the surrounding tissue located more centrally in the flow territory indicates a later transition of the label into the tissue compartment in these regions.

Flow territories

To get more detailed information about the hemodynamics within the major flow territories, the brain was divided into regions of interest, based on the RPI scan. The distribution of the average normalized GM ASL signal (with vascular crushing) for the different PLDs is shown in figure 5a for the ICA and posterior flow territories at eTE = 0 ms. The average GM ASL signal of the right ICA flow territory was similar to the left ICA, whereas within the posterior flow territories the label arrived slightly later.

The change in T_2-values of the vascular crushed data over time for the different flow territories is shown in figure 5b. Only positive T_2-values smaller than 1000 ms were included in the average value per flow territory to exclude voxels which were not fitted well. For 565 and 865 ms PLD the average T_2 in GM was 174 ms, which indicates that the spins are mainly in the arteries. Longer PLDs showed a steady decrease in T_2. After 2000 ms the T_2 stabilizes around 105 ms.

Border zone regions

In figure 6a a clear delay and lower ASL signal can be seen in the border zone regions compared with the central regions of the flow territories. After fitting the ASL signal to the kinetic perfusion model of Buxton, a significantly lower CBF was found in the border zone region than the central region: 37.8 ± 2.5 (mean ± SEM) and 47.8 ± 2.5 ml/100g/min in the posterior flow territory and 38.6 ± 2.6 and 50.1 ± 2.6 ml/100g/min in the MCA flow territory. The signal curves of the border zones sampled in both the posterior and MCA flow territory are almost identical. Also the steepness of up and down slopes are very similar between MCA and posterior flow territories, but the upslope of the central MCA curve rises earlier than the central posterior curve. The ATT was on average 978 ms in the posterior and 996 ms in the MCA border zone region. This was significantly longer than the 597 in the posterior and 457 ms in the MCA central region as can be seen in figure 6b. The ATT in the central posterior region was also significantly longer than in the central MCA region ($p<0.05$).

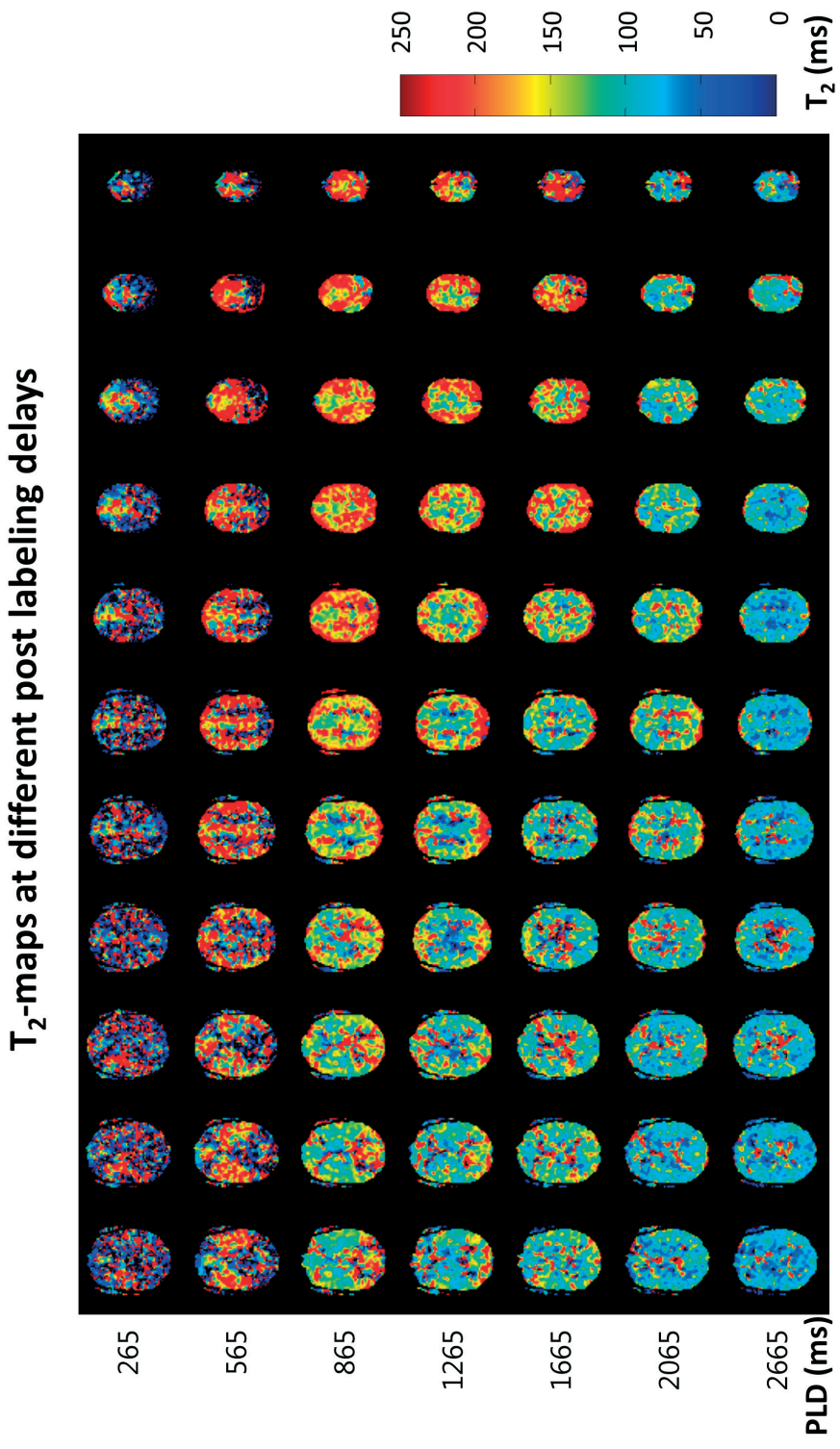

Figure 4 T_2-maps of a single subject for the different PLDs. Note the delayed decrease in T_2 in the posterior territory as well as in the border zone regions.

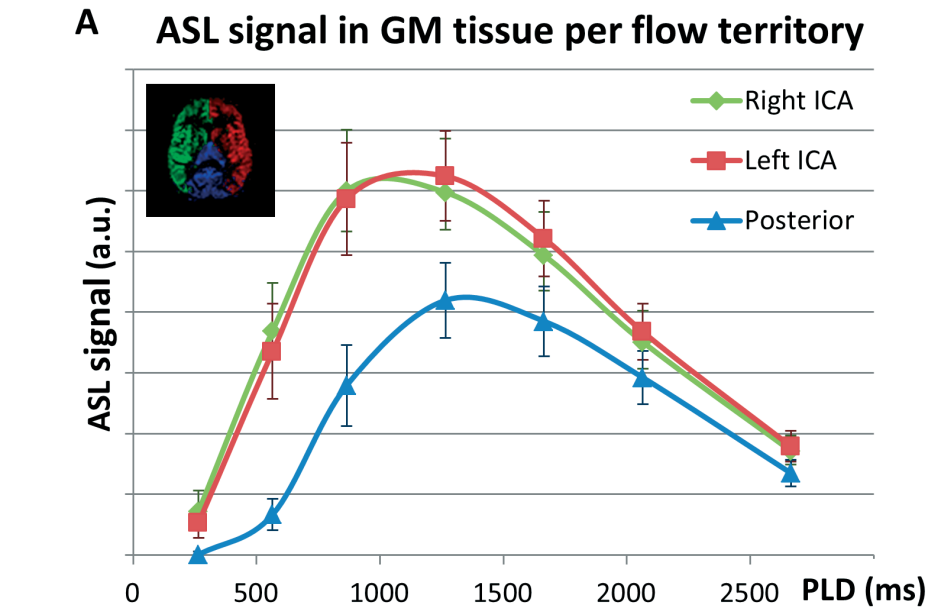

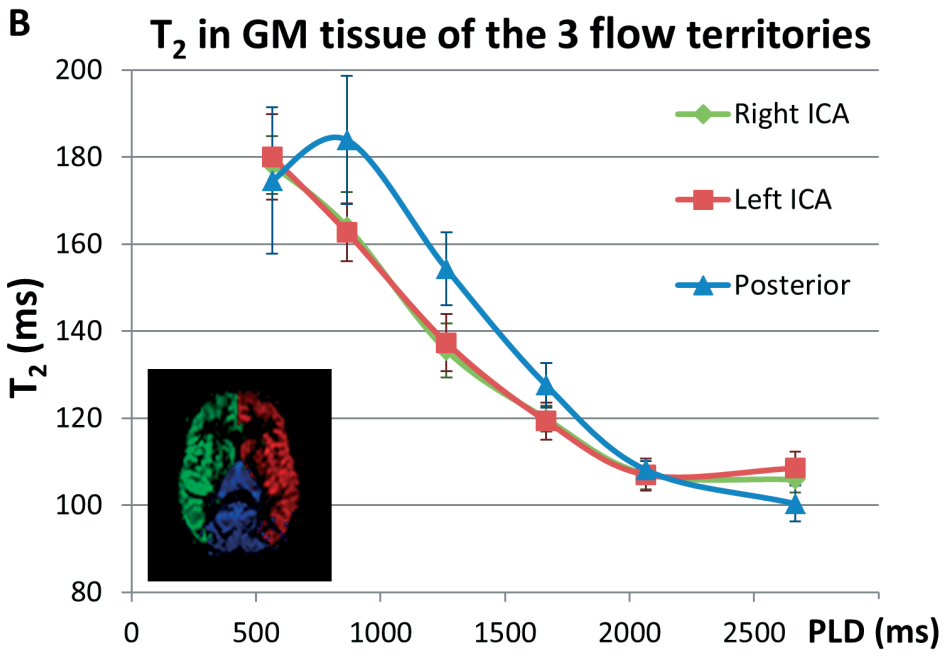

Figure 5 A) The average normalized grey matter ASL-signal at eTE = 0 ms in tissue of the right ICA (diamond), left ICA (square) and posterior (triangle) flow territory over the different PLDs. **B)** A slight delay was found in the T_2 of the posterior flow territory compared with the right and left flow territories. Especially for the shortest PLD the signal, the T_2 fit was not reliable due to absence of ASL signal and these values were therefore not included in the graph. Error bars show SEM.

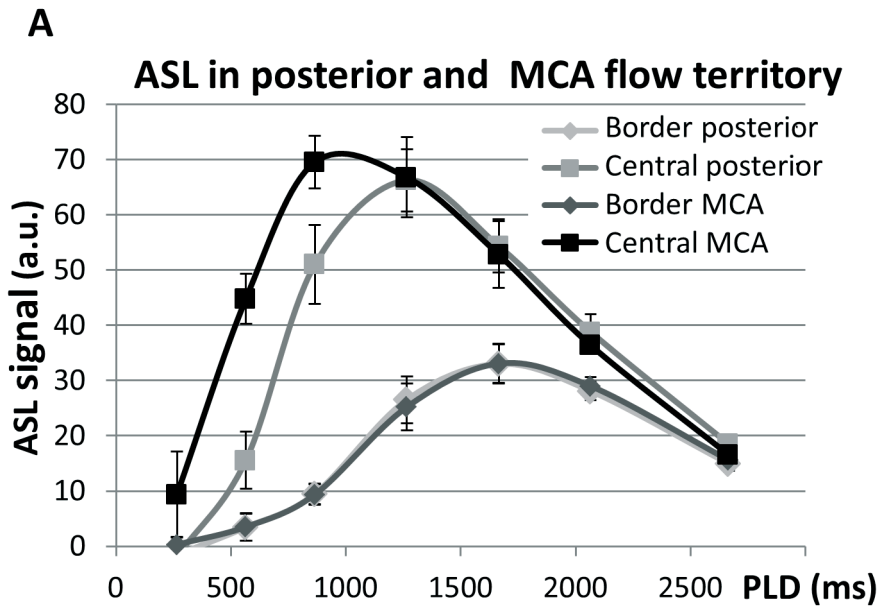

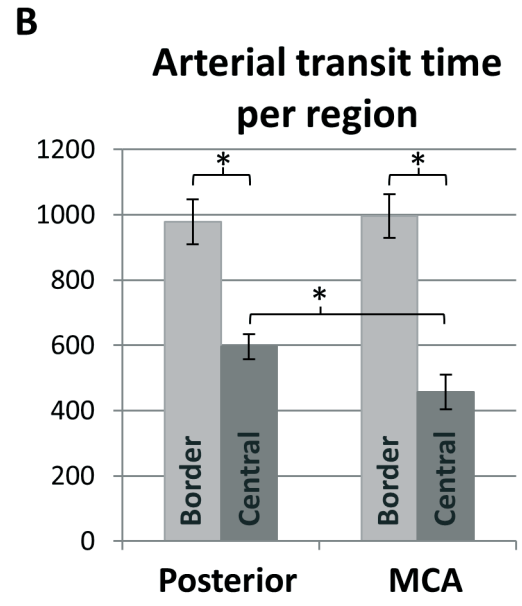

Figure 6 A) The normalized ASL signal in the posterior (light) and MCA (dark) flow territory GM sampled from the border zone (diamond) and central (square) regions over the different post labeling delays. **B)** The arterial transit time is significantly longer in the border zone than in the central regions for both the posterior as well as the MCA flow territory. * indicates $p<0.05$

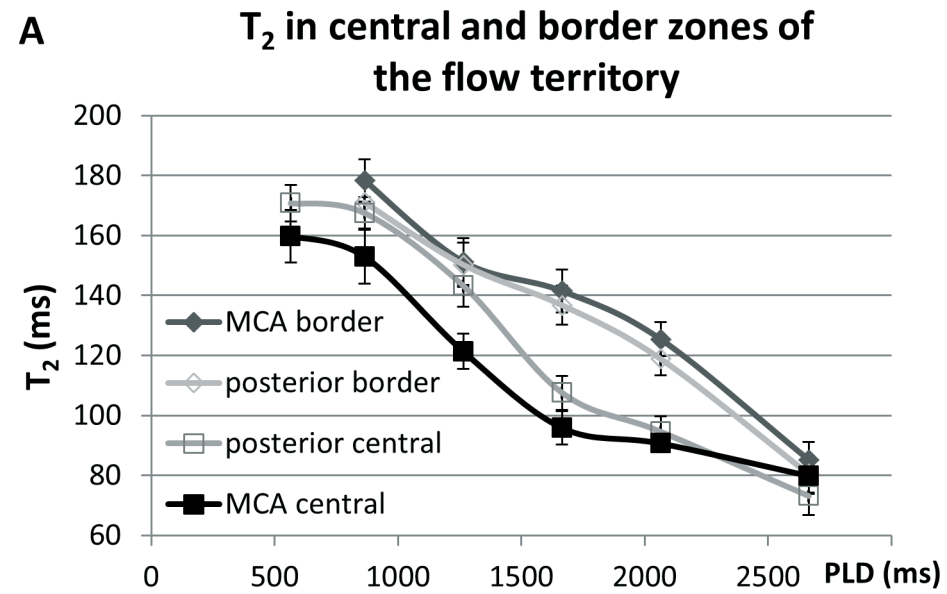

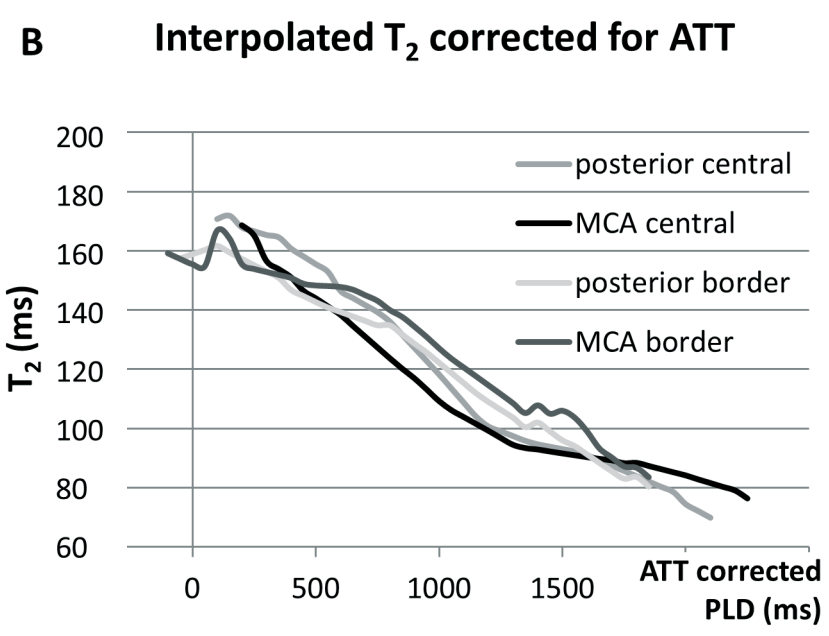

Figure 7 A) The T_2 in the posterior (light) and MCA (dark) flow territory over time, sampled in the border zone (open) and central (solid) regions. **B)** Showing the same data, but the T_2-curves are shifted by the individual arterial transit time delay of that territory and are interpolated at a 50 ms interval before averaging over all subjects

The transition of the signal from the vascular to the tissue compartment was delayed in the border zones as compared with the central region, as is demonstrated in figure 7a by the significant higher T_2 in the border zone regions compared with the central regions for PLDs of 1665 and 2065 ms (posterior) and 1265, 1665 and 2065 ms for the MCA flow territory. After shifting the T_2-curves by the subject specific ATT and interpolation at a 50 ms interval (see figure 7b), the statistical test showed no significant difference between the central and border zone regions. The interpolated curves in figure 7b are only displayed when data for two or more subjects were present at that time point. This causes the deviation from the original T_2-values at the beginning and end of the curves.

Discussion

In this work, te-pCASL was used in combination with TRUST to enable T_2-measurements of the ASL-labeled spins in a time-efficient manner. This method was used to evaluate the hemodynamics of the cerebral border zone regions. The most important findings of the present study are threefold. Firstly, by using te-pCASL-TRUST it was possible to distinguish spin compartments based on their T_2 and to enable voxelwise T_2-mapping of this dynamic process. Secondly, the exchange of the label from the intravascular to the tissue compartment in the border zone regions occurs later than in the central regions of the flow territories of healthy young volunteers, but at a comparable rate. This delay is predominantly caused by longer ATTs in the border zones. Finally, the use of te-pCASL-TRUST allows for acquisition of spin compartment information in a highly time-efficient manner.

Due to the different T_2-characteristics of the spin compartments, it was possible to distinguish intravascular label from label within the tissue compartment based on their T_2. Such a distinction cannot be made from the normal ASL signal at multiple PLD-times due to the small difference in T_1 between blood and tissue.[21-25] The following T_2-relaxation values at 3T are known from literature: ~175 ms (at a hematocrit of 42 ± 6.4 %) in the arterial compartment,[3] ~90 ms in GM tissue,[4] and ~50 ms in the venous compartment (at an oxygenation level of 60 %).[3]

For the early time points (see figure 5b), a T_2 was found similar to the arterial T_2 known from literature.[3] However, it was not always possible to fit the T_2 in each voxel at these early time points, due to the simple fact that the label had not arrived yet in all voxels and this explains the noisy images at a PLD of 265 ms in figure 4.

For the longest PLD of 2665 ms, the T_2 of the whole brain GM was approximately 105 ms, which is a little higher compared with the tissue value known from literature for GM tissue.[4] However, when looking at only a few voxels in the central regions of the flow territory, a T_{2-}

value of 90 ms was reached approximately 2 sec post labeling (see figure 7). This difference may be explained by the inclusion of the border zone regions in the analysis of the average T_2 for the 3 major flow territories. Moreover, some voxels which are mainly arterial and still filled with slow flowing spins could have attributed to the longer T_2-values in the large GM ROIs analysis.

The maximum intravascular ASL signal was found around 565 ms and decreased rapidly after this time point (see fig 2b). By looking at the difference in ASL signal between the vascular crushed and non-crushed scans of figure 2a, it can be seen that in individual scans locally still a high intensity in lateral vessels was found present around 1265 ms. This shows that vascular crushing efficiency is spatially variable, which may be caused by its dependency on vessel orientation in relation to the crusher gradient direction and therefore can only partially suppress vascular signal in the ASL signal.

In figure 6 no clear transition from the vascular to the tissue compartment can be observed, instead a gradual decrease in T_2-values is found. This may be explained by differences in timing per subject. Based on individual T_2-curves the moment of transition was easier to determine, which showed a wide range between 865 and 2065 ms for the different subjects. Another explanation for the rather linear, instead of sigmoidal T_2-curves, as shown in previous publications, could be that the data points represent a mixture of compartments. Especially the spins labeled in the block with the longest PLD could be present in the arterial, tissue as well as venous compartment. Also, blood in the arterioles and capillaries has previously been shown to already exhibit a lower oxygen saturation, leading to lowered T_2-values for shorter PLDs.[26] This also implies that one should keep in mind that short T_2-values do not provide the absolute proof that spins are extravascular, but could also point to lower oxygenation in microvascular blood compartment. Finally, the absence of clear sigmoid curve as observed in previous publications, made it more difficult to fit a model to the data to obtain a single summary parameter for the moment of transition, especially since such a model would be highly sensitive to assumptions of arterial and tissue T_2-values. It was therefore proposed to perform statistical testing per PLD with the data corrected for difference in large vessel transport, i.e ATT. The ATT found in this study was within the wide range of ATT (from approximately 500 ms up to 1600 ms) measured with multi-delay continuous ASL in earlier studies.[22, 23, 27-29] A significantly longer ATT was found in border zone regions compared with central regions, which was also clearly visible in the lower slices of the voxelwise T_2-map in figure 4, notice the higher T_2 at PLDs of 865, 1265 and 1665 ms in the border zone regions as compared with the central regions.

Also, a significantly longer ATT was observed in the central regions of the posterior flow territory compared with the central regions of the MCA flow territory. However, in the border zone regions no significant difference was found between the posterior and MCA flow territory. So despite that blood for the tissue in border zone regions is provided by the distal ends of two different arteries, there is no difference in ATT.

The ATT varies not only due to differences between the subjects, but is also influenced by the distance between labeling and imaging position. Within this study the location of the labeling slab was positioned such that it was perpendicular to the main brain feeding arteries and intercepted with the v3 segment of the vertebral arteries. Between subjects differences in the gap between the labeling and imaging could lead to small deviations in the ATT. In the example subject of Figure 2 in some locations in the tissue a signal decrease was observed in the first two PLDs; in other subjects an increase was found between these time points. Such tissue signal fluctuations at these early time points can mainly be attributed to noise, but it could also be partially caused by subtraction errors of the time-encoding scheme. For the analysis of the ATT all signal (i.e. also negative values) within the GM was included and therefore, the noise was averaged out and did not influence the ATT estimate much.

The border zone region CBF was on average 22% lower than CBF in the central part of the same flow territory. The CBF-values as obtained in this study in the central regions are in agreement with values reported in literature, while in the border zone region these values are on the lower side of the range as found in literature.[30-32]

A delayed T_2-change was found for the posterior flow territory in as compared with the left and right ICA flow territory (figure 5b). However, when the T_2-curves were corrected for the ATT, no significant difference were found between the central and border zone regions as shown in figure 7b. The exchange of the label from the vascular to the tissue compartment in the border zone regions appears therefore to be at a similar rate as in the central regions of the flow territories. Furthermore, for the border zone regions not only the ATT, but also the T_2-decay is similar for the MCA and posterior flow territory.

The use of time encode pCASL in combination with TRUST instead of sequential acquisition of single PLD pCASL scans, like in an earlier study,[6] provided several improvements: 1) a shorter bolus duration to be more sensitive to the compartment transition 2) three more PLD-values 3) a larger range in PLDs 4) a 26% shorter acquisition time 5) more than double the amount of averages and 6) provides a multi-slice acquisition. Despite these improvements, the scan duration of approximately 23 minutes will still be too long for most clinical applications. However, for this study we acquired scans with and without vascular crushing, whereas for characterization of the water transport into the tissue compartment, only the scan with vascular crushing is needed. Moreover, not all these averages were necessary to obtain a proper characterization of T_2-change as a function of PLD. By reducing the number of averages to five the scan could be performed in 12 min. For comparison, to obtain the same data with multi TI, this would take at least 45 min, so te-pCASL reduces the scan time to almost one

fourth. This makes te-pCASL a very time efficient method to acquire useful information about the ATT and could be used for example to recognize disturbances in blood supply due to stroke, vascular occlusions, and aging.

The duration of the labeling blocks was not chosen equally: a longer block duration was chosen for the blocks with a longer PLD to compensate for loss of signal due to T1-decay of label. The difference in block duration and the number of blocks was, therefore, a compromise between SNR, a large range in PLDs, improved characterization of the transition between compartments and scan-time. Compensation for the lower SNR for the longest PLDs, results in a longer effective labeling duration for these blocks and dispersion of the bolus could therefore be more significant for these longer PLDs than for the shorter labeling durations for the small PLD-blocks. Also, due to the rather long duration of the bolus with the longest PLD this is probably probing a mixture of compartments. This could be an explanation why the typical T_2-value of 50 ms for the venous compartment was not reached.

Especially, the spins that were labeled during the first labeling block, which had the longest block duration of 1300 ms, could be present in both the tissue and venous compartment. Proof that the labeled blood water spins reached the venous compartment was found in the increased ASL-signal in the sagittal sinus during the longest PLD.

A limitation of te-pCASL-TRUST compared with multi time point T_2-prepared ASL measurement is that all PLDs have the same eTE sampling scheme. For example for the short PLDs it would be more efficient to acquire longer spaced eTE times, while for the long PLDs closer spaced eTEs are more beneficial. Despite all degrees of freedom time encoded pCASL has, it does not provide the option to vary the distribution of eTEs in the TRUST module for the different PLDs.

Conclusion

In conclusion, the use of te-pCASL combined with TRUST provided a time efficient method to distinguish spin compartments based on their T_2. The ATT in the border zone is significantly longer than the central region of the same flow territory. However, the exchange of the label from the vascular to the tissue compartment appears to progress at a similar rate in the border zone and central regions.

References

1. Wu W-C, St Lawrence KS, Licht DJ, et al. Quantification Issues in Arterial Spin Labeling Perfusion Magnetic Resonance Imaging. Topics in Magn Res Im. 2010;21(2):65-73.
2. Levitt MH, Freeman R, Frenkiel T. Broadband Heteronuclear Decoupling. J Magn Res. 1982;47:328-330.
3. Chen JJ, Pike GB. Human whole blood T_2 relaxometry at 3 Tesla. Magn Reson Med. 2009;61(2):249-254.
4. Lu H, Clingman C, Golay X, et al. Determining the longitudinal relaxation time (T_1) of blood at 3.0 Tesla. Magn Reson Med. 2004;52(3):679-682.
5. Garcia DM, de Bazelaire C, Alsop D. Pseudo-continuous Flow Driven Adiabatic Inversion for Arterial Spin Labeling. Proc. Intl. Soc. Mag. Reson. Med. 2005; Miami, USA.
6. Liu P, Uh J, Lu H. Determination of spin compartment in arterial spin labeling MRI. Magn Reson Med. 2011;65(1):120-127.
7. Lu H, Ge Y. Quantitative evaluation of oxygenation in venous vessels using T_2-Relaxation-Under-Spin-Tagging MRI. Magn Reson Med. 2008;60(2):357-363.
8. Gregori J, Schuff N, Kern R, et al. T2-based arterial spin labeling measurements of blood to tissue water transfer in human brain. J Magn Reson Imaging. 2013;37(2):332-342.
9. Gunther M. Highly efficient accelerated acquisition of perfusion inflow series by cycled arterial spin labeling. Proc. Intl. Soc. Mag. Reson. Med. 2007; Berlin, Germany.
10. Wells JA, Lythgoe MF, Gadian DG, et al. In vivo hadamard encoded continuous arterial spin labeling (H-CASL). Magn Reson Med. 2010;63(4):1111-1118.
11. Dai W, Shankaranarayanan A, Alsop DC. Volumetric measurement of perfusion and arterial transit delay using hadamard encoded continuous arterial spin labeling. Magn Reson Med. 2013;69(4):1014-1022.
12. Teeuwisse WM, Schmid S, Ghariq E, et al. Time-encoded pseudocontinuous arterial spin labeling: Basic properties and timing strategies for human applications Magn Reson Med. 2014 72:1712–1722.
13. Schomer DF, Marks MP, Steinberg GK, et al. The Anatomy of the Posterior Communicating Artery as a Risk Factor for Ischemic Cerebral Infarction. New England Journal of Medicine. 1994;330(22):1565-1570.
14. Derdeyn CP, Khosla A, Videen TO, et al. Severe Hemodynamic Impairment and Border Zone-Region Infarction. Radiology. 2001;220(1):195-201.
15. Momjian-Mayor I, Baron J-C. The Pathophysiology of Watershed Infarction in Internal Carotid Artery Disease: Review of Cerebral Perfusion Studies. Stroke. 2005;36(3):567-577.
16. Botnar RM, Stuber M, Danias PG, et al. Improved Coronary Artery Definition With T_2-Weighted, Free-Breathing, Three-Dimensional Coronary MRA. Circulation. 1999;99(24):3139-3148.
17. Brittain JH, Hu BS, Wright GA, et al. Coronary Angiography with Magnetization-Prepared T_2 Contrast. Magn Reson Med. 1995;33(5):689-696.
18. Ordidge RJ, Wylezinska M, Hugg JW, et al. Frequency Offset Corrected Inversion (FOCI) Pulses for Use in Localized Spectroscopy. 1996.
19. Hendrikse J, van der Grond J, Lu H, et al. Flow territory mapping of the cerebral arteries with regional perfusion MRI. Stroke. 2004;35(4):882-887.
20. Jenkinson M, Bannister P, Brady M, et al. Improved optimisation for the robust and accurate linear registration and motion correction of brain images. NeuroImage. 2002;17(2):825-841.
21. Buxton RB, Frank LR, Wong EC, et al. A general kinetic model for quantitative perfusion imaging with arterial spin labeling. Magn Reson Med. 1998;40:383-396.
22. Alsop DC, Detre JA. Reduced transit-time sensitivity in noninvasive magnetic resonance imaging of human cerebral blood flow. J Cereb Blood Flow Metab. 1996;16:1236-1249.
23. Gonzalez-At JB, Alsop D, Detre JA. Cerebral perfusion and arterial transit time changes during task activation determined with continuous arterial spin labeling. Magn Reson Med. 2000 43:739–746.

24. Yang Y, Engelien W, Xu S, et al. Transit time, trailing time, and cerebral blood flow during brain activation measurement using multislice, pulsed spin-labeling perfusion imaging. Magn Reson Med. 2000;44:680–685.
25. Qiu M, Paul Maguire R, Arora J, et al. Arterial transit time effects in pulsed arterial spin labeling CBF mapping: insight from a PET and MR study in normal human subjects. Magn Reson Med. 2010;63(2):374-384.
26. Vazquez AL, Fukuda M, Tasker ML, et al. Changes in cerebral arterial, tissue and venous oxygenation with evoked neural stimulation: implications for hemoglobin-based functional neuroimaging. J Cereb Blood Flow Metab. 2009;30(2):428-439.
27. Ye FQ, Mattay VS, Jezzard P, et al. Correction for vascular artifacts in cerebral blood flow values measured by using arterial spin tagging techniques. Magn Reson Med. 1997;37:226-235.
28. Mildner T, Moller HE, Driesel W, et al. Continuous arterial spin labeling at the human common carotid artery: the influence of transit times. NMR Biomed. 2005;18(1):19-23.
29. Sousa I, Vilela P, Figueiredo P. Reproducibility of the quantification of arterial and tissue contributions in multiple postlabeling delay arterial spin labeling. J Magn Reson Imaging. 2014;40(6):1453-1462.
30. Hendrikse J, Lu H, van der Grond J, et al. Measurements of cerebral perfusion and arterial hemodynamics during visual stimulation using TURBO-TILT. Magn Reson Med. 2003;50(2):429-433.
31. Donahue MJ, Lu H, Jones CK, et al. An account of the discrepancy between MRI and PET cerebral blood flow measures. A high-field MRI investigation. NMR Biomed. 2006;19(8):1043-1054.
32. Petersen ET, Lim T, Golay X. Model-free arterial spin labeling quantification approach for perfusion MRI. Magn Reson Med. 2006;55(2):219-232.

7

Summary and general discussion

Summary and key findings

In this thesis I have described the introduction and validation of a new spatially non-selective arterial spin labeling (SNS-ASL) method in healthy subjects. Acceleration selective ASL (AccASL) was compared with pseudo continuous ASL (pCASL), a traditional ASL method, as well as other spatially non-selective ASL methods (velocity selective ASL, as introduced by Wong et al with two velocity-selective blocks, and using only a single labeling module), and with [^{15}O]-H_2O PET as the gold standard for brain perfusion imaging. By combining an AccASL with VSASL labeling module, the location of label origin in the vascular tree was assessed. Furthermore, time-encoded pCASL was explored in combination with SNS-ASL labeling modules to obtain insight into labeling at multiple post labeling delays (PLD). Finally, te-pCASL was combined with T_2-Relaxation-under-Spin-Tagging (TRUST) to provide a time-efficient method to distinguish spin compartments based on their T_2-values.

A general introduction about perfusion measurement techniques and the parameters that can be measured with these methods, arterial spin labeling and some of the recent developments in the ASL field were described in **chapter 1**.

In **chapter 2** it was shown that the use of an acceleration-dependent preparation module instead of a velocity-selective module, as used in the original spatially non-selective ASL technique (velocity-selective ASL), enables imaging brain perfusion without contamination from venous or CSF signal, which are present in single VSASL. In dual VSASL these contaminations were at a similar level as in pCASL and AccASL, although the amount of label signal and thus SNR was significantly reduced.

Even though dual VSASL is still the only SNS-ASL method that can provide quantitative cerebral blood flow (CBF), qualitatively all SNS-ASL methods provide similar CBF-maps as compared to [^{15}O]H_2O PET, as can be concluded from the results of **chapter 3**. From the SNS-ASL methods, AccASL best resembled the PET CBF-maps, showing only a 2% lower intracranial correlation coefficient compared with pCASL.

In **chapter 4** it was shown that AccASL is able to label spins in the macro-, meso- as well as micro-vascular regions. The label created with AccASL has a large overlap in terms of vascular region with VSASL, but depending on the A_{enc} the label from AccASL can also originate from regions closer to the tissue.

In **chapter 5**, the use of te-pCASL followed by an acceleration or velocity selective module that functioned as a crusher of the ASL-signal gave insight into the location in the vascular tree where the SNS-ASL methods create the label. Most signals were crushed at early time-points by the effects of crusher gradients in the main flow direction and flow rates within the cut-off range, while less signal was crushed at later time points, maybe because the label had already exchanged with tissue magnetization.

This gave further indications that AccASL creates more label within the microvasculature, whereas VSASL creates more signal in the large vasculature.

Furthermore, in **chapter 6** te-pCASL was combined with TRUST to provide a time-efficient method to measure the water transport time into the tissue compartment, based on the T_2 of the labeled spins. With this combined method we were able to measure the CBF, the ATT and the T_2 in a single sequence. It was found that the ATT in the border zone is significantly longer than the ATT of the central region of the same flow territory. However, the exchange of the label from the vascular to the tissue compartment appears to progress at a similar rate in the border zones and central regions.

Problems that were addressed

Pathologies with slow and collateral flow cause an underestimation of the CBF with traditional ASL methods using a labeling slab proximal to the imaging region.[1] When using a regular or slightly prolonged PLD the labeled blood still resides in the arteries and arterioles and does not fully reach the tissue, which is necessary for accurate perfusion mapping and especially for quantification of CBF. Prolongation of the PLD cannot solve this problem, because this leads to too low SNR due to enhanced decay of the label. The use of SNS-ASL methods could reduce these types of error, because labeling occurs within the imaging region with the result that the label is created closer to the tissue.

The disadvantage of the use of VSASL is that a single labeling module labels all spins flowing above the chosen cut-off velocity, independent of whether they are in the arterial or venous compartment. The presence of venous label within the perfusion image can be avoided by means of a second labeling module performed just before imaging, but at the cost of a strong reduction in the SNR. With AccASL we showed that it is possible to label primarily on the arterial side of the vasculature with a single labeling module. The choice of cut-off acceleration has a large influence on the amount of label created, as well as the location within the vasculature, where the label is created. By tuning the gradient amplitude, duration and time between the gradients, the acceleration encoding can be adapted. However, this also affects the diffusion-weighting of the labeling module, which is dependent on the same parameters. By choosing the gradient parameters carefully the influence of the diffusion weighting can be limited.

With the te-pCASL-TRUST method we were able to trace the label over time based on the changes in T_2. Whereas the regular ASL-signal does not provide any information about the compartment where the label is located, the vascular and tissue compartments can be distinguished using the T_2 values. The use of time-encoded ASL significantly decreased the total scan time as compared to the originally proposed protocol. As the voxelwise fit of the T_2 in the grey matter obtained with this method was of high enough quality, ATT information and exchange of label into the tissue could be studied within the flow territory border-zones.

Perspective

Acceleration selective ASL

In this thesis AccASL was introduced, compared, validated and explored, but more research is necessary to clarify the following questions and investigate the full potential of this new method.

Although the studies described in chapters 4 and 5 provided more insight into the labeling location of AccASL, it remains not completely clear which physiological processes are the basis for label generation. In hindsight AccASL should actually have been named deceleration selective arterial spin labeling, because it mainly labels decelerating spins in the arterial blood, but the exact location of the label generation within the vascular tree is strongly dependent on the settings of the motion sensitizing gradients and the subsequent A_{enc}. The possible origins of the label-generation process, such as general flow acceleration/deceleration in the vasculature, tortuosity of the vessels both at macro- and microvascular level, and cardiac cycle fluctuations probably all contribute to the label generation and all are dependent on physiological effects that may vary between persons and can vary by pathology. Only the influence from diffusion weighting, which is considered to be an artefactual source of label can be suppressed by an optimal choice of labeling parameters as explained before.

In general, the flow velocity decreases on the arterial side of the vascular tree when the blood moves closer to the capillaries, while on the venous side it increases when flowing into the sagittal sinus and other large veins. Branching of the vessels can cause local disturbances in the flow velocity. The largest deceleration occurs in the transition from the small arterioles to the capillaries, where the flow velocity is virtually zero. This velocity distribution along the vascular tree might change during the life-span and due to disease. The A_{enc} as employed in this thesis is optimized for young, healthy subjects, but for elderly subjects or patients with a disturbed flow, this A_{enc} could be suboptimal. Moreover, since in AccASL only a single gradient direction is employed, the flow direction might affect the amount of signal created with AccASL. In the macro-vasculature the main flow direction is considered to be along the feet-head axis, whereas the lateral direction becomes more prominent beyond the Circle of Willis, and the flow is in all directions within the capillary bed.

The tortuosity of the vessels could be investigated by using different gradient encoding directions. In the capillaries different gradient encoding directions should not have a large influence on the amount of signal created in that vascular region due to the random orientation of flow. However, in Moyamoya disease and brain-tumors, angiogenesis lead to new vasculature with a different structural organization than normal brain tissue, and an interesting application of the different gradient encoding directions could be to assess such a pathological change in vascular architecture.[2]

Fluctuations in flow velocity due to the cardiac cycle are most prominent in the arterial compartment, which could be one of the explanations why the AccASL signal has mostly an arterial origin. The influence of the cardiac cycle on the AccASL signal could be studied by using cardiac triggering. Preliminary data has shown that the cardiac cycle has only limited effect on the labeling, but this was again studied in young, healthy subjects. Nevertheless, it would be interesting to study this in elderly people, where it is known that the vasculature stiffens and less dampening of the pulsatility of the cardiac pressure occurs, also to see if this could be a measure for microvascular pulsatility.

Another factor that is still not completely clear is the proportion of CBV-weighting in AccASL, since it has been suggested that the signal is of mixed hemodynamic origin; including both CBF and CBV-weighting. Comparisons to [^{15}O]H_2O PET CBF and arterial CBV showed a greater correlation to the CBF. However, this does not mean that the same would be true for the full CBV.

In thesis, the feasibility of AccASL was only shown in healthy volunteers. Comparisons between several ASL methods and PET have been made and showed good potential for the application of AccASL in patients. At this point quantification of the CBF with AccASL is not possible, since the length of the bolus is not well defined. Therefore, AccASL will probably not be a suitable method for pathologies that affect the whole brain. Nevertheless, pathologies such as stroke or brain tumors are a good candidate to be evaluated with AccASL, since a qualitative comparison to other brain areas can be made.

Until now, the main benefit of the spatially non-selective AccASL methods has not been fully exploited. With the labeling occurring within the imaging region, it should be possible to decrease the inflow time and thereby to reduce the acquisition duration, since the transit time is shorter than in traditional ASL techniques. In chapter 5 was shown that by employing Acc- and VS-modules as crushers in a te-pCASL scan that around the time points when one would expect magnetization exchange to tissue, less pCASL-signal was crushed by AccASL. This could be explained by the fact that signal cannot be crushed when it already has exchanged. Since with these settings for AccASL and VSASL similar amount of signal is detected at a PLD of 1600ms, AccASL must have created more label close to the tissue than VSASL. This makes it interesting to examine the use of a shorter PLD for AccASL.

In VSASL this is not possible when quantification of the CBF is required, since shortening the time between the labeling modules would also reduce the amount of signal detected, while the SNR is already relatively low (compared to pCASL or AccASL) when using a standard PLD as shown in chapter 2.

Despite those questions and features of AccASL that can be further investigated, the work in this thesis opens up the possibility of exploring the clinical applications and validations of SNS-ASL with dual VSASL as a quantitative technique and AccASL for qualitative purposes.

The future of ASL

At this point, ASL is mainly used as a research tool in academic centres, but is still not commonly used as a standard method in the clinical setting. This can be ascribed to three main issues. First, in the case of an emergency it takes longer to make an MRI scan than a CT scan and it is difficult to quickly access MR-contra-indications, such as metal implants, in an acute situation. Second, until recently there was no standardized and optimized perfusion protocol. This can partially be attributed to the major MRI-vendors that did not provide ASL as standard package, as well as the fact that the methods they did implement were not comparable: pCASL (GE, Philips) or PASL (Siemens), 2D (Philips, Siemens) or 3D read-out (GE, Siemens). With the publication of the ASL consensus paper a standard has been set, and now highly comparable sequences are available on the systems of the three vendors as products or work-in-progress packages.[3] Third, even with a more standardized acquisition protocol ASL is still not a push-button method guaranteed to provide reliable results. The acquisition requires planning of the labeling slab and preferably some knowledge about the expected arrival time of the label. Furthermore, the ASL-images need post-processing before quantified perfusion maps are available. Moreover, a separate M0 scan needs to be measured and often motion correction needs to be performed and for longitudinal studies registration to an anatomical image is necessary. These more advanced post-processing steps depend on specialized software and frequently cannot be performed in real-time.

Despite the fact that the application of (advanced) ASL techniques in the clinical setting needs more support to be used actively, as a research application it can be expected to show some rapid, further developments, especially to yield *more* information in a *shorter* scan-time. For example, in chapters 5 and 6 it was shown that smart combinations of different ASL-modules, as wells as tracking of the signal over time, can produce important information on the hemodynamics and vascular architecture, beyond simply cerebral blood flow. With the use of time-encoded ASL, the PLD no longer serves as idle waiting time, but is used to efficiently gain knowledge about the cerebral hemodynamics of the subject. By integrating all such acquisition modules into a single scan, ASL measurements will no longer be limited to CBF, but will also include information on arterial and tissue arrival times, provide information about flow territories, watershed areas, blood-brain barrier, local vascular architecture, oxygen metabolism, or can combine MR angiography with perfusion imaging. By approaching ASL as a set of building blocks and combining their properties in a smart way our hemodynamic understanding of the brain and other organs can increase significantly.

References

1. Wong EC, Cronin M, Wu WC, et al. Velocity-selective arterial spin labeling. Magn Reson Med. 2006;55(6):1334-1341.
2. Wells JA, Thomas DL, Saga T, et al. MRI of cerebral micro-vascular flow patterns: A multi-direction diffusion-weighted ASL approach. J Cereb Blood Flow Metab. 2016; DOI:10.1177/0271678X16660985
3. Alsop DC, Detre JA, Golay X, et al. Recommended implementation of arterial spin-labeled perfusion MRI for clinical applications: A consensus of the ISMRM perfusion study group and the European consortium for ASL in dementia. Magn Reson Med. 2015;73(1):102–116.

Nederlandse samenvatting

In dit proefschrift werd een nieuwe spatieel-niet-selectieve arteriële spin labeling (SNS-ASL) methode geïntroduceerd en gevalideerd in gezonde deelnemers. Hiertoe werd deze methode, Acceleratie-selectieve ASL (AccASL), vergeleken met pseudo continue ASL (pCASL) als traditionele ASL-methode, met de andere spatieel-niet-selectieve ASL methodes (zowel de snelheid-selectieve ASL (VSASL), zoals geïntroduceerd door Wong et al met twee snelheids-selectieve alsmede met gebruik van slechts één labelingsmodule), en met [^{15}O]-H_2O PET als gouden standaard voor het afbeelden van de hersendoorbloeding. Door het combineren van een AccASL en VSASL labelingsmodule werd de locatie in de vaatboom waar het label gecreëerd wordt onderzocht. Bovendien werd tijdsgecodeerde pCASL (te-pCASL) in combinatie met SNS-ASL labelingsmodules gebruikt om inzicht te krijgen in de labelingslocatie op verschillende tijdspunten na labeling. Uiteindelijk is te-pCASL ook met T_2-metingen gecombineerd gebruikmakend van T_2-Relaxatie-onder-Spin-labeling (TRUST) om op een tijdsefficiënte manier onderscheid te kunnen maken tussen spin-compartimenten gebaseerd op hun T_2.

De verschillende medische beeldvormende technieken die de hersendoorbloeding kunnen meten, de parameters die gemeten kunnen worden met deze methodes, alsmede enkele recente ontwikkelingen in het ASL-veld worden beschreven in **hoofdstuk 1**.

In **hoofdstuk 2** wordt aangetoond dat het gebruik van een versnellingsafhankelijke voorbereidingsmodule het mogelijk maakt voor SNS-ASL om de doorbloeding van het hersenweefsel af te beelden zonder dat veneus signaal of signaal van hersenvocht het beeld vervuilen, terwijl deze vormen van vervuiling duidelijk aanwezig waren in VSASL met een enkele labelingsmodule. In VSASL met twee labelingsmodules waren deze verontreinigingen in gelijke mate aanwezig als in pCASL en AccASL, maar was de hoeveelheid signaal in de uiteindelijke perfusiebeelden significant lager.

Hoewel VSASL met twee labelingsmodules de enige SNS-ASL methode is die een kwantitatieve cerebrale bloed stroom (CBF) kan geven, geven alle SNS-ASL methoden kwalitatief gelijke CBF-beelden in vergelijking tot [^{15}O]H_2O PET, zoals in **hoofdstuk 3** te lezen is. Van de verschillende SNS-ASL methoden, is de signaalverdeling van AccASL het meest vergelijkbaar met PET CBF beelden, met slechts een 2% lagere intracraniale correlatie coëfficiënt ten opzichte van pCASL.

In **hoofdstuk 4** laat ik zien dat met AccASL labeling van bloed-spins zowel in de macro-, meso- als micro-vasculaire regio's kan plaatvinden. De locatie in de vaatboom waarin label gecreëerd wordt met AccASL heeft grote overlap met de regio's waar VSASL het label creëert, maar afhankelijk van de acceleration encodering (A_{enc}) kan het label ook gecreëerd worden in regio's dichterbij het weefsel.

In **hoofdstuk 5** wordt gepresenteerd hoe het gebruik van te-pCASL gevolgd door een versnellings- of snelheids-selectieve module als crusher, inzicht kan geven in de locatie in

de vaatboom waar het label gecreëerd wordt. Het meeste signaal werd weggeslagen op vroege tijdspunten, omdat de crushing gradiënten in dezelfde richting worden uitgespeeld als de stroomrichting in de grote arteriën en de snelheid in deze vaten groot genoeg is zodat saturatie optreedt. Terwijl op latere tijdspunten juist minder signaal weggeslagen kon worden, waarschijnlijk doordat het label al uitgewisseld was met de weefsel-magnetisatie. Uit deze experimenten kan geconcludeerd worden dat AccASL meer label creëert in de microvasculatuur, terwijl voor VSASL dit meer plaatsvindt in de grote vaten.

Tenslotte wordt in **hoofdstuk 6** te-pCASL gecombineerd met TRUST om een tijd efficiënte methode te ontwikkelen die onderscheid kan maken tussen de verschillende spin compartimenten gebaseerd op hun T_2. Met deze gecombineerde methode kon de CBF, arteriële transitie tijd (ATT) en T_2 gemeten worden. Er werd gevonden dat de ATT in de randgebieden van arteriële stroomgebieden significant langer was dan in de centrale regio's van hetzelfde stromingsgebied. Toch leek de uitwisseling van het label van de vasculaire naar het weefsel compartiment op een zelfde snelheid te verlopen in de randgebieden als in de centrale regio's.

Journal publications

1. **Advances in arterial spin labeling MRI methods for measuring perfusion and collateral flow**, MJP van Osch, WM Teeuwisse, Z Chen, Y Suzuki, M Helle, *S Schmid*, Journal of Cerebral Blood Flow & Metabolism, accepted April 2017
2. **Cerebral magnetic resonance imaging in quiescent Crohn's disease patients with fatigue,** S van Erp, E Ercan, P Breedveld, L Brakenhoff, E Ghariq, *S Schmid*, MJP van Osch, M van Buchem, B Emmer, J van der Grond, R Wolterbeek, D Hommes, H Fidder, N van der Wee, T Huizinga, D van der Heijde, H Middelkoop, I Ronen and A van der Meulen-de Jong, World Journal of Gastroenterology, accepted December 2016
3. **Insight into the labeling mechanism of Acceleration selective arterial spin labeling**, *S Schmid*, ET Petersen, and MJP van Osch, Magnetic Resonance Materials in Physics, Biology and Medicine, 2016: 30(2), 165-174
4. **Decreased cerebral perfusion in Duchenne muscular dystrophy patients**, N Doorenweerd,EM Dumas, E Ghariq, *S Schmid*, CSM Straathof, AAW Roest, BH Wokke, EW van Zwet, AG Webb, JGM Hendriksen, MA van Buchem, JJGM Verschuuren, I Asllani, EH. Niks, MJP van Osch, HE Kan, Neuromuscular Disorders 2016; 27(1), 29–37
5. **Time-efficient determination of spin compartments by time-encoded pCASL T_2-relaxation-under-spin-tagging and its application in hemodynamic characterization of the cerebral border zones**, *S Schmid*, WM Teeuwisse, H Lu and MJP van Osch, NeuroImage, 2015; 123, 72-79
6. **Comparison of velocity-and acceleration-selective arterial spin labeling with ^{15}O-H_2O positron emission tomography**, *S Schmid*, DFR Heijtel, HJMM Mutsaerts, R Boellaard, AA Lammertsma, AJ Nederveen and MJP van Osch, Journal of Cerebral Blood Flow & Metabolism, 2015; 35(8), 1296-1303
7. **PP09. 4–2839: Reduced cerebral blood flow in Duchenne muscular dystrophy and related to the Dp140 isoform**, EH Niks, N Doorenweerd, EM Dumas, E Ghariq, *S Schmid*, CSM Straathof, P Spitali, HB Ginjaar, BHA Wokke, DGM Schrans, JC van den Bergen, EW van Zwet, AG Webb, MA van Buchem, AAW Roest, MJP van Osch, JJGM Verschuuren, JGM Hendriksen and HE Kan, European Journal of Paediatric Neurology, 2015; 19, S65-S66
8. **Effects of background suppression on the sensitivity of dual-echo arterial spin labeling MRI for BOLD and CBF signal changes**, E Ghariq, MA Chappell, *S Schmid*, WM Teeuwisse and MJP van Osch NeuroImage, 2014; 103, 316-322
9. **GP 127: Reduced cerebral blood flow in boys with Duchenne muscular dystrophy**, N Doorenweerd, EM Dumas, E Ghariq, *S Schmid*, CSM Straathof, P Spitali, HB Ginjaar, BH Wokke, DGM Schrans, JC van den Bergen, EW van Zwet, A Webb, MA van Buchem, MJP van Osch, JJG Verschuuren, JGM Hendriksen, EH Niks and HE Kan, Neuromuscular Disorders, 2014;24(9), 838-839
10. **Acceleration-selective arterial spin labeling**, *S Schmid*, E Ghariq, WM Teeuwisse, A Webb and MJP van Osch, Magnetic resonance in medicine, 2014; 71(1): 191-199

11. **Time-encoded pseudocontinuous arterial spin labeling: Basic properties and timing strategies for human applications**, WM Teeuwisse, *S Schmid*, E Ghariq, IM Veer and MJP van Osch, Magnetic resonance in medicine, 2014; 72(6): 1712-1722
12. **Multi-parametric assessment of the anti-angiogenic effects of liposomal glucocorticoids**, E Kluza, M Heisen, *S Schmid*, DWJ van der Schaft, RM Schiffelers, G Storm, BM ter Haar Romeny, GJ Strijkers and K Nicolay, Angiogenesis, 2011;14(2), 143-153
13. **Anti-tumor activity of liposomal glucocorticoids: the relevance of liposome-mediated drug delivery, intratumoral localization and systemic activity**, E Kluza, SY Yeo, *S Schmid*, DWJ Van der Schaft, RW Boekhoven, RM Schiffelers, G Storm, GJ Strijkers and K Nicolay, Journal of controlled release, 2011; 151(1), 10-17

Oral presentations

1. **Arterial spin labeling - Data acquisition** *S Schmid*, ISMRM 2017 in Honolulu, Hawai, USA
2. **Effect of crushing with Acceleration and Velocity selective labeling modules on ASL signal at multiple PLDs** *S Schmid*, ET Petersen and MJP van Osch, ESMRMB 2016 in Vienna, Austria
3. **Hemodynamics of the cerebral border zone regions in healthy, young volunteers** *S Schmid*, WM Teeuwisse, H Lu, and MJP van Osch, ISMRM 2015 in Toronto, Canada
4. **Insight into the labeling mechanism of Acceleration selective arterial spin labeling**, *S Schmid*, ET Petersen, WM Teeuwisse, and MJP van Osch, ISMRM 2014 in Milan, Italy
5. **Comparison of velocity and acceleration selective arterial spin labeling with $[^{15}O]H_2O$ positron emission tomography**, *S Schmid*, DFR Heijtel, HJMM Mutsaerts, R Boellaard, AA Lammertsma, AJ Nederveen and MJP van Osch, ISMRM Benelux 2014 in Maastricht, The Netherlands
6. **Time efficient determination of spin compartments by Time Encoded Arterial Spin Labeling**, *S Schmid*, E Ghariq, WM Teeuwisse, A Webb, H Lu and MJP van Osch, ISMRM 2013 in Salt Lake City, Utah, USA
7. **Acceleration-selective arterial spin labeling**, *S Schmid*, E Ghariq, WM Teeuwisse, A Webb and MJP van Osch, ISMRM 2012 in Melbourne, Australia
8. **Acceleration-selective arterial spin labeling**, *S Schmid*, E Ghariq, WM Teeuwisse, A Webb and MJP van Osch, ISMRM Benelux 2012 in Leuven, Belgium

Poster presentations

1. **Cerebrovascular reactivity with a CO_2-challenge in HCHWA-D: a new, whole brain MRI-biomarker for CAA?** *S Schmid*, J Verbree, ES van Etten, PH Croll, M Redelijkheid, G Labadie, GM Terwindt, MJH Wermer, MA van Buchem, MJP van Osch, VasCog 2016 in Amsterdam, The Netherlands
2. **Study setup for whole brain assessment of the cerebrovascular reactivity in HCHWA-D with a CO_2-challenge?** *S Schmid*, J Verbree, ES van Etten, PH Croll, M Redelijkheid, G Labadie, GM Terwindt, MJH Wermer, MA van Buchem, MJP van Osch, International CAA conference 2016 in Boston, USA
3. **Hemodynamics of the cerebral border zone regions in healthy, young volunteers** *S Schmid*, WM Teeuwisse, H Lu and MJP van Osch, ISMRM Benelux 2015 in Gent, Belgium
4. **Comparison of velocity and acceleration selective arterial spin labeling with $[^{15}O]H_2O$ positron emission tomography** *S Schmid*, DFR Heijtel, HJMM Mutsaerts, R Boellaard, AA Lammertsma, AJ Nederveen and MJP van Osch, ISMRM 2014 in Milan, Italy
5. **Time efficient determination of spin compartments by Time Encoded Arterial Spin Labeling**, *S Schmid*, E Ghariq, WM Teeuwisse, A Webb, H Lu and MJP van Osch, ISMRM Benelux 2013 in Rotterdam, The Netherlands
6. **Improved selection of the venous blood pool for OEF determination: IQ-OEF**, *S Schmid*, ET Petersen, WM Teeuwisse, A Webb, and MJP van Osch, ISMRM 2012 in Melbourne, Australia

Awards

ESMRMB Young Investigator Award
ESMRMB 2016 in Vienna, Austria
ISMRM Magna Cum Laude Merit Award
in the category "Perfusion and Diffusion"
ISMRM 2015 in Toronto, Canada
ISMRM Magna Cum Laude Merit Award
in the category "Perfusion and Diffusion"
ISMRM 2014 in Milan, Italy
ISMRM Summa Cum Laude Merit Award
in the category "Perfusion and Diffusion"
ISMRM 2013 in Salt Lake City, Utah, USA
ISMRM Summa Cum Laude Merit Award
in the category "Perfusion and Diffusion"
ISMRM 2012 in Melbourne, Australia
ISMRM Benelux 2012 presentation award
for best presentation
ISMRM Benelux chapter meeting 2012 in Leuven, Belgium

Dankwoord

Tot slot wil ik graag iedereen bedanken voor hun bijdrage, steun en plezier bij de totstandkoming van dit proefschrift.

Allereerst veel dank aan mijn promotor Prof. dr. Andrew Webb en co-promotor Dr. ir. Thijs van Osch voor de zeer goede begeleiding en fijne samenwerking. Ik bewonder jullie betrokkenheid, eindeloze stroom aan ideeën en enthousiasme, die zich niet alleen beperken tot de wetenschap.

Uiteraard wil ik mijn collega's van het C.J. Gorter Center en het LUMC bedanken voor alle behulpzaamheid en gezelligheid. Het is boffen met een groep die zo voor elkaar klaar staat, op het werk en daarbuiten.

Graag wil ik de ASL groep bedanken voor de leerzame literatuur bijeenkomsten en open discussies. Door het samen bekijken van posters op congressen, het elkaar herinneren aan het aanpassen van de control parameters bij het scannen en het uitpluizen van de ASL papers, zijn we echt een team geworden.

Ook buiten het LUMC heb ik fijne contacten gelegd met de co-auteurs, bij de ISMRM (Benelux Chapter), de leden van het ASL Network en deelnemers van de EU-COST "ASL in Dementia" meetings. Bedankt voor de prettige samenwerkingen, de mogelijkheden om mijn werk te presenteren op mooie locaties, de diepgaande wetenschappelijk gesprekken en dat ik zoveel van jullie heb mogen leren.

Verder bedank ik ook STW en de gebruikerscommissie van het onderzoeksproject voor de opbouwende discussies. Dankzij jullie input is het onderzoek met sprongen vooruit gegaan.

Mijn dank gaat bovenal uit naar alle vrijwilligers die zo geduldig in de scanner hebben gelegen voor mijn onderzoek. Sorry dat de ASL-scans niet korter duren en we altijd het maximale uit de scantijd willen halen.

Mijn vriendinnen van Δγφδ wil ik bedanken voor de gezellige etentjes. Ook al zien we elkaar niet heel vaak, als we bij elkaar zijn kletsen we alsof er nooit iets veranderd is ondanks dat onze carrières en levens heel andere richtingen op gaan.

Mijn vrienden van Watersportcentrum 't Garijp bedank ik voor het uitwaaien op het water en het heerlijke vakantiegevoel van de zeilschool. Met jullie in Friesland was het geen probleem om het onderzoek even te vergeten.

Mijn familie en schoonfamilie wil ik bedanken voor hun betrokkenheid en vertrouwen. Mama en Papa, bedankt dat jullie mij de vrijheid geven om zelf alles te ontdekken en altijd achter me staan.

Daan, bedankt voor je liefde en dat je er altijd voor me bent.

Curriculum Vitae

Sophie Schmid was born in Delfzijl on 18 July 1987. After graduating from the Esdal College in Emmen in 2005, she studied Biomedical Engineering at the Eindhoven University of Technology. During her internship at the University of British Columbia MRI Research Centre in Vancouver, Canada, she worked on the quality assurance of a Philips Achieva 3T MRI scanner. In 2010, she finished her graduation project, which consisted of the assessment of monocyte recruitment to tumors treated with liposomal prednisolone phosphate with MR imaging as performed in collaboration with the Weizmann Institute of Science in Rehovot, Israel.

In February 2011, she started her PhD research at the CJ Gorter Center for high field MRI of the Leiden University Medical Center. Her main research topics are the development and optimization of arterial spin labeling (ASL) perfusion techniques, such as acceleration selective ASL (AccASL), time encoded pseudo continuous ASL (te-pCASL) and new oxygen extraction fraction measurement techniques that could help in the detection and characterization of e.g. small vessel disease.

Since February 2015 she is studying the cerebrovacular reactivity in Hereditary Cerebral Hemorrhage With Amyloidosis – Dutch type (HCHWA-D), also known as the Katwijk disease, a hereditary form of cerebral amyloid angiopathy (CAA). The vessels in the brain of HCHWA-D-patients are challenged with CO_2 and visual stimulation at 3T MRI and compared with age- and gender-matched healthy controls to get insight in the effect of the amyloid deposition in the cerebral vasculature on the reactivity of the vessels. This study is part of the CAVIA project, which has been made possible by ZonMW, part of the Dutch national ‘Deltaplan for Dementia’.